Low cost materials used to sorption process

Orbital - Vol. 5 No. 3 - July-September - Special Issue 2013

Table of Contents

Editorial

Guest Editors' Note

Dear Readers,

In recent years there has been considerable interest in the removal of pollutants from water and wastewater by using adsorption treatment. Adsorption technique is an economical and effective method and it has shown to be very attractive over traditional treatment methods because of its several advantages, including adsorption capacity and low cost. In fact, the adsorption process has proven to be an excellent way to treat industrial effluents, offering significant advantages, especially from economic and environmental viewpoints, such as: low cost, accessibility, ease of operation and efficiency in comparison with conventional methods. Various waste products from industrial operations such as fly ash, coal, oxides, lignocellulosic materials and agricultural waste and natural materials such as shell peanuts, coconut, sugar cane, clay, soil, among others, are being applied as inexpensive adsorbents in wastewater treatment. These adsorbents can be applied as a sustainable technique for sorption of many classes of organic and inorganic pollutants.

The Special Issue: **Low Cost Materials Used to Sorption Process** aimed to cover the recent progress in all aspects of this important field of Sorption Science. The thematic topics focused on: sorption using inexpensive material, wastewater treatment using alternative materials, low-cost materials applied to air and water. Articles addressing the use of various low-cost adsorbents- applied in the removal of organic and inorganic substances found in liquids-, provide a significant contribution on the subject. The use of experiments as batch and fixed-bed column, as well as various isotherm models was applied to explain the sorption phenomena, which will certainly be an improvement to this science field.

Currently, there is a great appeal for solutions considered "clean" or "green" including the reuse of waste materials, given the economic and environmental context. The technology of low cost material deserves further study and this special issue presents a significant contribution about the basic understanding of the theory and new scientific approaches on the use of low cost adsorbents.

Rivelino Martins Cavalcante
(Universidade Federal do Ceará)

Ronaldo Ferreira do Nascimento
(Universidade Federal do Ceará)

Francisco Wagner de Sousa
(Instituto Federal do Ceará)

Carta dos Editores Convidados

Prezados Leitores,

Nos últimos anos tem havido um interesse considerável na remoção de poluentes a partir de águas residuárias utilizando processos de adsorção. A técnica de adsorção é um método econômico e eficaz que tem se mostrado muito atraente em relação aos métodos tradicionais de tratamento por causa de suas várias vantagens, incluindo a capacidade de adsorção e o baixo custo. De fato, o processo de adsorção, tem provado ser um excelente meio para o tratamento de efluentes industriais, oferecendo vantagens significativas, em especial do ponto de vista econômico e ambiental, tais como: baixo custo, acessibilidade, facilidade de operação e eficiência em comparação com os métodos convencionais. Vários produtos residuais provenientes de operações industriais tais como: cinzas, carvão, óxidos e

materiais lignocelulósicos e resíduos agrícolas e materiais naturais como: casca de amendoim, coco, cana-de-açúcar, argila, solos, entre outros, são aplicados como adsorventes de baixo custo no tratamento de efluentes industriais. Estes adsorventes podem ser aplicados como uma técnica sustentável para sorção de muitas classes de poluentes orgânicos e inorgânicos.

A Edição Especial: **Materiais de Baixo Custo Utilizado para Processos de Adsorção** teve como objetivo cobrir o recente progresso em todos os aspectos deste importante campo da Ciência de sorção. Os tópicos temáticos foram organizados e focados em: sorção utilizando materiais de baixo custo, tratamento de efluentes utilizando materiais alternativos e materiais de baixo custo aplicados ao ar e à água. Os artigos referentes ao uso de vários adsorventes de baixo custo aplicados na remoção de compostos orgânicos e inorgânicos encontrados em efluentes proporcionaram uma contribuição significativa sobre o assunto. O uso de ensaios experimentais em batelada e leito fixo (coluna) bem como, os diversos mecanismos de adsorção foram aplicados para explicar os fenômenos de adsorção, o qual deverá ser uma melhoria a este campo da ciência.

Atualmente, há um grande apelo para as soluções consideradas "limpas" ou "verdes", incluindo a reutilização de resíduos, dado o contexto econômico e ambiental. A tecnologia de material de baixo custo merece um estudo mais aprofundado e esta edição especial apresenta uma contribuição significativa a cerca do entendimento básico da teoria e de novas abordagens científicas sobre o uso de adsorventes de baixo custo.

Rivelino Martins Cavalcante
(Universidade Federal do Ceará)

Ronaldo Ferreira do Nascimento
(Universidade Federal do Ceará)

Francisco Wagner de Sousa
(Instituto Federal do Ceará)

Full Paper

Kinetic and Thermodynamic Studies of the Adsorption of Crystal Violet onto Used Black Tea Leaves

Mohammad A. Hossain * and Md. T. al-Hassan

Department of Chemistry, University of Dhaka, Dhaka-1000, Bangladesh

Abstract: This study presents the kinetic and thermodynamic investigations of the adsorption of crystal violet (CV) on used black tea leaves (UBTL) from aqueous solution to evaluate the feasibility of the process. The effects of concentration, solution pH and temperature on adsorption kinetics were carried out in batch process. Kinetic studies have shown that the adsorption data partially follow simple first order, second order and pseudo second order kinetic equations for different initial concentrations at pH 2.0. The equilibrium amount adsorbed, equilibrium concentration and rate constant were calculated from better fitted pseudo second order kinetic plots for different initial concentrations. The equilibrium amount adsorbed (200 mg/g at 30 ^{o}C) increased with the increase of temperature, indicated endothermic nature of the adsorption. The apparent activation energy of adsorption was determined from Arrhenius plot using pseudo second order rate constant and the value, $E_a = 83.1$ kJ/mol, revealed the process is chemisorption. Thermodynamic parameters: ΔH^{o}, ΔG^{o} and ΔS^{o}, were determined from the equilibrium adsorption constant and the results obtained confirmed that the adsorption process was feasible, less spontaneous and endothermic. The equilibrium amount adsorbed was found to be increased with increase of solution pH from 2.0 to 6.0 indicating electrostatic interaction between cationic CV with anionic surface of UBTL dominated at higher pH due to the low zero point charge pH of UBTL.

Keywords: adsorption kinetics; crystal violet; used black tea leaves; adsorption thermodynamics

1. INTRODUCTION

Environmental pollution by industrial effluents is am important issue in recent years. Different types of dyes are common pollutants usually found in textile industries effluents in many developing countries. Moreover, rapid industrialization has led to disposal of synthetic dyes which are mostly used in relevant industries such as textile, leather, paper, plastic etc. to color their final products [1]. Most of dyes are toxic and carcinogenic compounds posing a serious threat to human and animal health which is not only limited to themselves but may be passed onto further generations [2]. Dyes from the wastewater of these factories must be removed before discharging into water. Crystal violet (CV) is one of the most useful dye uses in textile and paper dyeing, and 15% of such dyes produced worldwide are released to environment in wastewater. Crystal violet destroys cells and can be used as a disinfectant. Compounds related to CV are potential carcinogens [3]. Crystal violet binds to DNA which causes replication errors

in living tissue, possibly leading to mutations and cancer [3]. Thus crystal violet is a mutagen and mitotic poison; therefore concerns exist regarding the ecological impact of the release of CV into the environment. Numerous methods have been developed to treat CV pollution. The most common methods are chemical bleaching [4], biodegradation [5-6], photodegradation [7], photocatalytic degradation [8-10], electrochemical degradation [11-12], cation exchange membrane [13], micellar enhanced ultra filtration [14], fenton-biological treatment [15] and adsorption [16] onto various solids such as activated charcoal. Among the above methods, adsorption has proven to be more versatile and efficient for the removal of dyes from aqueous system. Among them, adsorption is a cost affective method for treatment of wastewater. Activated carbon has been recognized as a highly effective adsorbent for the treatment of heavy metals in wastewater [17]. However, high cost of activated carbon and regeneration difficulties has deterrent in the utilization of activated carbon in the developing countries [18].

---

* Corresponding author. E-mail: *hossainabul@yahoo.com*

Therefore, there is increasing research interest in using alternative low cost adsorbents. Recently, used black tea leaves (UBTL) are interested due to their high adsorption capacity, low cost and easy to recover the adsorbate from adsorbed UBTL [19]. Crystal violet was selected as a common basic dye available in textile effluent for its removal study. Main focus of the present study was to investigate the kinetics and thermodynamics of adsorption of CV onto UBTL under various operational conditions.

2. MATERIAL AND METHODS

21. Adsorbent

The used black tea leaves (UBTL) was prepared by using same method described Alam [20]. In this process, tea liquor was completely removed from fresh black tea leaves collected from local market in Dhaka, Bangladesh. Leaves were dried at room temperature and then dried in oven at 105 °C for 8 h. Dried leaves were sieved through the sieves of mesh size 212-300 µm and the particles in the size range of 212-300 µm in diameter were stored in a desiccator for adsorption experiments. Figure 1 shows the heterogeneous surface morphology of prepared UBTL observed by scanning electron microscope (SEM) (JSM-6490LA, JEOL, Japan).
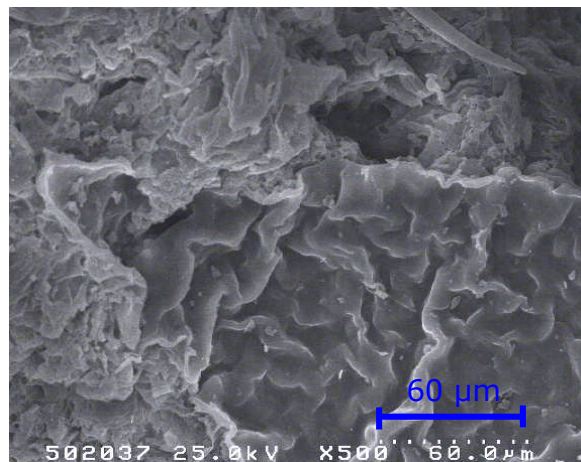

Figure 1. SEM micrograph of prepared UBTL×500.

2.2. Adsorbate

All chemicals used in the study were analytical grade. Crystal violet (CV) is a basic dye which exists as cationic form in acidic to neutral media. It is used as a pH indicator, with a range between 0 and 1.6. The protonated form (found in acidic conditions) is yellow, turning blue-violet above pH levels of 1.6. IUPAC name of CV is tris(4-(dimethylamino) phenyl)methylium chloride. Synonyms of crystal violet are methyl violet 10B, methyl violet 10BNS, aniline violet, baszol violet 57L, brilliant violet 58, gentian violet, pyoktanin, methylrosanilide chloride and hexamethyl-p-rosaniline chloride. Molecular formula of crystal violet is $C_{25}H_{30}N_3Cl$ and the structural formula is given in Figure 2. C.I. number and CAS number of crystal violet are basic violet 3 and 548-62-9, respectively. Molecular weight of crystal violet is 407.98 g.

A stock solution of 1000 mg/L was prepared by dissolving CV (Analytical grade) in distilled water from which different concentrated solutions were prepared. Concentration of CV in different solutions was determined by a computerized UV-visible spectrophotometer (UV-1650A, Shimadzu, Japan) using $\lambda_{max} = 582$ nm and solution pH was at 6.0 as an optimum pH for CV solution to analyze [21]. According to Beer-Lambert law, the calibration limit of CV was determined which was in the range of 0.1 to 20.0 mg/L at optimum pH 6.0 and the absorption coefficient was 0.109 L/mg.cm.
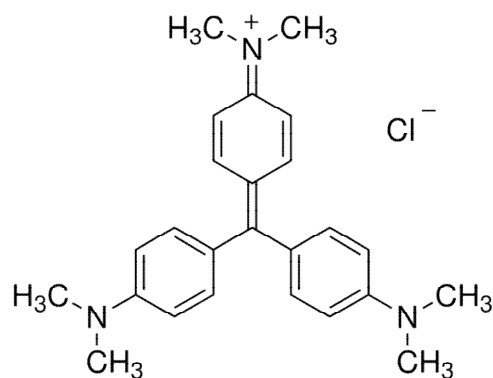
Figure 2. Molecular structure of crystal violet (CV).

2.3. Adsorption Kinetic Experiments

Adsorption study was conducted in batch process in a series of reagent bottles at a constant temperature. 0.0025g of UBTL was mixed with each of 25 mL of a definite concentrated CV solution (22.66 mg/L) at pH 2.0 as an optimum pH for UBTL [20] and was shaken in a thermostatic mechanical shaker (HAAKE SWB20, Fissions Ltd., Germany) at 30.0 ± 0.2 °C with a fixed agitation rate of 150 rpm. After shaking of different time of intervals, the mixtures were separated. The pH of supernatant of each bottles were adjusted at pH 6.0 with proper dilution and measured the absorbance using UV-vis spectrophotometer (UV-1650A, Shimadzu, Japan) at λ_{max} 582 nm. Before adsorption, the absorbance of the

149

Orbital: Electron. J. Chem. 5 (3):148-156, 2013

solution at pH 6.0 with proper dilution was also measured by UV-vis spectrophotometer at λ_{max} 582 nm to determine the initial concentration of the solution. Similar kinetic experiments were performed using different initial concentrations of crystal violet solutions. The amount adsorbed at different contact times for different initial concentration was calculated from the following equation (1).

$$q_t = \left(C_o - C_t\right) \times \frac{V}{W} \qquad (1)$$

where, C_o is the initial concentration of CV (mg/L), C_t is the concentration of CV at time t (mg/L), q_t is the amount adsorbed at time t (mg/g), V is the volume of solution in liter and W is the mass of adsorbent in g.

2.4. Effect of temperature on adsorption kinetics

To investigate the effect of temperature on the adsorption kinetics, kinetic experiments were conducted at three different temperatures using same initial concentration of about 100.2 mg/L of CV solution at pH 2.0, keeping other parameters constant. The change of amount adsorbed of CV with different contact time for different temperatures were recorded.

2.5. Effect of pH on adsorption kinetics

To observe the effect of solution pH on adsorption of CV, a series of adsorption kinetic experiments were conducted at three different pH values using initial concentration of about 51.6 mg/L of CV solution, keeping other parameters constant. The change of amount adsorbed with different contact time for different initial pH values were calculated.

3. RESULTS AND DISCUSSION

3.1. Effect of concentration on adsorption kinetics

Kinetic of adsorption is one of the important characteristics defining the efficiency of an adsorbent. To investigate the effect of CV concentration on adsorption kinetics, a series of kinetic experiments, change of concentration with contact time, were performed at different initial concentrations of CV for a constant temperature, solution pH, adsorbent dose and agitation rate. As the time passes, the CV adsorbed on the UBTL surface resultant the decreased of CV concentration in solution. Figure 3 (a-b) shows the variation of amount adsorbed of CV with contact time for a fixed amount of adsorbent. The adsorption of CV onto UBTL are quite rapid initially, however the adsorption rate becomes slower with progress of time. The initial faster rate of adsorption may be due to the availability of the uncovered surface sites of UBTL. Again, the amount of CV adsorbed per unit mass of UBTL increased with increase in CV concentration as shown in Figure 3 (a-b) which indicated that the extent of adsorption is highly dependent on the concentration of CV. This is because at low concentration, the ratio of the initial number of CV molecules to the available sites is low, resultant the finished of CV in solution before reach the saturation of UBTL surface; subsequently, the fractional adsorption becomes independent of the initial concentration. However, at high concentration of CV the available surface sites of adsorption become fewer, and hence the percent adsorption as well as adsorption amount depends on the initial concentration of CV up to a certain limit.
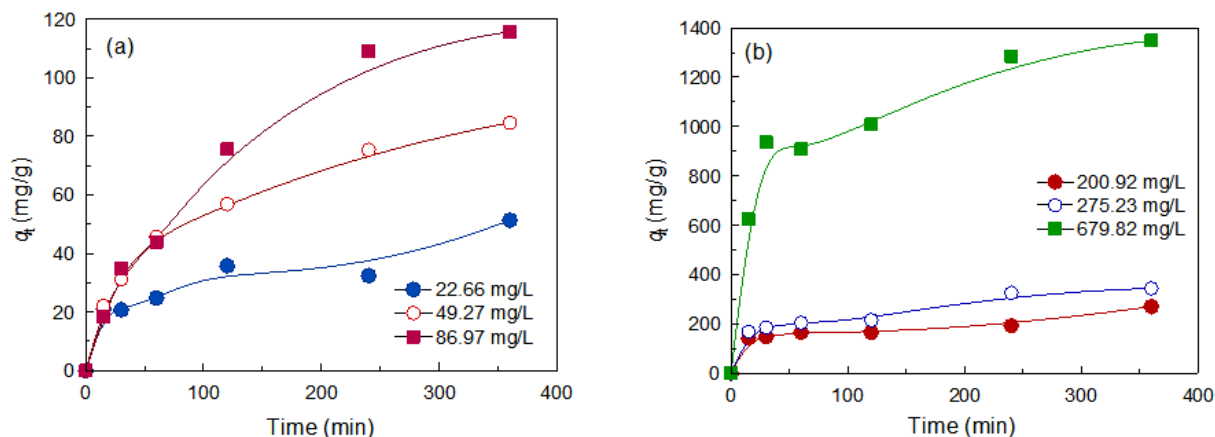

Figure 3. (a) and (b): Variation of the amount adsorbed of CV on UBTL with time for different initial concentrations of CV where solution pH 2.0, particle size: 212-300 μm and temperature: 30.0 ± 0.2 °C.

150

Orbital: Electron. J. Chem. 5 (3):148-156, 2013

The adsorption mechanism depends on the physicochemical characteristics of adsorbent and adsorbate and as well as on the mass transfer process. With the maximum agitation speed of 150 rpm, it was assumed to offer no mass transfer (both external and internal) resistance to the overall adsorption process. Therefore the adsorption kinetics can be studied through the residual adsorbate concentration in the solution. The kinetic experimental results obtained for different initial concentration of CV were analyzed using simple first order, second order and pseudo second order kinetic equations. Linear regression (R^2) value was used to determine the best fitting kinetic model for experimental data.

To evaluate the feasibility of the adsorption of CV on UBTL, simple first order kinetic model was verified using the following equation (2) [21-22]

$$\ln C_t = k_1 t + \ln C_o \qquad (2)$$

where, C_t is the concentration of dye after time t (mg/L), C_o is the initial concentration of dye (mg/L) and k_1 is first order rate constant. Applicability of the first order kinetic equation (2) was examined by plotting $\ln C_t$ *vs* t as shown in Fig. 4 (a-b) which shows that the adsorption of CV on UBTL partially follow the simple first order kinetic equation for different initial concentrations of CV and regression values are given in Table 1.

3.2. First order kinetics

Figure 4. (a) and (b): First order kinetics CV adsorption onto UBTL at various initial concentrations pH 2.0 and temperature 30.0 ± 0.2 °C.

Table 1. A comparison of the data fitness to the first, second and pseudo second order kinetic equations.

Initial concentration C_o (mg/L)	R^2 (-)		
	First order equation	**Second order equation**	**Pseudo second order equation**
22.66	0.862	0.837	0.892
49.27	0.928	0.939	0.916
86.97	0.913	0.929	0.873
200.92	0.970	0.918	0.932
275.23	0.946	0.944	0.967
679.82	0.855	0.832	0.979

3.3. Second order kinetics

Second order kinetic equation (3) was applied to evaluate the feasibility of the adsorption of CV on UBTL [21].

$$\frac{1}{C_t} = kt + \frac{1}{C_o} \qquad (3)$$

where, C_t is the concentration of dye at time t (mg/L), C_o is the initial concentration of dye (mg/L) and k_2 is second order rate constant (g/mg.min). The experimental results of the adsorption of CV on UBTL was investigated by plotting $1/C_t$ *versus* t. Figure 5 (a-b) shows the adsorption of CV on UBTL partially follow the simple second order kinetic

151

Orbital: Electron. J. Chem. 5 (3):148-156, 2013

equation for different initial concentration of CV and the regression factors are presented in Table 1. The values of average regression factor (R^2) for simple first order and second order kinetic equations are

0.912 and 0.899, respectively, which indicated that both kinetic models prediction deviated considerably from experimentally obtained data.
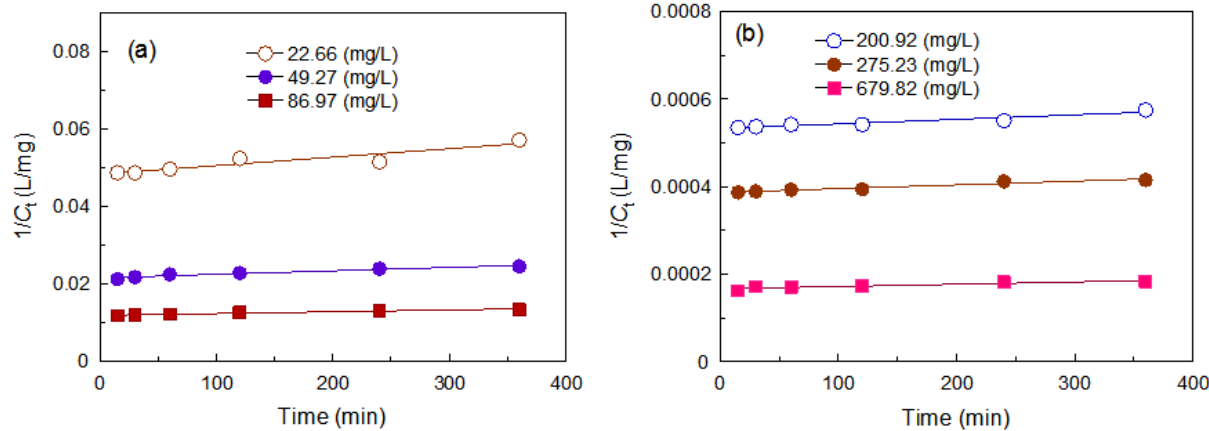
Figure 5. (a) and (b): Second order kinetics of CV adsorption onto UBTL at various initial concentrations at pH 2.0 and temperature 30.0 ± 0.2 °C.

3.4. Pseudo second order kinetics

Pseudo second order kinetic equation based on solid phase adsorption was applied to the experimental data obtained for different initial concentrations to investigate the feasibility of adsorption of CV on UBTL [24]. The linearized form of the Ho and McKay's pseudo second order rate equation (4) was verified by plotting t/q_t *vs. t* as shown in Figure 6 (a-b).

$$\frac{t}{q_t} = \frac{1}{kq_e^2} + \frac{t}{q_e} \qquad (4)$$

where, q_t is the amount adsorbed at time, t (mg/g), q_e is equilibrium amount adsorbed (mg/g) and k is pseudo second order rate constant (g/mg.min). Figure 6 (a-b) shows that each plot does not gives straight line with the whole range of concentration but the average value of regression factor ($R^2 = 0.933$) for different concentrations of CV is better than that of both simple first order and second order kinetic equations. A comparison of the regression factor for the fitness of simple first order, second order and pseudo second order kinetic equations to the adsorption kinetics of CV on UBTL at pH 2.0 is given in Table 1.
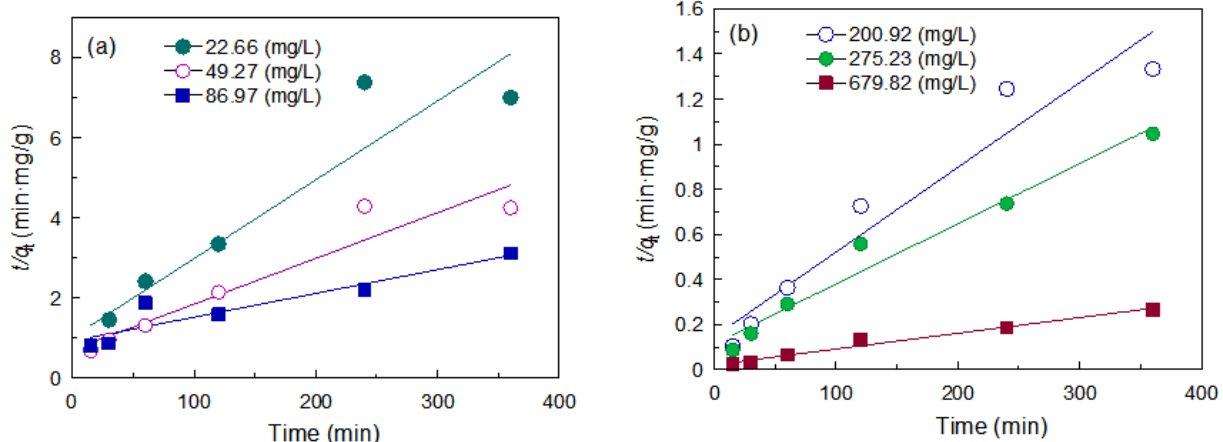

Figure 6. (a) and (b): Pseudo second order kinetics of CV adsorption onto UBTL at various initial concentrations at pH 2.0 and temperature 30.0 ± 0.2 °C.

152

Orbital: Electron. J. Chem. 5 (3):148-156, 2013

3.5 Effect of temperature on adsorption kinetics

To investigate the effect of temperature on the adsorption kinetics, kinetic experiments were performed at different temperatures using same concentration of CV solution at pH 2.0. Figure 7 shows the variation of amount adsorbed with time for different temperatures. Pseudo second order kinetic equation was also applied for the system at different temperatures (Figure not shown). From the slope of the each straight line, equilibrium amounts adsorbed were calculated (200 mg/g at 30 °C). Again, the equilibrium amount adsorbed was plotted against temperature as shown in Figure 8 which shows that the equilibrium amount adsorbed increases with temperature i.e. the process is endothermic indicating chemical interaction of the process.
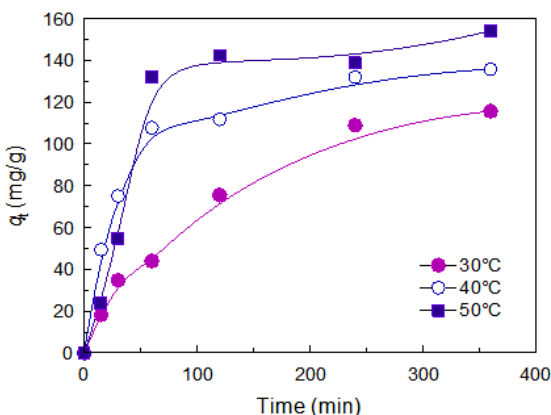
Figure 7. Change of the amount adsorbed with time during the adsorption of CV on UBTL at pH 2.0 for different temperatures.

Figure 8. Variation of equilibrium amount adsorbed with temperature for adsorption of CV on UBTL at pH 2.0.

3.6. Adsorption thermodynamics

Activation energy of adsorption

The effect of temperature on the reaction rate is well known and important in understanding reaction mechanism. The apparent activation energy of adsorption was calculated from the pseudo second order rate constant obtained at different temperatures using the following (6) Arrhenius equation [25]

$$\ln k = -\frac{E_a}{RT} + \ln A \qquad (6)$$

where, E_a is the apparent activation energy (kJ/mol), A is the Arrhenius temperature independent factor and k is the pseudo second order rate constant (g/mol·s). E_a was calculated from the slope of the plot of ln$k$ values at different temperatures against the reciprocal of absolute temperatures as shown in Figure 9. The calculated value of apparent activation energy was 83.10 kJ/mol, implying that adsorption occurs comparatively slowly by like as chemical reaction in which E_a is in the range 65–250 kJ/mol [26].

Thermodynamic equilibrium constant

The value of the equilibrium adsorption (K_C) at different temperatures was calculated according to the following equation (7) [27-30] to estimate the thermodynamic parameters of adsorption.

$$K_C = \frac{C_a}{C_e} \qquad (7)$$

C_a is the dye concentration on the adsorbent at equilibrium (mg/L) and C_e is the dye concentration in solution at equilibrium (mg/L).
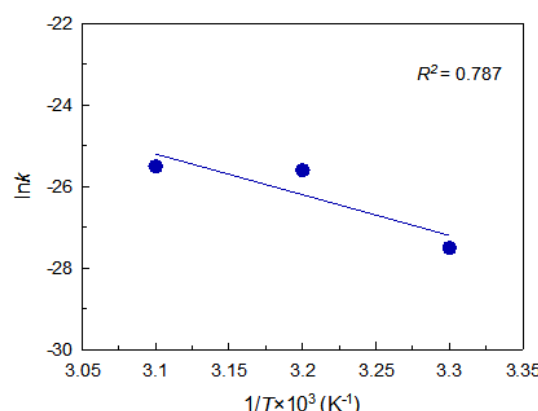
Figure 9. A plot of ln k against the reciprocal of absolute temperatures to determine the apparent activation energy.

153

Orbital: Electron. J. Chem. 5 (3):148-156, 2013

Standard enthalpy, entropy and free energy change were calculated by using equation (8) and (9), respectively [27-32].

$$\ln K_C = \frac{\Delta S^o}{R} - \frac{\Delta H^o}{RT} \qquad (8)$$

$$\Delta G^o = -RT \ln K_C \qquad (9)$$

where ΔG^o, ΔH^o and ΔS^o are the change of standard free energy (kJ/mol), enthalpy (kJ/mol) and entropy (kJ/mol·K), respectively. K_C is the equilibrium adsorption constant (-) and T is the absolute temperature (K). The values of ΔH^o and ΔS^o were calculated from the slope and intercept of the linear plot of $\ln K_C$ vs $1/T$ as shown in Figure 10.
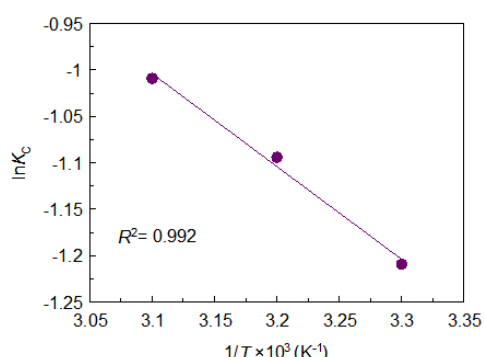
Figure 10. A plot of $\ln K_C$ vs $1/T$ for determination of enthalpy of the adsorption of CV on UBTL.

The value of ΔG^o was calculated from equation (9) and presented in Table 2 as well as the values of ΔH^o and ΔS^o. The results indicated that the adsorption of CV on UBTL was endothermic and chemical in nature. The calculated values of ΔH^o and ΔS^o were 8.32 kJ/mol and 0.0174 kJ/mol·K, respectively indicated that the adsorption of CV on UBTL was endothermic and less spontaneous. The positive value of ΔG^o which decreased with increasing temperature indicated the process is slow and less feasible [33]. The positive value of entropy predicted the increased randomness through the fragmentation of CV molecules during the adsorption on the UBTL surface.
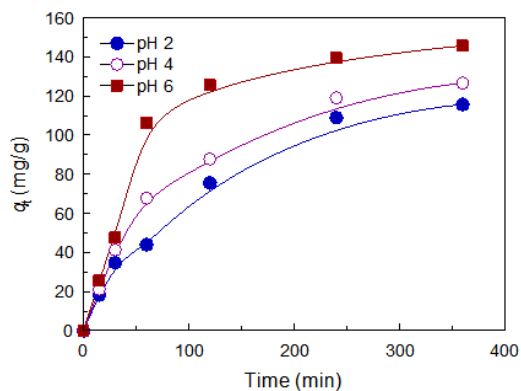
Effect of pH on Adsorption Kinetics

The pH of solution is one of the most important parameters in the adsorption of solid/liquid interface. Basically, the pH of solution affects the adsorbent surface charge through the protonation/deprotonation process based on adsorbent's zero point charge pH (pH$_{ZPC}$). In case of cationic CV as an adsorbate, solution pH has a large effect on its molecular structure through the protonation of the amino groups located at the aromatic rings. The number of positive charge decreases from 3 to 1 with the increase of solution pH. For the solution pH>5 the CV has a blue-violet color whereas at solution pH <2, the CV is green. The different colors are results of the different charged states of CV molecule. Therefore, to investigate the effect of solution pH on the adsorption kinetics as well as the adsorption capacity of CV on UBTL, a series of adsorption kinetic experiments were carried out at a fixed concentrated CV solution with different initial pH values from 2.0 to 6.0. All the solutions before and after adsorption were analyzed at a constant pH 6.0. The change of amount adsorbed with time at different initial pH is shown in Figure 11. Pseudo second order rate equation was verified for different initial pH values and respective parameters were determined. The variation of equilibrium amount adsorbed with pH is shown in Figure 12 which indicated the increase of equilibrium amount adsorbed with increase of solution pH from 2.0 to 6.0.

Figure 11. Variation of equilibrium amount adsorbed of CV with time for different initial pH with initial concentration of 51.6 mg/L at 30.0 ± 0.2 °C.
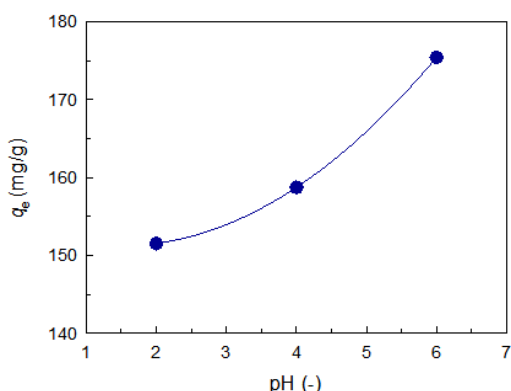
Figure 12. Change of the amount adsorbed with pH for adsorption of CV on UBTL at 30.0 ± 0.2 °C.

154

Orbital: Electron. J. Chem. 5 (3):148-156, 2013

The observation can be explain by the pHzpc on UBTL (pH$_{ZPC}$= 4.2) [34]. The cationic species of CV are expected to be adsorbed more at higher pH values of solution than the pH$_{ZPC}$ of UBTL surface which leads to negative surface. The result of investigation agreed with the expectation of electrostatic interaction between the positively charged cationic CV molecules and adsorbent, which is enhanced considering the negatively charged UBTL surface (i.e. gradual deprotonation as the solution pH increases) [35]. The same trend has also been reported in the adsorption of CV by other adsorbent materials such as Peel of Cucumis sativa Fruit [36], Chaetophora elegans algae [37], Coconut coir pith (CCP) [38], Jackfruit plant (*Artocarpus heterophyllus*) leaf powder (JPLP) [38], Pineapple (*Ananas comosus*) peel powder(PPP) [38], Teak tree (*Tectona grandis*) leaf powder (TTLP) [38], Chiku (*Manikara zopata*) leaf powder (CLP) [38] and Cinnamon Plant (*Cinnamonum zeylanicum*) leaf powder (CPLP) [38].

Table 2. Adsorption constant and thermodynamic parameters for CV adsorption on UBTL at different temperatures.

Equilibrium concentration on adsorbent C_a (mg/L)	Equilibrium concentration in solution C_e (mg/L)	Equilibrium adsorption constant K_C (-)	$\ln K_C$	ΔG^o (kJ/mol)	ΔH^o (kJ/mol)	ΔS^o (kJ/K.mol)
20.00	66.97	0.2986	-1.208	3.04		0.0174
22.33	66.68	0.3348	-1.090	2.85	8.32	0.0174
24.21	66.43	0.3644	-1.009	2.71		0.0174

3.7. Comparison studies

The adsorption kinetics as well as adsorption capacity and enthalpy of CV onto UBTL were compared with other biosorbents reported in literature and presented in Table 3. All the biosorbents given in Table 3 shows that the adsorption of CV follows pseudo second order kinetic equation and the process is favorable at neutral media and endothermic in nature. The adsorption capacity vary due to the properties of each adsorbent such as surface area, structure and functional groups, etc.

Table 3. A comparison of the adsorption kinetics, capacity and enthalpy of CV onto UBTL with different biosorbents.

Adsorbents	pH	q_e (mg/g)	Kinetics	ΔH (kJ/mole)	References
peel of *Cucumis sativa* fruit	7.0	34.2	Pseudo second order		[36]
Chaetophora elegans aJga	6.5	158.7	Pseudo second order	21.080	[37]
Coconut coir pith (CCP)	6.0	182.0	Pseudo second order	27.112	[38]
Jackfruit plant leaf powder	6.0	169.0	Pseudo second order	10.160	[38]
Pineapple peel powder(PPP)	6.0	153.5	Pseudo second order	10.999	[38]
Teak tree leaf powder (TTLP)	6.0	77.0	Pseudo second order	7.335	[38]
Chiku leaf powder (CLP)	6.0	73.5	Pseudo second order	5.326	[38]
Cinnamon Plant leaf powder (CPLP)	6.0	72.0	Pseudo second order	5.129	[38]
Used black tea leaves (UBTL)	2.0	200.0	Pseudo second order	8.314	Present Study

4. CONCLUSION

Kinetic study on the adsorption of CV on UBTL has shown that the adsorption kinetics partially follows simple first order or second order kinetic equation but mostly follows pseudo second order rate equation for different initial concentrations of CV at pH 2.0. Pseudo second order kinetic was used to calculate the equilibrium amount adsorbed, equilibrium concentration and pseudo second order rate constant for different initial concentrations. The equilibrium amount adsorbed obtained (200 mg/g at 30 °C) from pseudo second order kinetics were found to be increased with increase in temperature i.e. the process is endothermic and chemical in nature. Pseudo second order rate constant was used to determine the apparent activation energy of adsorption. The calculated apparent activation energy and standard enthalpy were 83.1 kJ/mol and 8.27 kJ/mol, respectively. The value of apparent activation energy supported the chemical nature of the

155

Orbital: Electron. J. Chem. 5 (3):148-156, 2013

adsorption. The positive value of standard free energy change indicated that the adsorption process is less spontaneous. The positive value of standard entropy means the fragmentation of adsorbed molecule might be occurred on the surface of UBTL. The equilibrium amount adsorbed was found to be increased with increase of solution pH from 2.0 to 6.0 suggesting electrostatic interaction between cationic CV with anionic UBTL surface dominated at neutral/basic solution.

5. ACKNOWLEDGMENTS

6. REFERENCES AND NOTES

[1] Carliell, C. M.; Barclay, S. J.; Naidoo, N.; Buckly, C. A. *Water S. A.* **1995**, *21*, 61.

[2] Crini, G. *Dyes Pigments*. **2008**, *77*, 415. [CrossRef]

[3] Sabnis, R. W. Handbook of Biological Dyes and Stains: Synthesis and Industrial Applications. John Wiley and Sons, **2010**. [CrossRef]

[4] Bhasikuttan, A.; Sapre, A. V.; Shastri, L. V. *J. Photochemistry and Photobiology A: Chemistry*. **1995**, *90*, 177.

[5] Bumpus, J. A; Brock, B. J. *Appl. and Environ. Microbiol.* **1988**, *54*,1143. [PubMed]

[6] Yatome, C.; Yamada, S., Ogawa, T.; Matsui, M. *Appl. Microbiol. and Biotechnol.* **1993**, 38, 4. [CrossRef]

[7] Senthilkumaar, S.; Porkodi, K. *J. Colloid and Interf. Sci.* **2005**, *288*, 184. [CrossRef][PubMed]

[8] Sohrabi, M. R.; Ghavami, M. *J. Hazard. Mater.* **2008**, *153*, 1235. [CrossRef][PubMed]

[9] Sleiman, M.; Vildozo, D. L.; Ferronato, C.; Chovelon, J. M. *Appl. Catal. B* **2007**, *77*, 1. [CrossRef]

[10] Sahoo, C.; Gupta, A.; Pal, A. *Dyes Pigments* **2005**, *66*, 189. [CrossRef]

[11] Fan, L.; Zhou, Y.; Yang, W.; Chen, G.; Yang, F. *Dyes Pigments* **2008**, *76*, 440. [CrossRef]

[12] Sanroman, M.; Pazos, M.; Ricart, M.; Cameselle, C. *Chemosphere* **2004**, *57*, 233. [CrossRef][PubMed]

[13] Wu, J. S.; Liu, C. H.; Chu, K. H.; Suen, S. Y. *J. Membr. Sci.* **2008**, *309*, 239. [CrossRef]

[14] Zaghbani, N.; Hafiane, A.; Dhahbi, M. *Desalination* **2008**, *222*, 348. [CrossRef]

[15] Lodha, B.; Chaudhari, S. *J. Hazard. Mater.* **2007**, *148*, 459. [CrossRef][PubMed]

[16] Zaghbani, M. X.; Lee, L.; Wang, H. H.; Wang, Z. *J. Hazard. Mater.* **2007**, *149*, 735. [CrossRef][PubMed]

[17] Huang, C. P.; Blankenship, B. W. *Wat. Res.* **1989**, *18*, 37. [CrossRef]

[18] Ho, Y. S.; Chiang T. H.; Hsueh Y. M. *Process Biochem.* **2005**, *40*, 119. [CrossRef]

[19] Hossain, M. A. Study on the Process Development for Removal of Cr (VI) from Waste Water by Sorption on Used Black Tea Leaves. [Doctoral dissertation.] Kanazawa University, Japan, 2006.

[20] Alam, M. S. Equilibrium and Continous Column Study on the Adsorption of Rhodamine B on Used Black Tea Leaves. *MS. Project*. Department of Chemistry, University of Dhaka, Bangladesh, 2010.

[21] Hasan, T. A. Study on the Adsorption Kinetics of Crystal Violet on Used Black Tea Leaves. *BS. Project*. Department of Chemistry, University of Dhaka, Bangladesh, 2012.

[22] Gupta, V. K.; Gupta, M.; Sharma, S. *Water Res.* **2001**, *34*, 735.

[23] Cimino, G.; Passerine, A.; Toscano, G. *Water Res.* **2000**, *34*, 2955. [CrossRef]

[24] Ho, Y. S.; McKay, G. *Water Res.* **2000**, *34*, 735. [CrossRef]

[25] Bayramoglu, G.; Altintas, B.; Arica, M. Y. *J. Chem. Eng.* **2009**, *152*, 339. [CrossRef]

[26] Yu, Y.; Zhuang, Y. Yi.; Wang, Z. H. *J. Colloid Interf. Sci.* **2001**, *242*, 288. [CrossRef]

[27] Singha, B.; Das, S. K. *Colloids and Surf. B: Biointerface,* **2011**, *84*, 221. [CrossRef][PubMed]

[28] Naiya, T. K.; Bhattacharya, A. K.; Das, S. K. *J. Colloid and Interf. Sci.* **2009**, *333*, 14. [CrossRef][PubMed]

[29] Bhattacharya, A. K.; Naiya, T. K.; Mandal, S. N.; Das, S. K. *Chem. Eng. J.* **2008**, *137*, 529. [CrossRef]

[30] Singha, B.; Das, S. K. *Environ. Sci. Pollut. Res.* **2012**, *19*, 2212. [CrossRef][PubMed]

[31] Ada, K.; Ergene, A.; Tan, S.; Yalcin, E. *J. Hazard. Matter.* **2009**, *165*, 637. [CrossRef][PubMed]

[32] Nandi, B. K.; Goswami, A.; Purkait, M. K. *Appl. Clay. Sci.* **2008**, *42*, 583. [CrossRef]

[33] Ali, A. S.; Hassan, A. *J. Phys. Chem. Biophys.* **2012**, *2*, 1.

[34] Hossain, M. A.; Islam, T. S .A. *J. Bangla. Acad. Sci.* **1998**, *22*, 91.

[35] Kannan, R. R.; Rajasimman, M.; Rajamohan, N.; Sivaprakash, B. *Front. Environ. Sci. Engin.* **2010**, *4*, 116. [CrossRef]

[36] Smithaa, T.; Thirummalisamy, S. A.; Manonmani, S. *E-J.Chem.* **2012**, *9*, 1091.

[37] Rammel, R. S.; Zatiti, S. A.; El-Jamal, M. M. *J. Univ. Chem. Technol. Metallur.* **2011**, *46*, 283.

[38] Patila, S.; Renukdasb, S.; Patelb, N. *J. Chem. Bio. Phy. Sci. Sec. D*, **2012**, *2*, 2158.

156

Orbital: Electron. J. Chem. 5 (3):148-156, 2013

Full Paper

Estudo Comparativo da Adsorção de Pb (II), Cd (II) e Cu (II) em Argila Natural Caulinítica e Contendo Montmorilonita

Débora M. Aragão[a], Maria Lara P. M. Arguelho[a], José do Patrocinio H. Alves[a]*, Carolina M. O. Prado[b]

[a]*Departamento de Química, Universidade Federal de Sergipe, Av. Mal. Rondon, s/n, 49100-000 São Cristóvão - SE, Brazil.*
[b]*Instituto Tecnológico e de Pesquisas do Estado de Sergipe, Rua Campo do Brito 371, São José, 49.020-380, Aracaju – SE, Brazil.*

Abstract: Natural clays containing kaolinite (AC) and montmorillonite (AM), obtained from State of Sergipe, Northeast of Brazil, were used as adsorbents for metal ions in aqueous solution. The adsorption equilibrium was reached in the first minutes and the contact time of 60 min was selected for the rest of the study. Adsorption increased with pH for AC and did not change significantly for AM. Montmorillonite showed a higher adsorption capacity for the metal ions with the Langmuir monolayer capacity (Qo) of 1.48 to 6.98 mg g^{-1} compared to that of 0.42 to 1.51 mg g^{-1} for kaolinite.

Keywords: metal ions; adsorption; natural clays

1. INTRODUÇÃO

A poluição por metais traço é um dos mais sérios problemas ambientais da atualidade, uma vez que esses elementos não são degradáveis e tendem a acumular-se nos organismos aquáticos, podendo como consequência causar intoxicação em seres humanos. Em muitos rios e lagos, o lançamento antropogênico desses metais já excede a quantidade que normalmente entra no ambiente aquático pela ação do intemperismo e mesmo nos oceanos, já é considerável o aporte resultante da atividade humana [1]. Desse modo, tornou-se uma preocupação especial, o tratamento de despejos para remoção de metais tóxicos [2, 3].

Dentre os processos físico-químicos usados para remoção de metais, a adsorção tem se destacado pela elevada eficiência, baixo custo, facilidade de operação e aplicabilidade em concentrações muito baixas [4-7].

As argilas minerais ocorrem em abundancia na natureza e agem como removedores naturais de poluentes catiônicos e aniônicos por troca iônica e/ou adsorção. Tem se mostrado excelentes matérias adsorventes pela sua elevada área superficial, grande capacidade de troca e estabilidade química e mecânica [5, 6, 8]. Argilas minerais com elevada capacidade de adsorção para íons metálicos, tais como, montmorilonita, caulinita e vermiculita vêm sendo usadas para remoção de metais tóxicos de soluções aquosas [9-12].

A caulinita tem uma composição teórica de 46,5 % de SiO$_2$, 39,5 % de Al$_2$O$_3$ e 14,0 % de água, não permitindo a substituição na camada tetraédrica, do Si^{4+} pelo Al^{3+} e nem do Al^{3+} por outros íons na camada octaédrica. A carga liquida da caulinita deveria ser zero, mas uma pequena carga negativa, resultante da quebra das bordas dos cristais, confere a sua superfície alguma atividade. A caulinita é a menos reativa das argilas, a adsorção está limitada à superfície externa e é acompanhada da liberação de íons H$^+$ dos vértices do mineral [11, 13, 14]. Mesmo com a baixa capacidade de troca catiônica, muitos estudos tem usado a caulinita para remoção de Pb (II), Cu (II) e Cd (II) em solução aquosa [11, 15-17].

A montmorilonita tem uma composição teórica de 66,7 % de SiO^2, 28,3 % de Al$_2$O$_3$ e 5,0 % de água, existindo na camada tetraédrica a substituição do Si^{4+} pelo Al^{3+} e na camada octaédrica do Al^{3+} pelo Mg^{2+}. Isso confere uma carga negativa a montmorilonita que

---
* Corresponding author. E-mail: larapalm@yahoo.com

é responsável pela sua maior atividade como adsorvente [11]. Nesse caso a adsorção pode se dá tanto na superfície externa quanto na intercamada, devido à carga negativa gerada pela substituição isomórfica [18]. Nesse estudo foi avaliada a possibilidade de utilização de argilas naturais, sem pré-tratamento, contendo caulinita e montmorilonita, abundantes no estado de Sergipe, nordeste do Brasil, como adsorventes de baixo custo, para remoção do Pb (II), Cu (II) e Cd (II), em solução aquosa. Foram investigadas as condições de adsorção incluindo tempo de contato, pH e isotermas de adsorção.

2. MATERIAL E MÉTODOS

Características das amostras de argila

A argila caulinita (AC) foi originária da área de lavra, localizada na Serra do Pinhão, município de Itabaiana e a argila contendo montmorilonita (AM) procedente do depósito argiloso situado no município de Nossa Senhora do Socorro, ambos no estado de Sergipe. As amostras foram secas a 80 ^{o}C por 3 h, pulverizadas e passadas em peneira de 75 µm antes de serem usadas como adsorventes.

As amostras foram coletadas e caracterizadas por Prado [19]. A análise por difratometria de raios X mostrou que a argila AC contém caulinita, haloisita, goetita e quartzo, enquanto a argila AM tem caulinita, dolomita, goetita, haloisita, montmorilonita, ilita e quartzo.

As características químicas são mostradas na Tabela 1. Os constituintes químicos principais foram sílica, alumínio e os óxidos de ferro. O SiO_2 foi muito maior na argila AC e o Fe_2O_3 na argila AM. A ocorrência dos óxidos de cálcio e magnésio, e de elevada quantidade de potássio, confirmam respectivamente, as presenças de dolomita e ilita na amostra AM. Os valores da razão SiO2/Al2O3, igual a 3,77 em AC e a 4,11 em AM, foram muito superiores a razão teórica da caulinita (1,18) e da montmorilonita (2,36), sugerindo que as argilas estão enriquecidas com sílica, provavelmente devido ao aporte detrital da região continental adjacente [11, 20, 21]. Espera-se, portanto, que com essas diferenças de propriedades mineralógicas e químicas, as amostras de argilas mostrem um comportamento variável em relação à adsorção de metais.

Tabela 1. Composição química das argilas usadas como adsorventes (% em massa, média ± desvio padrão, n = 3). AC: argila caulinita; AM: argila contendo montmorilonita.

Óxidos	AC	AM
SiO_2	74,3±0,3	59,2±0,4
Al_2O_3	19,7±0,2	14,4±0,2
Fe_2O_3	1,02±0,02	4,79±0,06
TiO_2	0,096±0,01	0,66±0,02
CaO	0,05±0,01	4,02±0,09
MgO	0,59±0,04	2,64±0,03
Na_2O	0,18±0,06	0,48±0,07
K_2O	2,01±0,04	3,11±0,06

Reagentes

Todos os reagentes utilizados foram de grau analítico. As soluções estoques dos metais (200 mg L^{-1}) foram preparadas dissolvendo a quantidade estequiométrica dos nitratos [$Cd(NO_3)_2$, $Cu(NO_3)_2$, $Pb(NO_3)_2$] em água deionizada (sistema Milipore Mili-Q) e as demais soluções foram preparadas pela diluição da solução estoque. O pH foi ajustado usando soluções de NaOH 0,1 mol L^{-1} e HNO_3 0,1 mol L^{-1}.

Efeito do tempo de contato

No estudo do tempo de contato foi utilizada uma massa de 0,5 g da argila e 20 mL da solução dos metais (Pb^{2+}, Cd^{2+}, Cu^{2+}) numa concentração de 20 mg L^{-1}, no pH da própria solução dos nitratos que se manteve em 5,2 ± 0,2. O sistema foi mantido sob agitação de 150 rpm, à temperatura ambiente de 25 ± 1 ^{o}C, nos tempos de contato de 20, 40, 60, 90, 120, 150, 180, 210 e 240 min. Brancos, sem adição das argilas, foram utilizados para o controle da concentração inicial dos metais e os experimentos foram executados em duplicata. Concluído o tempo de agitação, as soluções foram filtradas utilizando papel de filtração rápida e guardadas em frascos de polietileno para posterior determinação da concentração dos metais. As concentrações dos metais foram determinadas por absorção atômica.

A quantidade do metal adsorvido, Q_e (mg do metal/g do adsorvente), foi calculada pela equação 1:

$$Q_e = V(C_o - C_e) / m \qquad (1)$$

158

Orbital: Electron. J. Chem. 5 (3):157-163, 2013

onde V (L) é o volume de solução; Co (mg L^{-1}) a concentração inicial da solução de íon metálico, Ce (mg L^{-1}) a concentração final após o tempo de agitação e m (g) a massa de argila.

A percentagem de remoção do metal adsorvido foi calculada de acordo com a equação 2:

% Remoção = $(C_o – C_e) / C_o$ x 100   (2)

Efeito do pH

O efeito do pH sobre a adsorção foi investigado usando 20 mL da solução dos íons metálicos e 1,0 g do adsorvente, mantido em agitação constante de 150 rpm por um período de 60 min e temperatura de 25 ± 1,0 °C. O pH das soluções foram ajustados no intervalo de 2,0 a 8,0 com soluções de NaOH 0,1 mol L^{-1} ou HNO$_3$ 0,1 mol L^{-1}. Após o tempo de contato, as soluções foram filtradas e os metais determinados por absorção atômica. Brancos, sem adição das argilas, foram utilizados para o controle da concentração inicial dos metais e os experimentos foram executados em duplicata.

Isotermas de adsorção

Para obtenção das isotermas de adsorção foi utilizado uma massa de 1,0 g da argila, 20 mL das soluções dos metais nas seguintes concentrações: 20, 40, 60, 80, 100, 120 e 140 mg L^{-1} e agitação de 150 rpm durante 60 min a temperatura de 25 ± 1,0 °C. Em seguida as amostras foram filtradas e os metais determinados por absorção atômica. Brancos, em cada uma das concentrações e sem adição das argilas, foram utilizados para o controle da concentração inicial dos metais. Os experimentos foram executados em duplicata.

3. RESULTADOS E DISCUSSÃO

Efeito do tempo de contato

O efeito do tempo de contato sobre a adsorção do Cd (II), Cu (II) e Pb (II) foi investigado no intervalo de tempo de 20 a 240 min. A Figura 1 mostra a variação da adsorção nas argilas AC e AM, dos íons metálicos de uma solução aquosa contendo 20 mg L^{-1} de cada íon, sob agitação de 150 rpm e mantidas a uma temperatura constante de 25 ± 1 °C. Os resultados evidenciam claramente que a adsorção é um processo dependente do tempo, com uma remoção inicial muito rápida e com o equilíbrio sendo atingido

em poucos minutos. A velocidade e capacidade de adsorção dependem dos íons metálicos que são transportados da fase liquida e das características do adsorvente. Na argila AC o equilíbrio foi atingido num tempo de 60 min e a capacidade máxima de adsorção foi de 86,0% para Pb (II), 43,2% para Cd (II) e 34,2% para o Cu (II). Enquanto na argila AM a capacidade máxima de adsorção foi obtida em 30 min com remoção de 99,5% para Pb (II) e Cu (II), e de 93,4% para Cd (II).

Como esperado, a argila caulinítica (AC) mostrou-se muito menos reativa do que a argila montmorilonítica (AM), pois a adsorção está restrita a superfície externa, enquanto na montmorilonita a adsorção pode se dá tanto na superfície externa quanto na intercamada, devido à carga negativa gerada pela substituição isomórfica [11]. A cinética da troca catiônica é rápida e cátions como K^+, Ca^{2+} e Mg^{2+}, que existem em quantidade elevada na argila AM, são facilmente trocáveis pelos íons metálicos da solução [11, 18].
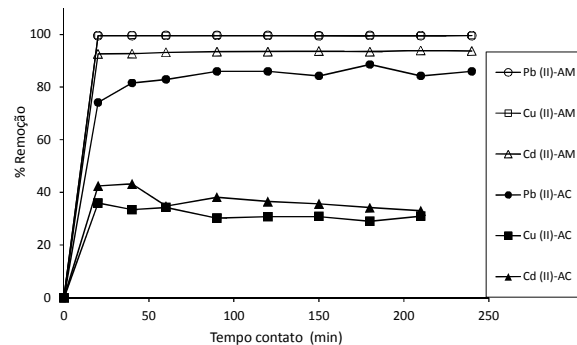
Figura 1. Efeito do tempo de contato sobre a adsorção de Pb (II), Cd (II) e Cu (II) em argila caulinita (AC) e argila contendo montmorilonita (AM). Concentração inicial: 20 mg L^{-1}; pH da solução: 5,2 ± 0,2; velocidade de agitação: 150 rpm e temperatura 25 ± 1 °C.

Efeito do pH

A influência do pH sobre a adsorção do Pb (II), Cu (II) e Cd (II), nas argilas AC e AM foi avaliada no intervalo de pH de 2,0 a 8,0. Os resultados obtidos são apresentados na Figura 2. Para a argila AC o efeito é fortemente evidenciado para os três metais, com uma variação na percentagem de adsorção de 46,6 a 99,9% para Pb (II), de 6,1 a 82,9% para Cd (II) e de 4,6 a 97,9% para Cu (II), entre pH 2,0 a 7,0. Esses resultados são similares aos observados na literatura, para a remoção desses

159

Orbital: Electron. J. Chem. 5 (3):157-163, 2013

mesmos metais, usando argila caulinita natural [17]. Para a argila AM não se observou, para os três metais, uma mudança na quantidade do metal adsorvido com a variação do pH da solução.
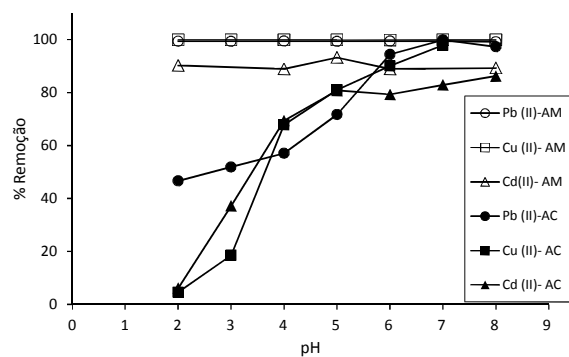
**Figura 2**. Efeito do pH sobre a adsorção de Pb (II), Cd (II) e Cu (II) em argila caulinita (AC) e argila contendo montmorilonita (AM). Concentração inicial: 20 mg L^{-1}; tempo de contato: 60 min; velocidade de agitação: 150 rpm e temperatura ambiente 25 ± 1 °C.

A literatura em geral, tem registrado uma adsorção crescente desses metais, com o aumento do pH da solução [10, 11, 17, 22]. Esses aumentos de adsorção são variáveis em função do tipo da argila utilizada. A caulinita tem mostrado variações maiores devido a baixa remoção em meio muito ácido (pH 2 - 3) e uma remoção superior a 80% acima de pH 6. Para a montmorilonita tem sido obtido no intervalo de pH de 2 a 7, pequenas variações, como cerca de 10% para o Cd (II) até variações em torno de 60% para o Cu (II) [10, 22].

O processo de adsorção em argilas pode ser controlado por dois mecanismos: (1) Troca catiônica nas intercamadas (ex. $2 XNa + M^{2+} = X_2M + 2 Na^+$) e (2) através da reação de complexação na superfície externa, pelos grupos SiO- e AlO- (ex. $SOH + M^{2+} = SOM + H^+$) [10, 23, 24]. A troca catiônica é independente do pH, já a adsorção através dos grupos SiO- e AlO- decresce com o decréscimo do pH, pois em pH baixo esses grupos estão mais protonados e menos disponíveis para remoção dos metais. Na caulinita a adsorção está restrita a complexação na superfície externa, enquanto na motmorilonita a adsorção se dá através dos dois mecanismos e de acordo com Barbier et al. [24] a densidade dos sítios de troca catiônica é muito mais importante que a densidade dos grupos hidroxila da superfície. Eles ainda afirmam que os sítios do aluminol são mais reativos que os sítios do silanol. É provável, portanto que na argila AM aqui estudada, o mecanismo de troca catiônica seja o mecanismo dominante na

remoção do Pb (II), Cd (II) e Cu (II), e por isso não se observa uma variação da adsorção com o pH da solução. Esse comportamento pode estar relacionado ao fato da argila AM conter uma grande quantidade de cátions trocáveis (K^+, Ca^{2+} e Mg^{2+}) e uma elevada relação SiO_2/Al_2O_3 (4,11), maximizando a contribuição da troca catiônica no processo de adsorção, em relação a participação dos grupos silanol e aluminol, devido a menor presença do grupo aluminol, mais reativo. Sprynskyy et al. [25] encontraram como principal mecanismo, na remoção catiônica por zeólitas e argilas minerais, a troca iônica com cátions trocáveis tipo Ca^{2+}, Mg^{2+}, K^+ e Na^+.

Isotermas de adsorção

Usualmente o equilíbrio entre a concentração dos íons metálicos na solução e na fase sólida é descrito por uma isoterma, cujos parâmetros da equação expressam as propriedades da superfície e a afinidade do adsorvente. Os modelos mais utilizados para gerar as isotermas de adsorção são o de Langmuir e o de Freundlich.

O modelo de Langmuir assume que a adsorção ocorre numa superfície homogênea, na forma de uma monocamada cobrindo a superfície do adsorvente. Admite ainda que o adsorvente tem um número finito e idêntico de sítios ativos e que não existe nenhuma interação entre as espécies adsorvidas [26-28]. O modelo de Freundlich é aplicado à adsorção sobre uma superfície heterogênea que suporta sítios com afinidades variáveis [29].

As equações de Langmuir (3) e Freundlich (4) na forma linear podem ser escritas como:

$$C_e / Q_e = 1 / (Q_o \, b) + C_e / Q_0 \qquad (3)$$

$$\log Q_{\neg e} = \log Kf + (1/ n) \log C_e \qquad (4)$$

onde Q_e é a quantidade adsorvida por massa do adsorvente (mg g^{-1}), Ce a concentração do íon metálico no equilíbrio (mg L^{-1}), Qo a capacidade máxima de adsorção e b constante de equilíbrio relacionada a energia de adsorção. Kf e n são constantes indicadoras da capacidade de adsorção e intensidade de adsorção respectivamente. Valores de n superiores a 1 indicam uma adsorção favorável, por outro lado, quanto mais heterogêneos o sistema, mais n se aproxima de zero [30].

Os dois modelos foram aplicados aos dados obtidos para a adsorção de Pb (II), Cd (II) e Cu (II),

160

Orbital: Electron. J. Chem. 5 (3):157-163, 2013

nas argilas AC e AM. As Figuras 3 e 4 mostram as isotermas lineares e os parâmetros de adsorção, calculados usando o método dos mínimos quadrados, estão apresentados na Tabela 2. Os dados experimentais ajustaram-se bem aos dois modelos, contudo um melhor ajuste foi alcançado para isoterma de Langmuir, o que resultou em coeficientes de correlação mais elevadas tanto para a argila AC como para AM. A capacidade de adsorção de Langmuir em monocamada (Q_o) variou de 0, 42 a 1,51 mg g^{-1} para AC e de 1,48 a 6,98 mg g^{-1} para AM, enquanto a

capacidade de adsorção de Freundlich mostrou uma variação de 0,16 a 0,33 mg g^{-1} para AC e de 0,41 a 4,93 mg g^{-1} para AM, confirmando, portanto a maior capacidade de adsorção da argila AM. A montmorilonita (AM) tem uma maior densidade de carga superficial, devido às substituições isomórficas nas folhas tetraédricas e octaédricas, enquanto na caulinita (AC) essas substituições são muito menores, por isso essa a grande diferença de capacidade de adsorção entre as duas argilas [31].
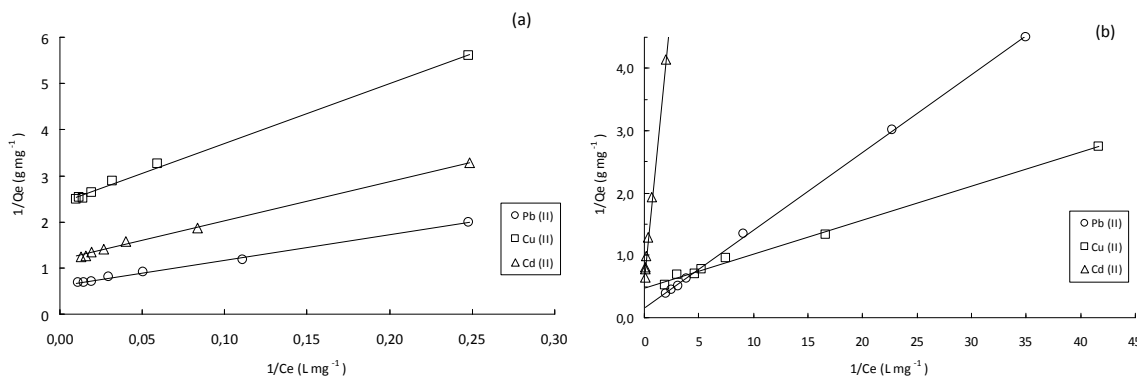
Figura 3: Isoterma linear de Langmuir para a adsorção de Pb (II), Cd (II) e Cu (II) em argila caulinita (a) e argila contendo montmorilonita (b). Concentração inicial: 20 a 140 mg L^{-1}; pH da solução: 5,2 ± 0,2; tempo de contato: 60 min; velocidade de agitação: 150 rpm e temperatura de 25 ± 1 ^{o}C.
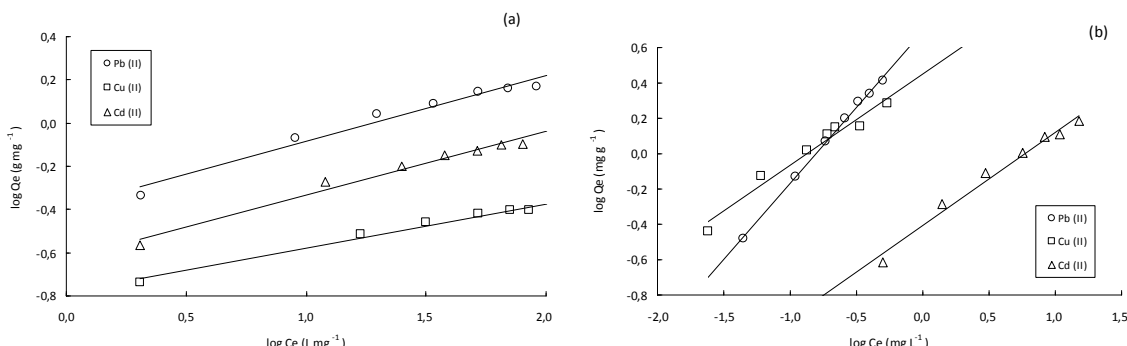
Figura 4: Isoterma linear de Freundlich para a adsorção de Pb (II), Cd (II) e Cu (II) em argila caulinita (a) e argila contendo montmorilonita (b). Concentração inicial: 20 a 140 mg L^{-1}; pH da solução: 5,2 ± 0,2; tempo de contato: 60 min; velocidade de agitação: 150 rpm e temperatura de 25 ± 1 ^{o}C.

Tabela 2: Parâmetros das isotermas de adsorção, usando o modelo de Langmuir e Feundlich, para Pb (II), Cd (II) e Cu (II). AC: argila caulinita; AM: argila contendo montmorilonita.

Argila	Íon	Langmuir			Freundlich		
		Q_o (mg g^{-1})	b (L mg^{-1})	R^2	K_f (mg g^{-1})	n	R^2
	Pb(II)	1,51	0,157	0,998	0,33	2,78	0,924
AC	Cd(II)	0,85	0,138	0,998	0,22	1,78	0,951
	Cu(II)	0,42	0,184	0,995	0,16	4,66	0,949
	Pb(II)	6,98	1,126	0,999	4,93	1,16	0,998
AM	Cd(II)	1,48	0,435	0,993	0,41	1,95	0,987
	Cu(II)	2,07	8,924	0,996	2,83	1,94	0,966

161

Orbital: Electron. J. Chem. 5 (3):157-163, 2013

Os valores dos fatores de separação ($R_L = 1/(1+bC_o)$), calculados a partir das constantes b (0,065 – 0,643 para AC e 0,007 – 0,155 para AM), juntamente com os valores de n suportam um processo de adsorção favorável (n>1 e 0<RL<1) para os íons metálicos nas duas argilas.

Em resumo, os valores dos parâmetros computados a partir das isotermas de adsorção, indicam que as duas argilas satisfazem as condições para serem usadas como adsorventes para Pb (II), Cd (II) e Cu (II).

4. CONCLUSÕES

Os resultados mostraram que as argilas podem ser usadas para remover Pb (II), Cd (II) e Cu (II) de soluções aquosas. Para a argila caulinítica (AC) a adsorção aumentou com o pH e uma remoção máxima de 99,9% para Pb (II), 82,9% para Cd (II) e 97,9% para Cu (II), foram obtidas em pH 7,0. Para argila contendo montmorilonita (AM) não se observou efeito significativo do pH sobre adsorção, obtendo-se uma remoção máxima foi de 99,4% para Pb (II), 93,2% para Cd (II) e 99,9% para Cu (II). Esse comportamento pode estar relacionado ao fato da argila AM conter uma grande quantidade de cátions trocáveis (K^+, Ca^{2+} e Mg^{2+}) e uma elevada relação SiO_2/Al_2O_3 (4,11), maximizando a contribuição da troca catiônica no processo de adsorção. Os dados experimentais ajustaram-se bem aos modelos de Langmuir e Freundlich, mas o melhor ajuste foi alcançado com a isoterma de Langmuir, evidenciando que o processo de adsorção ocorreu preferencialmente em monocamada. Os coeficientes de adsorção indicaram um processo de adsorção favorável para as duas argilas. Como esperado, a capacidade de adsorção da argila AM foi muito maior que a da AC para todos os três íons metálicos.

5. AGRADECIMENTOS

6. REFERÊNCIAS E NOTAS

[1]   Drever, J. I. The geochemistry of natural waters: surface and groundwater environments. New Jersy: Prentice-Hall, 1997.

[2]   Fu, F.; Wang, Q. *J. Environ. Manage* **2011**, *92*, 407. [CrossRef][PubMed]

[3]   Singh, D. K.; Lal, J. *Pollut. Res.* **1992**, *11*, 37.

[4]   Bailey, S. E.; Olin, T. J.; Bricka, R. M.; Adrian, D. D. *Water Res.* **1999**, *33*, 2469. [CrossRef]

[5]   Babel, S.; Kurniawan, T. A. *J. Hazard. Mater.* **2003**, *97*, 219. [CrossRef]

[6]   Wang, Y.H.; Lin, S.H.; Juang, R. S. *J. Hazard. Mater.* **2003**, *102*, 291. [CrossRef]

[7]   Alvarez-Ayuso, E.; Nugteren, H. W. *Water Res.* **2005**, *39*, 2535. [CrossRef][PubMed]

[8]   Sljivic, M.; Smiciklas, I.; Pejanovic, S.; Plecas, I. *Appl. Clay Sci.* **2009**, *43*, 33. [CrossRef]

[9]   Adebowale, K. O.; Unuabonah, I. E.; Olu-Owolabi, B. I. *J. Hazard. Mater.* **2006**, *134*, 130. [CrossRef][PubMed]

[10] Abollino, O.; Giacomino, A.; Malandrino, M.; Mentasti, E. *Appl. Clay Sci.* **2008**, *38*, 227. [CrossRef]

[11] Bhattacharyya, K. G.; Gupta, S. S. *Adv. Colloid Interface Sci.* **2008**, *140*, 114. [CrossRef][PubMed]

[12] Malandrino, M.; Abollino, O.; Giacomino, A.; Aceto, M.; Mentasti, E. *J. Colloid Interface Sci.* **2006**, *299*, 537.

[13] Spark, K. M.; Wells, J. D.; Johnson, B. B. *Eur. J. Soil Sci.* **1995**, *46*, 633. [CrossRef]

[14] Aguiar, M. R. M. P.; Novaes, A. C. *Quim. Nova* **2002**, *25*, 1145. [CrossRef]

[15] Yavuz, O.; Altunkaynak, Y.; Guzel, F., *Water Res.* **2003**, *37*, 948. [CrossRef]

[16] Jiang, M.; Wang, Q.; Jin, X.; Chen, Z. *J. Hazard. Mater.* **2009**, *170*, 332. [CrossRef][PubMed]

[17] Jiang, M.; Jin, X.; Lu, X.; Chen, Z. D*esalination* **1010**, *252*, 33.

[18] Elzing, E. J.; Sparks, D. J. *J. Colloid Interface Sci.* **1999**, *213*, 506.

[19] Prado, C. M. O.; Caracterização Química e Mineralógica das Argilas Utilizadas na Produção de Cerâmica Vermelha no Estado de Sergipe. [Dissertação de Mestrado.], São Cristovão, Brazil: Núcleo de Pós-Graduação em Química, Universidade Federal de Sergipe, 2011. [Link]

[20] Sdiri, A.; Higashi, T.; Hatta, T.; Jamoussi, F.; Tase, N. *Environ. Earth Sci.* **2010**, *61*, 1275. [CrossRef]

[21] Sdiri, A.; Higashi, T.; Hatta, T.; Jamoussi, F.; Tase, N. *Chem. Eng. J.* **2011**, *172*, 37. [CrossRef]

[22] Grupta, S. S.; Bhattacharyya, K. G. *J. Hazard. Mater.* **2006**, *128*, 247. [CrossRef][PubMed]

[23] Kraepiel, A. M. L.; Keller, K.; Morel, F. M. M. *J. Colloid Interface Sci.* **1999**, *210*, 43.

162

Orbital: Electron. J. Chem. 5 (3):157-163, 2013

[24] Barbier, F.; Duc, G.; Petit-Ramel, M. *Colloids and Surfaces A: Physicochem. Eng. Aspects* **2000**, *166*, 153. [CrossRef]

[25] Sprynskyy, M.; Buszewski, B.; Terzyk, A.P.Namiesnik, J. *J. Colloid Interface Sci.* **2006**, *304*, 21. [CrossRef][PubMed]

[26] Ozkzya, B. *J. Hazard. Mater*. **2006**, *129*, 158. [CrossRef][PubMed]

[27] Rodrigues, L. A.; Silva, M. L. C. P. *Quim. Nova* **2009**, *32*, 1206. [CrossRef]

[28] Carvalho, T. E. M.; Fungaro, D. A.; Izidoro, J. C. *Quim. Nova* **2010**, *33*, 358. [CrossRef]

[29] Oubagaranadin, J. U. K.; Murthy, Z. V. P. *Appl. Clay Sci.* **2010**, *50*, 409. [CrossRef]

[30] Asci, Y; Nurbas, M.; Acikel, Y. S. *J. Hazard. Mater*. **2008**, *154*, 663. [CrossRef][PubMed]

[31] Chantawong, V.; Harvey, N. W.; Bashking, V. N. *Water Air Soil Pollut.* **2003**, *148*, 111. [CrossRef]

163

Orbital: Electron. J. Chem. 5 (3):157-163, 2013

Full Paper

Pseudo-Stem Banana Fibers: Characterization and Chromium Removal

Helena Becker*, Regiane F. de Matos, Joseane A. de Souza, Daniel de A. Lima, Francisco Thiago C. de Souza and Elisane Longhinotti*

Departamento de Química Analítica e Físico-Química, Centro de Ciências, Universidade Federal do Ceará - Fortaleza – CE - Brazil, CEP 60.455-760.

Abstract: In this work, pseudo-stems of the banana tree were collected, characterized and used as adsorbent materials for the removal of the chromium ions from aqueous solution. The characterization of pseudo-stems by FTIR suggests the presence of cellulose, hemicellulose and lignin. The predominant groups were carbonyls (0.312 ± 0.010 mmol g^{-1} adsorbent), phenols (0.237 ± 0.021 mmol g^{-1} adsorbent), lactones (0.041 ± 0.003 mmol g^{-1} adsorbent) and basic groups (0.096 ± 0.006 mmol g^{-1} adsorbent). The textural propriety of the adsorbent, surface area, pore volume and pore diameter were found to be 0.383 $m^2 g^{-1}$, 0.003525 $cm^3 g^{-1}$ and 368.3 Å, respectively. The pHpzc value was found 7.5 and so the adsorption assays of chromium removal from solution were more efficiently at acidic pH values. The experiments show that approximately 95% and 78% of the Cr (VI) was removed from solution by untreated and treated fiber, respectively, in 300 minutes of the contact time.

Keywords: pseudo-stem banana fibers; agricultural by-products; removal; chromium

1. INTRODUCTION

The banana occupies second place in terms of volume of fruit produced and consumed in Brazil. The banana tree belongs to the family Musaceae, and is a native of the south of Asia and Indonesia. The Brazilian production of bananas is distributed across the entire national territory, with the Northeast being the largest producer (34%). The area planted in Brazil is about 520.000 ha, where the state of Ceará participates with about 42.767 ha. Banana plantations are a permanent cultivation because banana trees produce new shoots. The pseudo-stem is the part of the banana tree that rises from the ground to the fruit, and after the crop is harvested, the pseudo-stem becomes an agricultural by-product. Shah [1] stated that each hectare of banana plantation generates approximately 220 tons of garbage, which is discarded by the farmers into the rivers, lakes and on highways, causing a serious environmental problem. The pseudo-stem of banana trees is most often utilized in the building industry. Agricultural by-products are usually composed of lignin and cellulose, and other functional groups, including carboxylic acids, phenols, carbonyls and ethers. The presence of these functional groups, together with the low-cost, makes agricultural by-products very interesting as adsorbents for the removal of metal ions and dyes from wastewater [2-4].

The presence of potentially toxic substances in natural reservoirs has very large repercussions in the economy and on public health. Environmental control laws, reflecting a tendency to preserve and protect the environment, have been requiring more rigorous limits of water contamination in domestic or industrial waste. The conditions and patterns of effluent release in Brazil are regulated by the Environment National Council [5], which specifies the maximum values allowed for Cr (III) and Cr (VI) species as 0.5 and 0.05 mg L^{-1}, respectively. This fact has prompted several research groups to search for efficient alternatives for the treatment of liquid effluents containing toxic metals. Low cost natural organic materials have often been suggested as alternative adsorbents for the removal of metals from

---

*Corresponding author. E-mail: becker@ufc.br (H. Becker) and elisane@ufc.br (E. Longhinotti). Tel.: +55 85 33669964, Fax: +55 85 33669982.

liquid effluents [2, 6]. Some researchers already reported its potentiality of the banana fiber as biosorbents [7-10]. Thereby, this work is aimed at the characterization and use of pseudo-stem banana fibers as adsorbents for the removal of Cr from aqueous solutions.

2. MATERIAL AND METHODS

Characterization of pseudo-stem banana fibers

The pseudo-stem banana fiber samples (Musaceae) were collected from the Northeast area of Ceará State (Baturité). After the sap was extracted, the fiber was washed with distilled water, dried for 48 h, triturated and sifted through 2-mm sieves (untreated fiber). A pre-treating of the biosorbent (treated fiber) was realized using 1.0 mg L^{-1} HCl solution, were 10.0 g of banana fibers were mixed with 100 mL of acid solution and agitated for 24 h. The biosorbent was washed thoroughly with distilled water until the pH reached nearly neutral, and then the material was dried at 60oC for 48 h.

The textural characterization of the untreated fibers was obtained by N_2 adsorption/desorption isotherms at 77 K using an Automated Physisorption Instrument (Autosorb-MP, Quantachrome Instruments). Prior to measurement, the samples were outgassed in a vacuum at 623 K for 2 h. Specific surface areas were calculated according to the Brunauer–Emmett–Teller (BET) method, and the pore size distribution was obtained according to the Barret–Joyner–Halenda (BJH) method from the adsorption data. The organic materials and ash content were determined by calcination of 1.0 g of the fiber at 500 ^{o}C and incineration at 900 ^{o}C.

Acidic or basic functional groups of the banana fibers were determined via the Boehm method [11, 12]. A volume of 20.0 mL of solution was added to vials containing 0.20 g of fiber sample and agitated for 24 h. Then, the samples were filtered and the excess acid or base was determined by titration with NaOH or HCl solutions. Five blank samples were also prepared in the same way.

The pH of the point of zero charge (pHpzc) was determined as previously described [7]. $NaNO_3$ (0.01 mg L^{-1}) solutions of pH 3, 6 and 11 were prepared using NaOH or HCl. Several amounts of untreated banana fibers (0.07, 0.1, 0.5, 0.7, 1, 3, 5, and 7%) were added to 100 mL of solution of different initial pH values, and the equilibrium pH

was measured after 24 h of agitation (100 rpm) at 25 $\pm$ 2 ^{o}C.

The analysis of metals in the composition of the untreated fiber samples was determined using Inductively Coupled Plasma Spectroscopy (ICP–OES by PERKIN ELMER model 4000). The dried fiber was solubilized in 2:1 HNO_3 and H_2O_2 in a digestor block for 4 h at 140 ºC.

The structure of the banana fibers was studied by Fourier Transform Infrared (FTIR) spectroscopy. FTIR spectra were recorded with a FTIR SPECTRUM 1000 spectrometer in the range of 4000–400 cm^{-1} with a resolution of 2 cm^{-1}. The analyses were performed on KBr pellets containing 1.0 wt.% of the sample. Elemental analysis for CHN and S was performed in an elementary analyzer CARLO ERBA.

Thermogravimetric analysis was performed to obtain more information about the fiber sample. The analysis was performed with a SHIMADZU thermoanalysis system (DSC-50 differential exploratory calorimetry system and a TGA-50 thermobalance) using 5.0 mg of sample with a heating rate of 10 °C min^{-1} under nitrogen flow of 50 mL min^{-1}.

The morphology and average diameter of the fibers were examined via scanning electron microscopy, obtained with a SERIES scanning microscope, model Philips XL30, operating at an accelerating voltage of 15 kV.

Adsorption Assays

Solutions were prepared in deionized water (milli-Q) with analytical grade reagents. All of the experiments were performed in triplicate with slow agitation at 25 $\pm$ 2 ^{o}C. The adsorption tests were performed using $K_2Cr_2O_7$ as the adsorbate. The concentration of the Cr (VI) ions in solution, after adsorptions tests, was determined by absorption spectrophotometry with 1,5-diphenylcarbazide as complexing agent [13]. The analysis were performed in a UV-Vis spectrophotometer (VARIAN model 1E) using a 1 cm cell at 540 nm. Each trial was performed in triplicate. The total Cr after the adsorption test was determined with the ICP–OES. The reduced Cr (III) was calculated by the difference between the Cr (total) and Cr (VI) in the solution.

The effect of pH on chromium removal was studied using 100 mL of a 10 mg L^{-1} $K_2Cr_2O_7$ solution and 1.0 g of the untreated banana fibers, by

165

Orbital: Electron. J. Chem. 5 (3):164-170, 2013

300 minutes. Different volumes of acid (0.1 mol L^{-1} HCl) or alkali (0.1 mol L^{-1} NaOH) were added to adjust the pH of the mixture. The final concentration of Cr (VI) and Cr (total) were examined with the same methods the above said.

The influence of contact time on the adsorption process was evaluated in 250 mL Erlenmeyer flasks containing 100 mL of HCl (0.01 mg L^{-1} solution) at a fixed banana fiber mass (1.0 g), and dichromate ion concentration (50 mg L^{-1}). Aliquots of the solution were removed at fixed time by 300 minutes. The adsorption assays were realized with untreated and treated banana fiber.

Figure 1. SEM image showing surface morphologies of the pseudo-stem banana fibers.

3. RESULTS AND DISCUSSION

Pseudo-stem banana fiber characterization

Table 1 lists the physic-chemical characteristics of the pseudo-stem banana fibers. The surface morphology and bulk structure of the pseudo-stem fibers were studied with SEM and adsorption isotherms (not shown). The SEM images of the fiber surface, Figure 1, show a dense interfibrillar structure, similar to coconut [14-16].

Low porosity was observed in the SEM analysis of the untreated fibers. According to results obtained by adsorption isotherms, the surface area, pore volume and pore diameter of the pseudo-stem fibers were 0.383 m^2 g^{-1}, 0.003525 cm^3 g^{-1} and 368.3 Å, respectively. These surface properties can be considered to be a factor providing an increase in the total surface area. In addition, the pore structures of the fibers could reduce the diffusional resistance and facilitate mass transfer because of their high internal surface area.

Table 1 . Characterization chemistry and physic of the pseudo-stem banana fibers.

Pore volume	0.003525 $cm^3.g^{-1}$
Pore diameter	368.3 Å
Surface area (BET)	0.3828 $m^2.g^{-1}$
Organic material	88.0 ± 0,4 (wt%)
H	6.25 ± 0.08 (wt %)
C	45.9 ± 0.2 (wt %)
N	0.18 ± 0.01 (wt %)
O	47.6 ± 0.4 (wt %)
Ash	4.65 ± 0.11(wt %)
Carbonyl groups	0.312 ± 0.010 mmol. g^{-1}adsorbent
Phenolyc groups	0.237 ± 0.021 mmol. g^{-1}adsorbent
Lactonic groups	0.041 ± 0.003 mmol. g^{-1}adsorbent
Basic groups	0.096 ± 0.006 mmol. g^{-1}adsorbent
Metals	*(mg Kg^{-1})*
Ca	3928 ± 236
Mg	2287 ± 106
Fe	84.0 ± 6.9
Na	73.3 ± 5.1
K	23267 ± 465

Figure 2 shows the FTIR spectra of the untreated pseudo-stem banana fibers. The absorptions bands at 3600-3100 cm^{-1} can be assigned to stretching vibrations and other polymeric associations of hydroxyl groups. Symmetric stretching at 2913 cm^{-1} assigned to the CH_2 groups present in polysaccharides. Angular deformations of C–H linkages of aromatic groups were observed at 858,

761, 668 and 576 cm^{-1}. An overlapping of peaks was observed between 1654–1327 cm^{-1} and 1244–1026 cm^{-1} due to C–C, C=C, OH, CO, CH_n, CH, and C–O–C vibrations. These are generally observed in cellulose, hemicellulose and lignin, suggesting an aromatic and ethereal character of the sample. The results indicate a similarity with the composition of banana fibers of another species [17], and are

166

Orbital: Electron. J. Chem. 5 (3):164-170, 2013

important because they demonstrate that the pseudo-stem banana fibers contain functional groups that allow interactions between metallic ions and the biosorbent. The FTIR spectra for the treated fibers (not shown) didn't present significant changes, suggesting a small reduction of organic compounds of the adsorbent.
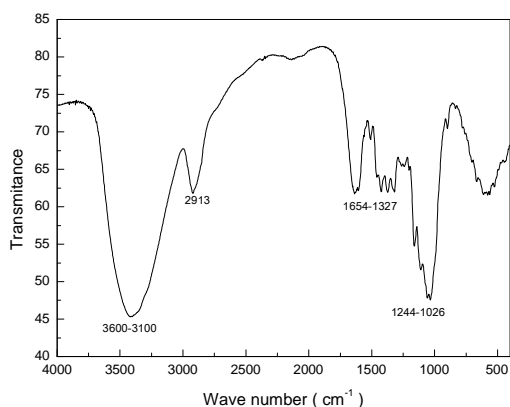

Figure 2. FTIR spectrum of pseudo-stem banana fibers.

The analysis for metals in the pseudo-stem fibers of the banana tree, Table 1, showed larger potassium and calcium concentrations in relation to other metals. This low concentration of metals should favor the use of this material in adsorption processes. The elemental analysis results to the untreated pseudo-stem banana fibers (Table 1) are similar to other materials containing cellulose, hemicellulose and lignin [17]. The functional groups at the surface of the pseudo-stem banana fibers were predominantly carbonyls (0.312 ± 0.010 mmol g^{-1} adsorbent), phenols (0.237 ± 0.021 mmol g^{-1} adsorbent), lactones (0.041 ± 0.003 mmol g^{-1} adsorbent) and basic groups (0.096 ± 0.006 mmol g^{-1} adsorbent). The pHpzc value determined for pseudo-stem banana fibers was found to be between 7.15 and 7.7, as shown in Figure 3. It was observed that the data also converges on a pHpzc value of approximately 7.5. This result is interesting for the use of pseudo-stem banana fibers acting as biosorbents, since at pH values above 7.5, negative charges prevail on the surface, and the adsorption of cationic species should be favored. In contrast, the adsorption of anionic species would be favored at pH values below the pHpzc, since the surface would present an excess of positively charged functional groups.

The thermal analysis of the pseudo-stem banana fibers (Figure 4) showed good thermal stability, even at about 200 °C, with degradation process in two stages with different mass rate losses.
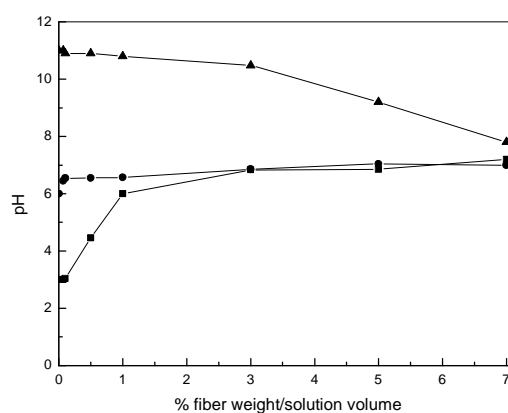
Figure 3. Experimental curves for PZC determination. Initial pH: (■) 3.0; (●) 6.0 and (▲) 11.0. The solid line is only illustrative, not representing the adjustment of data.
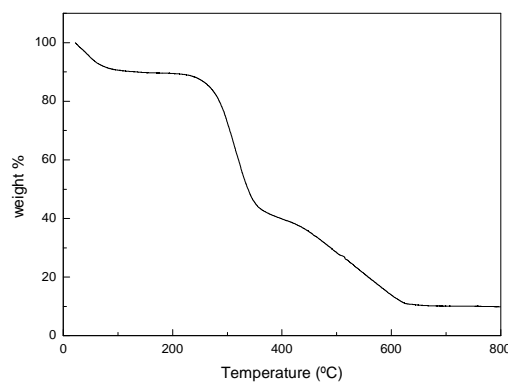
Figure 4. Thermogravimetric curve for pseudo-stem banana fibers using 5.0 mg of sample with a heating rate of 10 °C min^{-1} under a nitrogen flow of 50 mL min^{-1}.

The first stage of mass loss, between 30 °C and 100 °C (11% mass variation), with a maximum rate of elimination at around 100 °C, was associated with the dehydration of surface water molecules. This process was an endothermic event according to DSC (not shown). Thereafter, water could be removed by drying the samples at 150 °C. At the second stage, ranging from 200 to 400 °C, a larger mass loss was observed of approximately 55%, which can be attributed to hemicelluloses decomposition, breakdown of cellulose linkages, and volatile substance release. This stage was an exothermic event according to the DSC (not shown). The thermal behavior of the pseudo-stem banana fibers is similar to that of the natural fibers used by industry [17-19]. Therefore, pseudo-stem banana fibers are a promising material for use in the industrial sector and in the development of new biomass-derived materials.

Adsorption Assays

167

Orbital: Electron. J. Chem. 5 (3):164-170, 2013

The literature report different anionic species to Cr (VI) ions in aqueous solution, depending on the pH value [20-23]. A simplified equilibrium equation is represented as follows [22]:

$$HCr_2O_7^-{}_{(aq.)} \xrightleftharpoons[pH<1]{pH>1} Cr_2O_7^{2-}{}_{(aq.)} \xrightleftharpoons[pH<7]{pH>7} CrO_2^{2-}{}_{(aq.)}$$
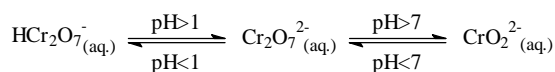
The organic matter present in environmental samples it can promote chromium (VI) reduction during analysis, which takes place preferably in acidic solution. Thereby the mechanism of hexavalent chromium biosorption it cannot be considered as a simple adsorption process of anionic Cr (VI) onto cationic functional groups of the adsorbent.

In this work, the experiments of hexavalent chromium adsorption by banana fibers treated and untreated were carried evaluated using 50 mg L^{-1} of dichromate solution and a temperature of 25 ^{0}C. The experiments to removal chromium ions from the solution, have been accomplish in pH values 2.0, because in low pH value the Cr (VI) ions are removed more efficiently from the solution, Figure 5.

The removal of chromium species by untreated and treated banana fibers, for different intervals of time, is presented in Figure 6a and 6b, respectively. The concentration of Cr (VI), Cr (III) an Cr (total) species in solution during the adsorption were monitored for 300 minutes and observed that the hexavalent chromium concentration decrease while the Cr (III) increase for both untreated and treated

biosorbent. As can be observed, with 300 minutes of contact, the concentration of hexavalent chromium in solution becomes undetectable for untreated fiber (Figure 6a), c.a. 95% of the removal (c.a. 27% by adsorption and 68% by reduction). For the treated fiber (Figure 6b), it is observed that, within 300 minutes, c.a. 78% of the Cr (VI) is removed from the solution (c.a. 51% by adsorption and 27% by reduction). This observation can be attributed to the presence of reductive compounds in the untreated adsorbent. In fact, under highly acidic conditions these compounds can be partially removed from the adsorbent, decreasing the amount of the Cr (VI) ions that can be reduced [24].
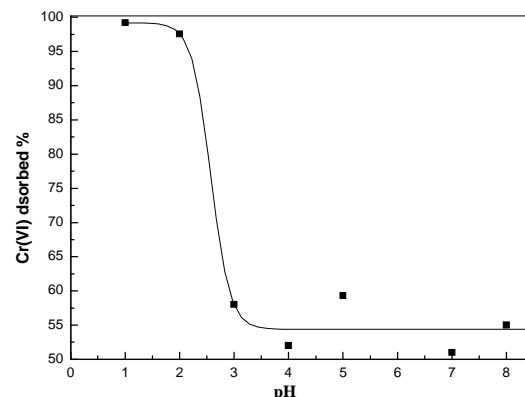
Figure 5. Effect of pH on the adsorption Cr (VI). anionic species by pseudo-stem banana fibers, by 300 min and 25 ^{o}C. The solid line is only illustrative.
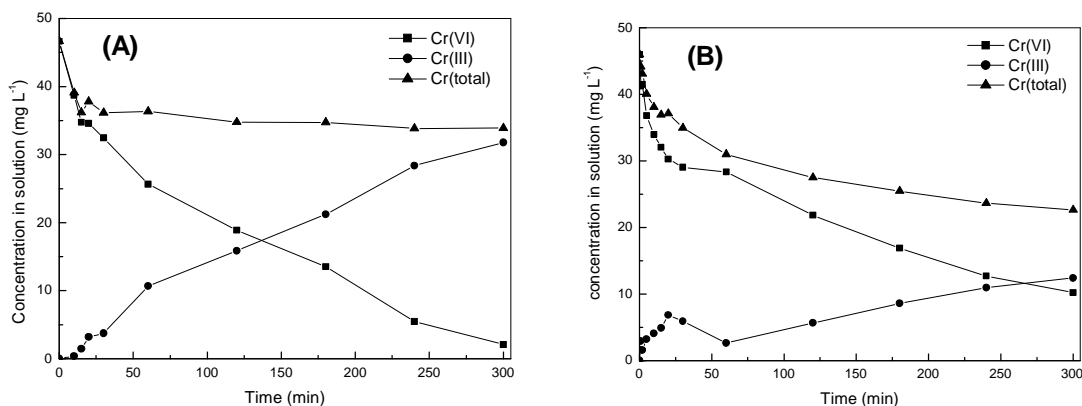
Figure 6. Effect of contact time on removal of the chromium ions by pseudo-stem banana fibers, (A) untreated fiber and (B) treated fiber, at pH 2.0.

The Figure 6 show also that, for the untreated and treated fiber, the trivalent chromium ions reduced remain in solution, evidencing that the Cr (III) ions, under lower pH, is not (or is less) adsorbed by biosorbent. The Figure 7 reinforce the fact of the Cr

(III) species they be not adsorbed for the banana fiber, in any concentrations studied at pH 2.0.

The adsorption of the trivalent chromium has been observed for several biosorbent [25-35]. It is

168

Orbital: Electron. J. Chem. 5 (3):164-170, 2013

reported that the adsorption follows by two processes, initially happen the chemical reduction of the Cr (VI) to Cr (III) followed by the adsorption of the Cr (III) onto adsorbent surface [26]. As our interest, in this work, went to investigate only the potential of the banana fibers front to the of the hexavalent chromium in solution is very more toxic then trivalent chromium, this difference can be justified for the fact of Cr (VI) to penetrate through the cellular membrane with a lot of easiness and to be an agent very strong oxidizer. In spite of that, it is very important to reduce the concentration of the Cr (III) species in solution because in the nature this species can be chemically oxidize to Cr (VI), your more toxic form for man.
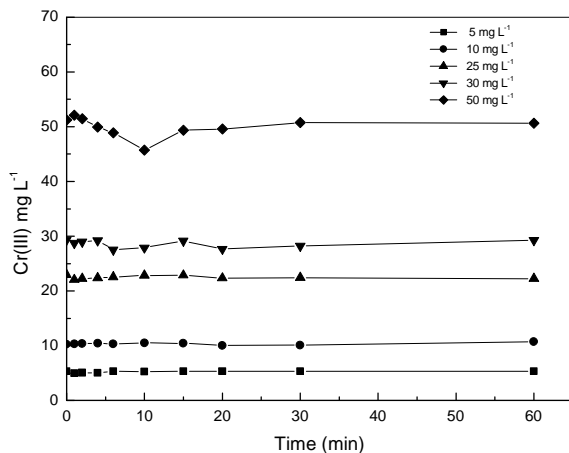
Figure 7. Variation of the Cr (III) concentration in solution at pH 2.0.

4. CONCLUSION

Natural organic materials of low cost have been used as alternative adsorbents for the removal of metals from aqueous solutions. Pseudo-stem banana fibers have been studied with respect to their chemical and textural properties. The remove of the Cr (VI) species by banana fibers was found to be pH dependent, and increased with decreasing pH, reaching a maximum removal at pH 1.00. The untreated adsorbent reduce more efficiently of the hexavalent chromium species then treated fibers and although the banana fibers present low surface area and porosity in relation to other materials, the pseudo-stem banana fibers show promise as a material for the removal of anionic Cr (VI) species from aqueous solution.

5. ACKNOWLLDMENTS

6. REFERENCE AND NOTES

[1] Shah, M. P.; Reddy, G. V.; Banerjee, P.; Babu, P. R.; Kothari, I. L. *Process Biochem.* **2005**, *40*, 445. [CrossRef]

[2] Bailey, S. E.; Olin, T. J.; Bricka, R. M.; Adrian, D. *Water Res.* **1999**, *33*, 2469. [CrossRef]

[3] Demirbas, A. *J. Hazard. Mater.* **2008**, *157*, 220. [CrossRef][PubMed]

[4] Mukhopadhyay, S.; Fangueiro, R., Shivankar, V.; *Text. Res. J.* **2009**, *79*, 387. [CrossRef]

[5] Environment National Council, CONAMA 397, of March 04, 2008.

[6] Fungaro, D. A.; Izidoro J. C.; Almeida, R. S. *Eclét. Quím.* **2005**, *30*, 31.

[7] Hameed, B. H.; Mahmoud, D. K.; Ahmad, A. L. *J. Hazard. Mater.* **2008**, *158*, 499. [CrossRef][PubMed]

[8] Anirudhan, T. S.; Senan, P.; Unnithan, M. R. *Sep. Purif. Technol.* **2007**, *52*, 512. [CrossRef]

[9] Shibi, I. G.; Anirudhan, T. S. *J. Chem. Technol. Biotechnol.* **2006**, *81*, 433. [CrossRef]

[10] Noeline, B. F.; Manohar, D. M.; Anirudhan, T. S. *Sep. Purif. Technol.* **2005**, *45*, 131. [CrossRef]

[11] Valdés, H.; Sánchez-Polo, M.; Rivera-Utrilla, J.; Zaror, C. A. *Langmuir* **2002**, *18*, 2111. [CrossRef]

[12] Oliveira, W. E.; Franca, A. S.; Oliveira, L. S.; Rocha, S. D. *J. Hazard. Mater.* **2008**, *152*, 1073. [CrossRef][PubMed]

[13] Standard Methods for Examination of Water and Wastewater. American Water Work Association (APHA), New York, USA, 2005.

[14] Ishizaki, M. H.; Visconte, L. L. Y.; Furtado, C. R. G.; Leite, M. C. A. M.; Leblanc, J. L. *Polím.: Ciênc. e Tecnol.* **2006**, *16*, 182. [CrossRef]

[15] Bhattacharya, D.; Germinario, L. T.; Winter, W. T. *Carbohydr. Polym.* **2008**, *73*, 371. [CrossRef]

[16] Megiatto Jr., J. D.; Silva, C. G.; Rosa, D. S.; Frollini, E. *Polym. Degrad. Stab*. **2008**, *93*, 1109. [CrossRef]

[17] Bilba, K.; Arsene, M.A.; Ouensanga, A. *Bioresour. Technol.* **2007**, *98*, 58. [CrossRef][PubMed]

[18] Chand, N.; Sood, S.; Singh, D. K.; Rohatgi, P. K. *J. Therm. Anal. Calorim.* **1987**, *32*, 595. [CrossRef]

[19] Varma, D. S.; Varma, M.; Varma, I. K. *Thermochim. Acta* **1986**, *108*, 199. [CrossRef]

[20] Shen-Yang, T.; Ke-An, L.; *Talanta* **1986**, *33*, 775. [CrossRef]

[21] Tandon, R. K.; Crisp, P. T.; Ellis, J. *Talanta* **1984**, *31*, 227. [CrossRef]

[22] Krishna, B. S.; Murty, D. S. R.; Jai Prakash B. S. *J. Colloid Interface Sci.* **2000**, *229*, 230. [CrossRef][PubMed]

[23] Pezzin, S. H.; Rivera, J. F. L.; Collins, C. H.; Collins, K. E. *J. Braz. Chem. Soc.* **2004**, *15*, 58. [CrossRef]

[24] Singh, V.; Kumari, P.; Pandey, S.; Narayan, T. *Bioresour. Technol.* **2009**, *100*, 1977. [CrossRef][PubMed]

[25] Elangovan, R.; Philip L.; Chandraraj, K. *Chem. Eng. J.*

169

Orbital: Electron. J. Chem. 5 (3):164-170, 2013

2008, *141*, 99. [CrossRef]

[26]   Yang, l.; Chen, J. P. *Bioresour. Technol.* **2008**, *99*, 297. [CrossRef][PubMed]

[27]   Elangovan, R.; Philip, L.; Chandraraj, K. *Chem. Eng. J.* **2008**, *141*, 99. [CrossRef]

[28]   Elangovan, R.; Philip, L.; Chandraraj, K. *J. Hazard. Mater.* **2008**, *152*, 100. [CrossRef][PubMed]

[29]   Gao, H.; Liu, Y.; Zeng, G.; Xu, W.; Li, T.; Xia, W. *J. Hazard. Mater.* **2008**, *150*, 446. [CrossRef][PubMed]

[30]   Kumar, P. A.; Ray, M.; Chakraborty, S. *J. Hazard. Mater.* **2007**, *143*, 24. [CrossRef][PubMed]

[31]   Suksabye, P.; Thiravetyan, P.; Nakbanpote, W.; Chayabutra, S. *J. Hazard. Mater.* **2007**, *141*, 637. [CrossRef][PubMed]

[32]   Park, D.; Lim, S. R.; Yun, Y.-S.; Park, J. M. *Chemosphere* **2007**, *70*, 298. [CrossRef][PubMed]

[33]   Chen, G.-Q.; Zeng, G.-M.; Tu, X.; Niu, C.-G.; Huang, G.-H.; Jiang, W. *J. Hazard. Mater.* **2006**, *135*, 249. [CrossRef][PubMed]

[34]   Deng, S.; Ting, Y.P.; Yu, G. *Water Sci. Technol.* **2006**, *54*, 1-8. [CrossRef] [PubMed]

[35]   Deng, S.; Ting, Y. P. *Environ. Sci. Technol.,* **2005**, *39*, 8490. [CrossRef] [PubMed]

170

Orbital: Electron. J. Chem. 5 (3):164-170, 2013

Full Paper

Use of Low-cost Adsorbents to Chlorophenols and Organic Matter Removal of Petrochemical Wastewater

Aretha Moreira de Oliveira[a], Maria Aparecida Liberato Milhome[b], Tecia Vieira Carvalho[c], Rivelino Martins Cavalcante[d] and Ronaldo Ferreira do Nascimento[a]*

[a]*Universidade Federal do Ceará (UFC), Departamento de Química Analítica e Físico-Química, Bl 940. Av. Humberto Monte s/n- Campus do Pici, Fortaleza, CE, CEP 60451-970. Brazil.*
[b]*Fundação Núcleo de Tecnologia Industrial do Ceará - NUTEC, Rua Rômulo Proença s/n, CEP: 60451-970. Fortaleza – CE, Brazil.*
[c]*Parque de Desenvolvimento Tecnológico - PADETEC, Rua do Contorno, S/N Campus do Pici, Bloco 310. CEP: 60455-970. Fortaleza – CE, Brazil.*
[d]*Universidade Federal do Ceará (UFC), Instituto de Ciências do Mar-LABOMAR, Av. Abolição, 3207 – Meireles, CEP: 60165-081 - Fortaleza-CE, Brazil.*

Abstract: The removal of 2,4 diclorophenol (2,4-DCF) and 2,4,6 trichlorophenol (2,4,6 TCF) present in petrochemical wastewater was evaluated using low-cost adsorbents, such as chitin, chitosan and coconut shells. Batch studies showed that the absorption efficiency for 2,4 DCF and 2,4,6 TCF follow the order: chitosan > chitin > coconut shells. Langmuir and Freundlich models have been applied to experimental isotherms data, to better understand the adsorption mechanisms. Petrochemical wastewater treatment with fixed bed column system using chitinous adsorbents showed a removal of COD (75%), TOG (90%) and turbidity (74-89%).

Keywords: chlorophenols; low cost adsorbent; adsorption; chitosan; petrochemical wastewater

1. INTRODUCTION

It very well know that one of the major problems of the petrochemical industry is the great amount of wastewater produced and the high investment needed for the treatment of this effluent before it is released in the environment.

Chlorophenols are organic compounds considered priority pollutants by the American Environmental Protection Agency (USEPA) because of their toxicity and adverse effects that can cause to human health [1]. These compounds are generally present in effluents from pharmaceutical, plastics, pesticides, fertilizers and petroleum refineries [2]. In Brazil, legislations based on CONAMA 430/2011 and SEMACE 154/2002, consider the maximum limit of 0.5 mg.L^{-1} total phenols in wastewater [3].

Despite the efforts that oil refineries have been demonstrating in recent decades for their effluents fit the standards set by legislation are still found significant levels of phenolic compounds in industrial wastewater, which often are not removed by conventional treatment. Several techniques have been evaluated for phenolic compounds removal, such as ozonization [4], advanced oxidation processes [5], solvent extraction [6], membrane [7] and biological treatment [8-9]. However, these processes are not really efficient. An alternative for wastewater treatment is the use of adsorption process, which allows a high efficiency in the removal and recovery of persistent organic pollutants [10]. Activated carbon has been widely applied for phenolic removal, despite some disadvantages such as high costs and difficult regeneration, but the low-cost solid residues from agricultural activities have been applied such as wood and coir [11], sugarcane bagasse [12], chitin (QTI) and chitosan (QTS) [13].

In Brazil, huge amounts of waste are produced by large scale agriculture, mainly sugar cane bagasse and green coconut shell [14-15]. The use of these materials for removal of organic pollutants [16] and metals [17-18] from wastewater can be advantageous

because reduce the environmental impact and to reduce the cost of processing. In addition, special attention has been paid to chitin, a natural polymer extracted from shells of crustaceans such as crab, shrimp and chitosan, a derivative obtained by alkaline deacetylation of chitin [19]. Due to its characteristics of biodegradability, biocompatibility and hydrophobicity of these materials have attracted great interest. Several authors have investigated the efficiency of chitinous materials as adsorbents for removal of organic compounds [20-22], metals [23, 24] and anions [25].

The purpose of this study was to investigate the adsorption features of adsorbents from chitinous and agricultural residues with respect to removal of chlorophenols, chemical oxygen demand (COD), Total oil and grease (TOG), nitrate, ammonia and turbidity from petrochemical wastewater. Results were compared with performances of some adsorbents used in practice.

2. MATERIAL AND METHODS

Reagents and solutions

Chromatographic grade solvents and 2,4 dichlorophenol (2,4 DCP) and 2,4,6-trichlorophenol (2,4,6 TCP) standards with purity > 99% were purchased from Sigma-Aldrich (Brazil). Stock solutions of 2,4-DCP and 2,4,6 TCP (1,000 mg.L^{-1}) were prepared in methanol. Calibration curves of chlorophenols were prepared by diluting the stock solution to concentrations of 5 to 400 mg.L^{-1}.

Effluent samples were obtained from LUBNOR - Lubricants and Petroleum products, located in Fortaleza-Ceará, Brazil. Samples were spiked with concentrations of 2,4 DCP and 2,4,6 TCP ranging from 10 to 300 mg.L-1 for the batch study. The samples were filtered through a membrane (0.45 µm) before being injected into the GC

Adsorbents

Were used as adsorbents green coconut shells obtained from EMBRAPA (60-200 mesh), chitin (white powder, 80 mesh, molecular weight 400,000 g.mol^{-1}, pH 4.28) and chitosan (yellowish powder, 80% grade of deacetylation, 80 mesh particle, molecular weight 174,205 g.mol^{-1}, pH 7.93), obtained from company POLYMER SA (Fortaleza-Ceará, Brazil). Also were studied for a comparison, the commercial adsorbents, activated carbon (100 mesh, Merck), silica (80 -200 Merck), Amberlite (80-100 mesh, Carlo Erba), bentonite (20 mesh, Merck).

Chromatographic analysis

The initial and final concentrations of 2,4-DCP and 2,4,6 TCP were determined by gas chromatography with flame ionization detector (GC-FID), Shimadzu 17A model, using a DB-5 capillary column (30 m x 0.25 mm x 0.32 µm). The chromatographic conditions were: detector and injector temperature 250 ºC, temperature program 60 °C (10 °C.min^{-1}) → 190°C (3 min) → 225 °C (10 °C.min^{-1}) for 5 min. It was used a flow of carrier gas (H$_2$) of 1 mL.min^{-1}, at a injected volume of 1.0 µL and split ratio 1:30

Batch adsorption

In glass vials containing 0.2 g of dry adsorbent were added to 10 mL aliquot of effluent samples, filtered and spiked with known amounts (10-300 mg.L^{-1}) of 2,4 DCP and 2,4,6 TCP. The vials were sealed and placed on the shaker and kept under agitation (150 rpm) at room temperature (28 ± 2 ºC) until it reaches equilibrium. After stirring the residual analyte concentrations were determined by GC-FID system. The adsorption capacity (Q_e) for each compound was calculated by equation 1:

$$Q_e = \frac{(C_o - C_e)V}{m} \qquad \text{Equation 1}$$

Where C_o and C_e are the concentrations (mg.L^{-1}) of solute in the initial solution and equilibrium, V is the volume of solution (L) and m the mass of adsorbent (g).

Study of pH effect was performed with effluent solutions at pH 3.0, 6.5 and 9.0 using the adsorbents such as chitin, chitosan and coconut shell. The pH value was controlled using acetate buffer and ammonia buffer.

The adsorption isotherms were obtained by correlating the parameters of concentration versus equilibrium adsorption. Adsorption isotherms were studied using the Langmuir (Equation 2) and Freundlich models (Equation 3).

Langmuir: $\dfrac{1}{Q} = \dfrac{1}{Q_{max}} + \left(\dfrac{1}{Q_{max}K_L}\right)\left(\dfrac{1}{C_e}\right)$ (Equation 2)

Freundlich: $\log Q = \log K_F + \dfrac{1}{n}\log C_e$ (Equation 3)

172

Orbital: Electron. J. Chem. 5 (3):171-178, 2013

Where Q is the amount of solute adsorbed (mg.g^{-1}), Q_{max} is the maximum adsorption capacity (mg.g^{-1}), K_L is the equilibrium constant of Langmuir isotherm (L.mg^{-1}), C_e is the equilibrium concentration of solute in solution (mg.L^{-1}), 1/n is the Freundlich constant, K_F constant Freundlich adsorption. 1/n and K_F values represent the intensity of adsorption and adsorption capacity of adsorbent.

Different materials such as bentonite, actived carbon, silica and amberlit were evaluated through batch adsorption, for a comparison with the adsorbents studied in this work.

Wastewater treatment in fixed bed

50 mL of effluent contained chlorophenols at pH 7.5 and flow rate of 1.0 to 2.0 mL.min-1 were percolated through the column (20 cm x 4.0 mm ID), packed with 0.2 g of the adsorbent material in stages interspersed with cotton. The column adsorption capacity was determined by measuring the compound concentration in the solution by GC-FID system, before and after passing through the column.

Wastewater samples collected for analysis of ammonia, nitrate, pH, turbidity, conductivity and chemical oxygen demand (COD) were performed at the Laboratory of Environmental Sanitation of the Federal University of Ceara (LABOSAN-UFC) as recommended by the procedures described in Standard Methods for the Examination of Waters and Wastewater (2005) [26]. The determination of oil and grease (TOG) in the wastewater effluent was carried out in the laboratory from company LUBNOR.

3. RESULTS AND DISCUSSION

Batch adsorption

pH effect

The pH effect on the compounds adsorption was studied at pH values of 3.0, 6.5 and 9.0 using the adsorbents chitin (QTI), chitosan (QTS) and coconut shell. The results showed that the pH influences on the adsorption of 2,4 DCP (pka=8.09) and 2,4,6 TCP (pka=6.21), this occur due to change in the ionization degree of these compounds. At pH < pKa, the molecular form predominates and at pH > pKa the anionic form prevails in solution as shown by equation 4. This behavior is directly influenced by adsorbate and adsorbent characteristics.

$$C_6H_nCl_nOH \leftrightarrows H^+ + C_6H_nCl_nO^- \quad \text{(Equation 4)}$$

Chitin and chitosan contain some functional groups such as acetamides, amines and hydroxyl which are capable of interacting with 2,4 DCP and 2,4,6 TCP through hydrogen bonding, Van der Waals interactions or ion exchange. In addition, changes at solution pH may induce a protonation or deprotonation process influencing in the adsorption capacity. For chitosan, in acid conditions, the amino groups are protonated, as showed by Equation 5.

$$R-NH_2 + H^+ \leftrightarrows R-NH_3^+ \quad \text{(Equation 5)}$$

The results obtained for chitosan indicated that the chlorophenols adsorption decreased at pH 3.0 to 9.0. In addition, was selected an intermediate value of pH 6.5. Zheng et al. [27] obtained similar results with the removal of chlorophenols from groundwater by chitosan. In contrast, for the chitin and coconut shells no significant changes on the adsorption of 2,4 DCP and 2,4,6 TCP was observed, probably due to the low influence of pH variation on the structure of these adsorbents.

Adsorption isotherm

The isotherms adsorption for chitin, chitosan and coconut shell were obtained by relating the amount of solute adsorbed (Q_e) with the solute concentration in the fluid phase at equilibrium (pH=7.5). The experimental data of adsorption isotherms were applied to the Langmuir and Freundlich models.

After fitting the equilibrium adsorption data, Freundlich and Langmuir parameters were obtained from straight regression lines. The values of adsorption capacity (Q_{max}) and the parameters K_L, K_F and 1/n are given in Table 1.

The results showed in Table 1 indicated that the adsorption efficiency of the solutes on the adsorbents follows 2,4 DCP < 2,4,6-TCP indicating that tends to increase with more chlorine in the molecule.

Satisfactory correlation coefficients were noted (r > 0.90). In order to more clearly define the model which represented the experimental data most correctly, the normalized percent deviation (*P*) [28] was applied, according to the following Eq. 6.

$$P = \left(\frac{100}{N}\right) \sum \left(\frac{|q_e - q_{teor}|}{q_e}\right) \quad \text{(Equation 6)}$$

173

Orbital: Electron. J. Chem. 5 (3):171-178, 2013

Where q_e is the experimental adsorption capacity, q_{teor} is the level theoretical adsorption capacity, N the number of trials.

For the lower P value, greater the correlation between the experimental and theoretical, and therefore more favorable to the model. P values were calculated for the Langmuir and Freundlich isotherms for both adsorbents, as shown in Table 1, being considered acceptable P values <5.

Table 1. Experimental parameters of 2,4 DCP < 2,4,6-TCP obtained from batch adsorption isotherms.

Compound	Langmuir				Freundlich			
	K_L (L.mg^{-1})	Q_{max} (mg.g^{-1})	R	*P*	1/n	K_F	r	*P*
2,4 DCP								
Chitosan	0.005	6.00	0.951	4.65	0.574	0.140	0.915	5.69
Chitin	0.014	4.58	0.979	11.57	0.455	0.313	0.903	5.08
Coconut	0.002	3.36	0.985	22.62	0.487	0.163	0.992	1.23
2,4,6 TCP								
Chitosan	0.002	27.55	0.995	3.61	0.808	0.106	0.990	4.71
Chitin	0.002	20.41	0.953	8.60	1.043	0.032	0.978	4.11
Coconut	0.003	4.73	0.952	15.29	0.599	0.264	0.966	2.04

Chitosan adsorption

Figures 1a and 1b show the experimental and theoretical isotherms for chitosan, which suggests that the adsorption of 2,4 DCP and 2,4,6 TCP on the chitosan follows the Langmuir model, which indicates a mono-layer adsorption.

The low P value observed for the Langmuir model (Table 1) confirms that the approach to the model. The adsorption efficiency of the chlorophenols by the chitosan can be explained due to the high amount of free groups (amino and hydroxyl) present in its structure. The amino groups (R-NH$_2$), in the protonated form, adsorbs strongly ionic solutes such as chlorinated phenols (Eq. 7). The hydroxyl groups present in chlorophenols can also contribute to hydrogen bonds and provide a greater stability and adsorption of solutes on the surface of chitosan [27].

$$R-NH_3^+ + C_6H_nCl_n-O^- \leftrightarrows R-NH_3^+\cdots^- O-Cl_nH_nC_6 \qquad \text{(Equation 7)}$$
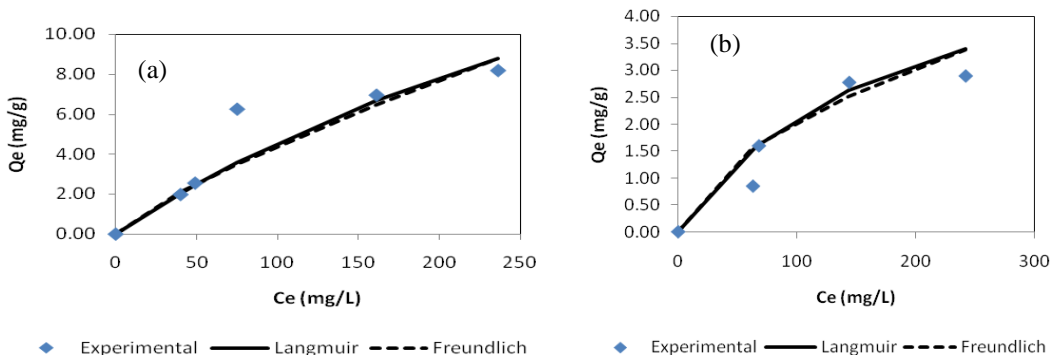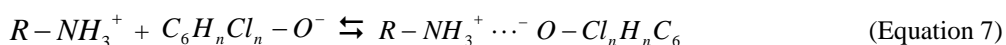
Figure 1. Adsorption isotherm of chitosan (a) 2,4 DCP, (b) 2,4,6 TCP.

Chitin adsorption

The results of adsorption isotherms with chitin are shown in Figures 2a and 2b, and it can be noted that the experimental data, evidenced by the lower value of P, are well described by Freundlich model. Therefore, it is assumed a heterogeneous adsorption, where the energy distribution to the sites is essentially

174

Orbital: Electron. J. Chem. 5 (3):171-178, 2013

exponential. Other authors [20, 27] also observed the similar process for phenol adsorption onto chitin. Chitin has a similar structure to cellulose, and its adsorptive properties are probably due to the groups acetamide (-NHCOCH₃) and carbonyl of the glucose units. The phenol adsorption onto chitin could be described by equation 8.

$$R - NHCOCH_3 + C_6H_nCl_n - O^- \leftrightarrows R - NHCOCH_3 \cdots^- O - Cl_nH_nC_6 \qquad \text{(Equation 8)}$$
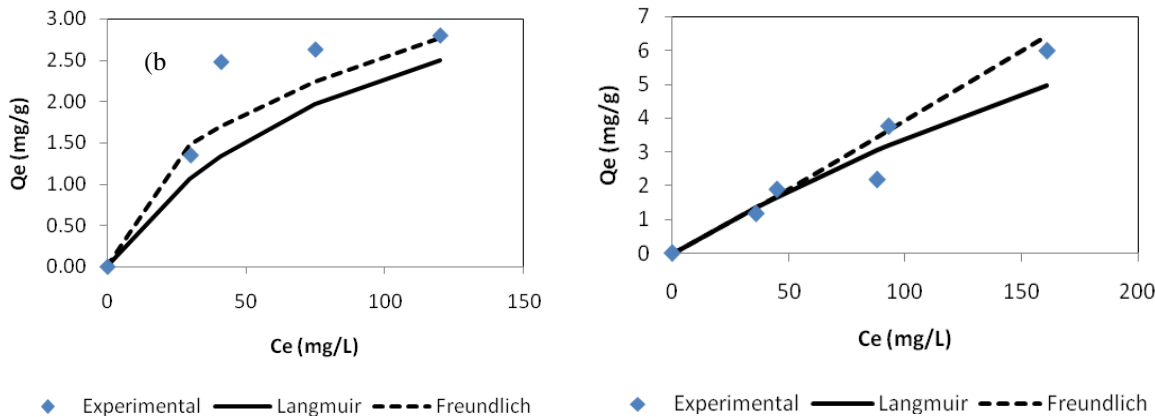
Figure 2. Adsorption Isotherm in Chitin (a) 2,4 DCP, (b) 2,4,6 TCP.

Coconut shell adsorption

The adsorption isotherms of 2,4 DCP and 2,4,6 TCP on the coconut bagasse are showed in Figures 3a and 3b. It can be observed that the experimental data are well described by the Freundlich model, which indicates a double-layer adsorption.

The composition of coconut shell contains largely cellulose, lignin and pentosanes [29]. These constituents present in its structure some functional groups such as alcohols, aldehydes, carboxylics, ketones and phenolic hydroxides, which may engage in processes that combine forces of attraction and repulsion ionic, hydrogen bonding, dipole-dipole forces and Van der Waals forces in interactions with solutes. The chlorophenols adsorption onto coconut bagasse could be described by process in equation 9.

$$R - CO_nH_n + C_6H_nCl_n - O^- \leftrightarrows R - CO_nH_n \cdots^- O - Cl_nH_nC_6 \qquad \text{(Equation 9)}$$
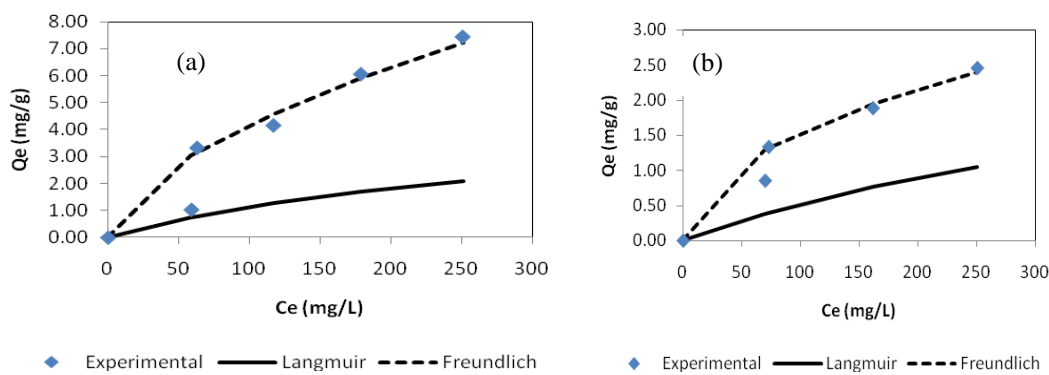
Figure 3. Adsorption isotherm in coconut bagasse (a) 2,4 DCP, (b) 2,4,6 TCP.

Comparison of adsorption capacity with other adsorbents

Adsorption capacity obtained for chitosan, chitin and coconut shells has been compared for other commercial adsorbents such as activated carbon, amberlite, bentonite and silica, as shown in Figure 4. As noted the 2,4,6 TCP is more easily removed from

175

Orbital: Electron. J. Chem. 5 (3):171-178, 2013

wastewater than 2,4 DCP by the chitinous materials. In contrast, coconut shell and other commercial adsorbents exhibit a removal efficiency for 2,4-DCP (Figure 4).

Table 2 shows the adsorption capacity values for some materials studied reported in literature [8, 20, 27, 29-32]. The high adsorption capacity of 2,4,6 TCP by chitin (27.55 mg.g^{-1}) and chitosan (20.41 mg.g^{-1}) for our study, is approaches to the fly ash (23.83 mg.g^{-1}) [29, 30]. Chitinous materials have different adsorption capacities depending on the experimental condition, such as pH, contact time and particle size. In addition, the performance of coconut shell can be efficiently improved by chemical or physical activation [29]. Removal of 2,4 DCP and 2,4,6 TCP about 55% and 95%; 50% and 99% were obtained using chitosan and chitin, respectively.
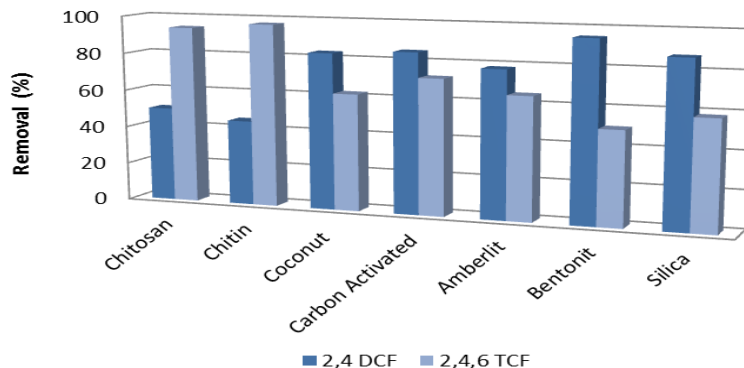
Figure 4. Removal (%) of 2,4 DCP and 2,4,6 TCP in commercial adsorbents.

Table 2. Comparison of adsorption capacity on various adsorbents.

Adsorbent	Compound	q (mg/g)	Particle size (mm)	pH	T ($^{\circ}$C)	Contact time (h)	References
Chitin	2,4 DCP	6.00	0.18	7.5	28±2	4	This paper
Chitosan	2,4 DCP	4.58	0.18	7.5	28±2	4	This paper
Coconut	2,4 DCP	3.36	0.18	7.5	28±2	4	This paper
Chitin	2,4,6 TCP	27.55	0.18	7.5	28±2	4	This paper
Chitosan	2,4,6 TCP	20.41	0.18	7.5	28±2	4	This paper
Coconut	2,4,6 TCP	4.73	0.18	7.5	28±2	4	This paper
Chitin	Phenol	25.06	0.15 - 0.30	1.0	40	1.6	[20]
Chitosan (Flake)	2,4,6 TCP	0.14	2.0 x 3.0 x 0.03	natural	5	96	[27]
Fly Ash	Phenol	23.83	0.04 – 1	6.5	30	24	[30]
Activated Carbon (Derived from coconut bagasse)	2,4 DCP	50.53	0.07- 0.58	4 ± 0.2	25	30	[29]
Biomass	Phenol	0.33	2.36 -4.75	5.1	21±1	30	[8]
Rice Rusk	p-chlorophenol	14.36	0.03 – 0.15	-	-	72	[31]
Petroleum coke	p-Chlorophenol	9.33	0.03 – 0.15	-	-	72	[31]
Lignite	Phenol	10.00	0.5	Natural	25	-	[32]

Wastewater treatment in fixed bed

For evaluate the efficiency of the adsorbents in the wastewater petrochemical treatment was employed a system of fixed bed, through which the effluent was percolated and the physicochemical parameters of the solutions were analyzed before and after leaving the fixed bed.

The effluent sample from process of oil refinery company (LUBNOR) presented an alkalinity median, high load of organic matter (COD), high oil and grease (TOG) and turbidity.

The results show that after effluent treatment with chitin, the reduction of COD reached approximately 75.0% (reduction 320.4 to 79.9 mg.L^{-1}), and therefore higher than the reduction observed for the treatment used by the company (LUBNOR), which was around 45% (from 320.4 to 184.2 mg.L^{-1}). These results are satisfactory, considering that the maximum limit (ML) established by environmental law (SEMACE 154/2002) is 200.0 mg.L^{-1}. In contrast, chitosan shows a low efficacy for COD removal.

The performance of chitin and chitosan for

176

Orbital: Electron. J. Chem. 5 (3):171-178, 2013

removal of oil and grease (TOG) reached about 90%. These results also are significant since the SEMACE determines that the maximum TOG for the release of effluent is 20 mg.L^{-1}.

Wastewater treatment with chitin and chitosan, showed no significant changes in pH and conductivity. The reduction in the concentration of ammonia and nitrate after sample treatment with chitin was satisfactory. In contrast, the performance of

the chitosan was not satisfactory. The turbidity removal from wastewater sample by the chitin and chitosan achieved 89% and 74% respectively.

The all the results obtained with coconut shell (not showed) were not satisfactory, probably due to the large increase in organic matter caused by the dissolution of the polysaccharides present in the its structure.

Table 3. Results of the physical-chemical parameters of wastewater before and after treatment.

Parameters	E_{Raw}	E_{Comp}	E_{QTI}	E_{QTS}	ML Semace 154/2002
COD (mg.L^{-1})	320.4	184.2	79.9	332.5	200
TOG (mg.L^{-1})	81.6	-	8.4	8.4	20
pH	7.66	7.79	7.85	7.90	5-9
Conductivity (μs.cm^{-1})	2.42	2.30	2.63	2.67	-
Nitrate (mg.L^{-1})	32.3	29.7	18.6	53.5	-
Ammonia (mg.L^{-1})	5.05	4.40	3.39	7.92	5.0
Turbidity (NTU)	23.2	4.41	2.40	6.01	-

E_{Raw} = raw wastewater
E_{Comp} = effluent treated by the company,
E_{QTI} = effluent treated with chitin adsorbent
E_{QTS} = = effluent treated with chitosan

4. CONCLUSION

Based on the results can be concluded that chitosan, chitin and coconut bagasse have a performance considerable on the adsorption of 2,4 dichlorophenol and 2,4,6 trichlorophenol. The order of adsorption capacity was as follow: chitosan> chitin> coconut shell. The wastewater treatment employed chitin showed high removal efficiency for COD and TOG with performance around 90%. In contrast, coconut shell showed low performance. The adsorption capacity of chitin was comparable to those of conventional adsorbents. The results indicated that a fixed bed column using chitinous materials can be very practical for organic compounds removal from petrochemical wastewater..

5. ACKNOWLEDMENTS

6. REFERENCE AND NOTES

[1] Tan, I. A. W.; Ahmad . A. L.; Hameed, B. H. *J. Hazard. Mater.* **2008**, *154,* 337. [CrossRef][PubMed]

[2] Chaliha S.; Bhattacharyya, K. G. *Chem. Eng. J.* **2008**, *139,* 575. [CrossRef]

[3] Milhome, M. A. L., Emprego de quitina e quitosana para adsorção de fenol de efluente de refinaria de petróleo. [Dissertação Mestrado.] Fortaleza, Brazil: Universidade Federal do Ceará (UFC), 2006.

[4] Yang, L. P.; Hu, W.Y.; Huang, H. M.; Yan, B. *Desalination and Water Treatment*. **2010**, *21,* 87. [CrossRef]

[5] Freire, R. S.; Pelegrini, R.; Kubota, L. T.; Duran N.; Zamora, P. *Quím. Nova* **2000**, *23*, 504. [CrossRef]

[6] Li, Z.; Wu, M.; Jiao, Z.; Bao, B.; Lu, S. *J. Hazard. Mater.* **2004**, *114,* 111. [CrossRef][PubMed]

[7] Ipek, U. *Filtr. Sep*. **2004**, *4*, 39. [CrossRef]

[8] Rao, J.; Viraraghavan, R. *Bioresour. Technol*. **2002**, *85,* 165. [CrossRef]

[9] Hamitouche, A.; Amrane, A.; Bendjam Z.; Kaouah, F. *Desalin. Water Treat*. **2011**, *25*, 20.

[10] Zaghouane-Boudiaf, H.; Boutahala, M. *Desalin. Water Treat.* **2010**, *24*, 47. [CrossRef]

[11] Cooney, D. O. Adsorption Design for Wastewater Treatment. Ed. CRC Press LLC. 1999.

177

Orbital: Electron. J. Chem. 5 (3):171-178, 2013

[12] Kalderis, D. Koutoulakis, D. Paraskeva, P. Diamadopoulos, E. Otal E., Valle J. and Fernández-Pereira. C. *Chem. Eng. J.* **2008**, *144*, 42. [CrossRef]

[13] Milhome, M. A. L.; Keukeleire, D.; Ribeiro, J. P.; Carvalho, T. V.; Queiroz. D. C.; Nascimento. R. F. *Quim. Nova* **2009**, *32,* 2122. [CrossRef]

[14] Moreira, S. A.; Sousa, F. W.; Oliveira, A. G.; Nascimento. R. F. *Quím. Nova* **2009**, *32,* 1717. [CrossRef]

[15] Sousa, F. W.; Oliveira, A. G.; Rosa, M. F.; Moreira, S. A.; Cavalcante, R. M.; Nascimento, R. F. *Quim. Nova* **2007**, *30,* 1153. [CrossRef]

[16] Crisafulli, R.; Milhome, M.A.L.; Cavalcante, R. M.; Silveira, E. R.; Keukeleire, D.; Nascimento, R. F. *Bioresour. Technol.* **2008**, *99,* 4515. [CrossRef][PubMed]

[17] Sousa, F. W.; Oliveira, A. G.; Ribeiro, J. P.; Rosa, M. F.; Keukeleire, D.; R. F. Nascimento. *J. Environ. Manage.* **2010**, *91,* 1634. [CrossRef][PubMed]

[18] Sousa, F. W.; Sousa, M. J.; Oliveira, I. R. N.; Oliveira, A. G.; Cavalcante, R. M. Fechine, P. B.; Neto, V. O. S.; Keukeleire, D.; Nascimento, R. F. *J. Environ. Manage.* **2009**, *90,* 3340. [CrossRef][PubMed]

[19] Ng, J. C. Y.; Cheung W. H.; Mckay, G. *Chemosphere* **2003**, *52,* 1021. [CrossRef]

[20] Dursun A. Y.; Kalayci, Ç. S. *J. Hazard. Mater.* **2005**, *123*, 151. [CrossRef][PubMed]

[21] Guibal, E. *Prog. Polym. Sci.* **2005**, *30,* 71. [CrossRef]

[22] Figueiredo, S. A.; Loureiro, J. M.; Boaventura, R. A. *Water Res.* **2005**, *39,* 4142. [CrossRef][PubMed]

[23] Ngah, W. S. W.; Endud C. S.; Mayanar, R. *React. Funct. Polym.* **2002**, *50,* 181. [CrossRef]

[24] Barros, F. C. F.; Sousa, F.W.; Cavalcante, R. M.; Carvalho, T. V.; Dias, F. S.; Queiroz, D. C.; Vasconcelos, L. C. G.; Nascimento, R. F. *Clean – Soil, Air.* **2008**, *36*, 292.

[25] Vijaya, Y. Popuri, S. R. Reddy G. S.; Krishnaiah, A. Desalin. *Water Treat.* **2011**, *25*, 159. [CrossRef]

[26] APHA, Standard Methods for the examination of water &wastewater, 21st Edition, Washington, **2005**.

[27] Zheng, S.; Yang, Z.; Jo D. H.; Park, Y. H. *Water Res.* **2004**, *38*, 2315. [CrossRef][PubMed]

[28] Ayranci, E.; Duman, O. *J. Hazard. Mater.* **2005**, *124,* 125. [CrossRef][PubMed]

[29] Sing, P.; Malik, A.; Sinha S.; Ojha, P. *J. Hazard. Mater.* **2008**, *150,* 626. [CrossRef][PubMed]

[30] Srivastava, V. C.; Swamy, M. M.; Mall, I. D.; Prasad B.; Mishra, I. M. *Colloids Surf., A: Physicochem, Eng. Aspects.* **2006**, *272,* 89. [CrossRef]

[31] Ahmaruzzaman, M.; Sharma, D. K. *J. Colloid Interface Sci.* **2005**, *287,* 14.

[32] Polat, H.; Molva, M.; Polat, M. *Int. J. Miner. Process.* **2006**, *79*, 264. [CrossRef]

178

Orbital: Electron. J. Chem. 5 (3):171-178, 2013

Full Paper

Adsorption of Crystal Violet Dye from Aqueous Solution onto Zeolites from Coal Fly and Bottom Ashes

Tharcila C. R. Bertolini*, Juliana C. Izidoro, Carina P. Magdalena, Denise A. Fungaro

Chemical and Environmental Center, Nuclear and Energy Research Institute, Av. Prof. Lineu Prestes, 2242, CEP 05508-000, São Paulo, Brazil.

Abstract: The adsorption of the cationic dye Crystal Violet (CV) over zeolites from coal fly ash (ZFA) and bottom ash (ZBA) was evaluated. The coal fly ash (CFA) and the coal bottom ash (CBA) used in the synthesis of the zeolites by alkaline hydrothermal treatment were collected in Jorge Lacerda coal-fired power plant located at Capivari de Baixo County, in Santa Catarina State, Brazil. The zeolitic materials were characterized predominantly as hydroxy-sodalite and NaX. The dye adsorption equilibrium was reached after 10 min for ZFA and ZBA. The kinetics studies indicated that the adsorption followed the pseudo-second order kinetics and that surface adsorption and intraparticle diffusion were involved in the adsorption mechanism for both the adsorbents. The equilibrium data of ZFA was found to best fit to the Langmuir model, while ZBA was best explained by the Freundlich model. The maximum adsorption capacities were 19.6 mg g^{-1} for the CV/ZFA and 17.6 mg g^{-1} for the CV/ZBA.

Keywords: crystal violet; coal fly ash; coal bottom ash; zeolite; adsorption

1. INTRODUCTION

The manufacture and use of synthetic dyes for dyeing fabrics has become an industry solid. It is estimated that around 700,000 tons of dyes are produced annually around the world. Of this amount about 20% is unloaded the industrial wastes without previous treatment. However, their use has become a matter of serious concern to environmentalists. Synthetic dyes are highly toxic causing negative effects on all life forms because they present sulfur, naphthol, vat dyes, nitrates, acetic acid, surfactants, enzymes chromium compounds and metals such as copper, arsenic, lead, cadmium, mercury, nickel, cobalt and certain auxiliary chemicals [1-2].

The crystal violet (CV) dye is a synthetic cationic dye and transmits violet color in aqueous solution. It is also known as Basic Violet 3, gentian violet and methyl violet 10B, belonging to the group of triarylmethane [3]. This dye is used extensively in the textile industries for dying cotton, wool, silk, nylon, in manufacture of printing inks and also the biological stain, a dermatological agent in veterinary medicine [3-4]. The CV is toxic and may be absorbed through the skin causing irritation and is harmful by inhalation and ingestion. In extreme cases, can lead to kidney failure, severe eye irritation leading to permanent blindness and cancer [5-6]. Therefore, removal of this dye from water and wastewater is of great importance.

Various methods of treatment exploited through the years by industries for removing colorants include physicochemical, chemical, and biological methods, such as flocculation, coagulation, precipitation, adsorption, membrane filtration, electrochemical techniques, ozonation, and fungal decolorization [7]. However, due to the fact that effluents contain different dyes, and these dyes contain complex structures, is very difficult to treat using conventional methods [8].

The adsorption is one of the most effective processes of advanced wastewater treatment, which industries employ to reduce hazardous pollutants present in the effluents. This is a well-known and superior technique to other processes for removal of dyes from aqueous worldwide due to initial cost, operating conditions and simplicity of design [9]. Currently, the most common procedure involves the use of activated carbon as adsorbent for this purpose

---
*Corresponding author. E-mail: thacolachite@yahoo.com.br

by offering greater adsorption capacities. However, due to their relatively high cost, many lower-cost adsorbents have been investigated as adsorbent for removing contaminants from wastewater. The low-cost adsorbents can be made from waste materials, thus collaborating with the environment and also getting economic advantages. A wide variety of low-cost adsorbents have been prepared from different materials utilizing industrial, biomass, and municipal wastes [10-14].

Thermoelectric power stations produce a great quantity of residues from combustion of coal. The major solid waste by-product of thermal power plants based on coal burning is fly ash. The coal-fired power plants in the southern of Brazil produce approximately 4 Mt of ash per year, of which 65–85% is fly ash and 15–35% bottom ash. The main uses of fly ash include pozzolanic cement, paving, bricks, etc., but only 30% of what is produced in the year are recycled [15-16]. The bottom ash are previously disaggregated and transported to the settling ponds through pumping hydraulic [17]. This may lead to environmental problems through leaching of toxic substances present in the ashes. One way to reduce the environmental impact of the disposal of these wastes is to expand its utilization. An alternative solid waste is recycling of the transformation of the coal ash at a low cost adsorbent able to remove toxic substances from contaminated waters [18-22].

The coal ash can be converted into zeolites due to their high contents of silicon and aluminum, which are the structural elements of zeolites. The most common method involves a hydrothermal treatment with sodium hydroxide [23-24]. This technique of recycling coal ashes has been extensively investigated for water treatment due to its large specific surface area and cation exchange capacity, low cost, and mechanical strength [25-29].

The aim of this work was to evaluate the efficiency of synthesized zeolites from Brazilian coal fly and bottom ashes as adsorbent in the removal of basic dye crystal violet from aqueous solutions. Batch kinetic experiments were performed to provide appropriate equilibrium times. The Langmuir and Freundlich isotherm models were used to model the isotherm data for their applicability.

2. MATERIAL AND METHODS

All chemicals used in this study were of analytical grade. Crystal Violet (CV) which was used

as a model cationic dye in this work was purchased from Proton-Research and considered as purity 100%. The general characteristics of CV are summarized in Table 1 and the chemical structure is in Fig. 1. A stock solution (5.0 g. L^{-1}) was prepared with deionized water (Millipore Milli-Q) and the solutions for adsorption tests were prepared by diluting. The samples of coal fly and bottom ashes were obtained from Jorge Lacerda coal-fired power plant located at Capivari de Baixo County, in Santa Catarina State, Brazil.

Table 1. General characteristics of CV dye.

Chemical name	Crystal Violet
Color index	CI 42555
λ_{max} (nm)	590
Molar mass (g mol^{-1})	408
Chemical formula	$C_{25}H_{30}N_3Cl$
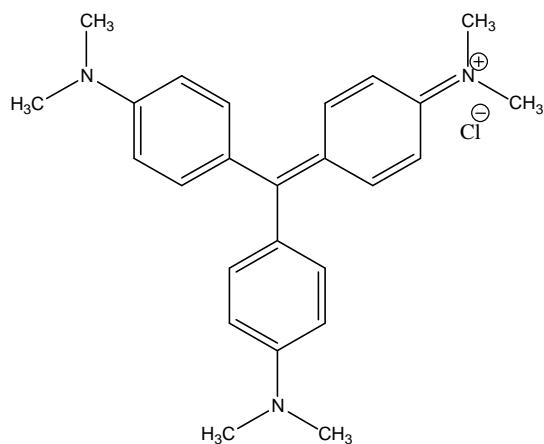
Figure 1. Chemical Structure of CV.

Zeolite synthesis

The zeolite was synthesized by hydrothermal activation of 20 g of coal fly (CFA) or coal bottom ashes (CBA) at 100 °C in 160 mL of 3.5 mol L^{-1} NaOH solution for 24 h. The zeolitic material was repeatedly washed with deionized water to remove excess sodium hydroxide until the washing water had pH ~ 10, then it was dried at 50 °C for 12 h [30]. The zeolitic products obtained were labeled as ZFA and ZBA for zeolite prepared with fly ash and bottom ash, respectively.

Adsorbents characterization

The mineralogical compositions of the samples (ZFA and ZBA) used as adsorbents and the samples saturated with dye (CV/ZFA and CV/ZBA) were determined by X-ray diffraction analyses (XRD) with

180

Orbital: Electron. J. Chem. 5 (3):179-191, 2013

an automated Rigaku multiflex diffractometer with Cu anode using Co Kα radiation at 40 kV and 20 mA over the range (2θ) of 5–80°with a scan time of 0.5°/min.

The chemical composition of CBA and ZBA, in the form of major oxides, was determined by X-ray fluorescence (XRF) in a Rigaku RIX- 3000 equipment. The bulk density and the specific surface area of CBA and ZBA was determined by a helium picnometer (Micromeritcs Instrument Corporation — Accupyc 1330) and by a BET Surface Area Analyser (Quantachrome Nova — 1200), respectively. Prior to determination of the specific surface area, samples were heated at 423.15 K for 12 h to remove volatiles and moisture in a degasser (Nova 1000 Degasser). The BET surface areas were obtained by applying the BET equation to the nitrogen adsorption data.

For the cation exchange capacity (CEC) measurements, the samples CBA and ZBA were saturated with sodium acetate solution (1 mol L^{-1}), washed with 1L of distilled water and then mixed with ammonium acetate solution (1 mol L^{-1}) [31]. The sodium ion concentration of the resulting solution was determined by optical emission spectrometry with inductively coupled plasma — ICP-OES (Spedtroflame — M120).

The pH and the conductivity were measured as follows: the bottom ashes and zeolite bottom ashes (0.25 g) were placed in 25 mL of deionized water and the mixture was stirred for 24 h in a shaker at 120 rpm (Ética — Mod 430). After filtration, the pH of the solutions was measured with a pH meter (MSTecnopon — Mod MPA 210) and the conductivity was measured with a conductivimeter (BEL Engineering - Mod W12D).

The determination of the zero point charge (pH$_{PZC}$) of ZFA and ZBA was carried out as follows: the samples (0.1 g) were placed in 50 mL of potassium nitrate (0.1 mol L^{-1}) and the mixtures were stirred for 24 h in the mechanical stirrer (Quimis – MOD Q-225M) at 120 rpm. The initial pH of solutions was adjusted to the values of 2, 4, 10, 11, 12 and 13 by addition of 0.1 and 1 mol L^{-1} HCl or 3 mol L^{-1} NaOH solution. The difference values between the initial and final pH (pH Δ) were placed in a graph in function of the initial pH. The point x where the curve intersects the y = 0 is the pH of PCZ.

The content of loss of ignition (LOI) of coal bottom ashes in this study were calculated according to the weight loss of the samples subjected to heating at 1050°C for 4 h in a muffle furnace and expressed in percentage. The mass of the material used was 0.5 g.

The chemical composition and the some physicochemical properties (bulk density, BET area, total and cation exchange capacity, pH) of CFA and ZFA have been described in a previous paper [26].

Adsorption studies

The adsorption was performed using the batch procedure. Kinetic experiments were carried out by agitating 0.25 g of adsorbent with 25 mL of dye solution with initial concentration of 185 mg L^{-1} at room temperature (25 ± 2 °C) at 120 rpm for 1-12 min for both adsorbents. The collected samples were then centrifuged (3000 rpm during 30 min for ZFA and during 10 min for ZBA) and the concentration in the supernatant solution was analyzed using a UV spectrophotometer (Cary 1E, Varian) by measuring absorbance at λ = 590 nm and pH = 5.

The adsorption capacity (mg·g^{-1}) of adsorbents was calculated using Eq. 1:

$$q = \frac{V(C_o - C_f)}{M} \qquad (1)$$

where q is the adsorbed amount of dye per gram of adsorbent, C_0 and C_f the concentrations of the dye in the initial solution and equilibrium, respectively (mg L^{-1}); V the volume of the dye solution added (L) and M the amount of the adsorbent used (g).

The efficiency of adsorption (or removal) was calculated using the equation:

$$R = 100\frac{(C_o - C_f)}{C_o} \qquad (2)$$

where R is the efficiency of adsorption (%), C_o is the initial concentration of dye (mg L^{-1}), C_f is the equilibrium concentration of dye at time t (mg L^{-1}).

Adsorption isotherms were carried out by agitating 0.25 g of zeolite with 25 mL of crystal violet over the concentration ranging from 24.4 to 236 mg L^{-1} for ZFA and 24.4 to 247.9 mg L^{-1} for ZBA till the equilibrium was achieved. The adsorption capacity (mg g^{-1}) of adsorbents was calculated using a Eq.1.

3. RESULTS AND DISCUSSION

Characterization of the adsorbents material

The X-ray diffractograms of ZFA and ZBA are

181

Orbital: Electron. J. Chem. 5 (3):179-191, 2013

shown in Fig. 2 and 3, respectively. The identification and interpretation of PXRD patterns of the materials are prepared by comparing the diffraction database provided by "International Centre for Diffraction Data/Joint Committee on Power Diffraction Standards" (ICDD/JCPDS). The phases in zeolitic materials were hydroxysodalite (JCPDS 31-1271) and NaX (JCPDS 38-0237) with peaks of quartz (JCPDS 85-0796) and mullite (JCPDS 74–4143) of ashes that remained after the treatment. The mineralogical composition of ash used as raw material for the synthesis of zeolites depends on the geological factors related to the formation and deposition of coal and its combustion conditions.
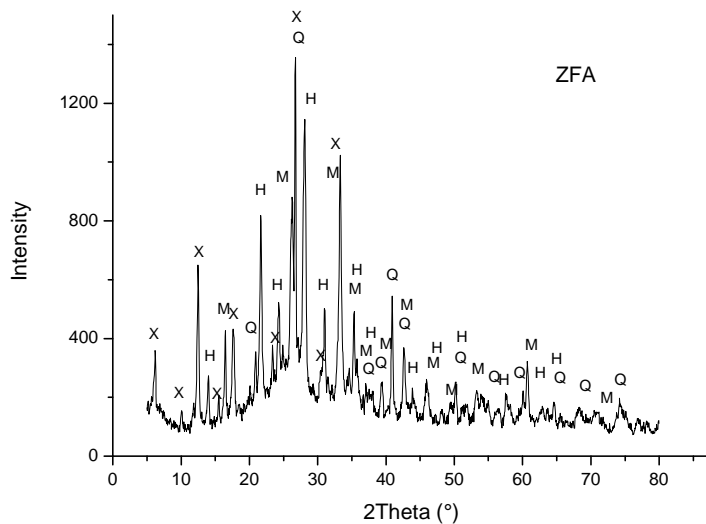
Figure 2. XRD Patterns of ZFA (Q = Quartz, M = Mullite, H = Hydroxysodalite zeolite, X = NaX zeolite).
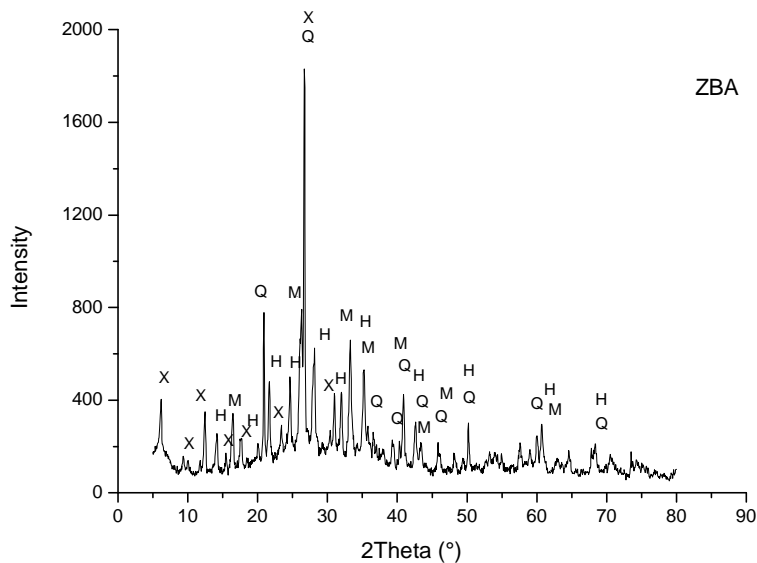
Figure 3. XRD Patterns of ZBA (Q = Quartz, M = Mullite, H = Hydroxysodalite zeolite, X = NaX zeolite).

The diffraction patterns of the zeolites obtained before and after adsorption of CV are shown in Fig. 4. The structural parameters of saturated ZFA and ZBA were very close to those of the corresponding ZFA and ZBA before adsorption. The crystalline nature of the zeolites remained intact after adsorption of molecules CV.

The chemical composition of CBA and ZBA determined by X-ray fluorescence (XFR) is shown in Table 2. The chemical compositions of CFA and ZFA have been described in detail in previous paper [26].

182

Orbital: Electron. J. Chem. 5 (3):179-191, 2013
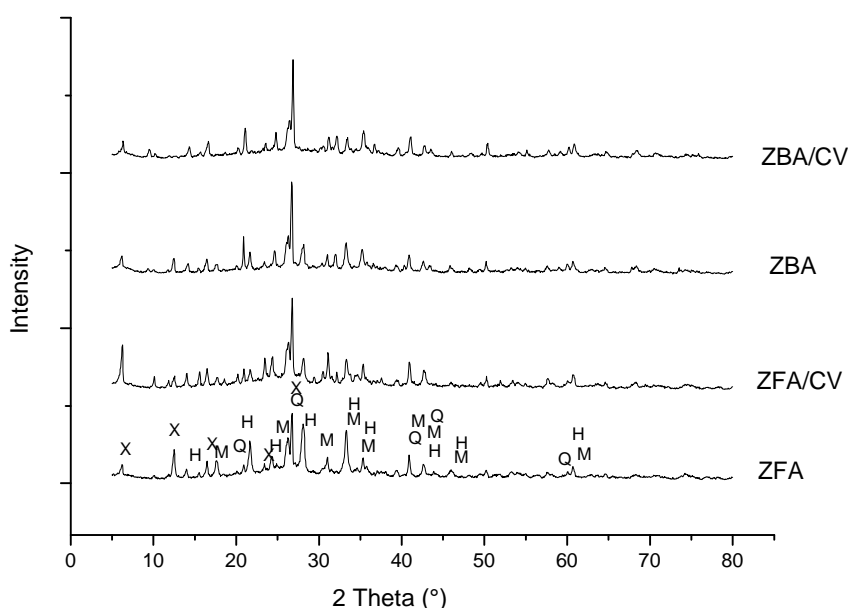
Figure 4. XRD Patterns of zeolites and zeolites saturated with dye (Q = Quartz, M = Mullite, H = Hydroxy-sodalite zeolite, X = NaX zeolite).

Table 2. Chemical composition of CBA and ZBA.

Elements (wt. %)	CBA	ZBA
SiO_2	49.6	35.1
Al_2O_3	27	32.9
Fe_2O_3	10.9	16.1
Na_2O	1.9	7.7
CaO	1.8	3.2
K_2O	4.4	0.7
TiO_2	1.9	2.4
SO_3	0.7	0.3
MgO	1.3	1.3
ZnO	0.03	0.03
ZrO_2	0.03	0.04
SiO_2/ Al_2O_3	1.84	1.06

The main constituents of CBA are silica (SiO_2), alumina (Al_2O_3), and ferric oxide (Fe_2O_3). Quantities below 5 wt.% of K_2O, CaO, TiO_2, SO_3 and MgO are also observed.

The main constituents observed for CBA were the same of CFA: 50.3 wt.% of SiO_2, 29.8 wt.% of Al_2O_3, and 6.70 wt.% of Fe_2O_3. It has found also oxides of calcium, titanium, sulfur and other compounds in amounts below 5 wt.%. The SiO_2/Al_2O_3 ratio was 1.69 and 1.84 for CFA and CBA, respectively, indicating good source to synthesize zeolites [32].

The coal and its ash generated in Jorge Lacerda coal-fired power plant were analyzed by Silva et al 2010. The results indicated that coal is bituminous-type, highly volatile (C/A). Samples of fly ash showed the following ranges of the main elements of higher concentration (wt.%): 57.98 – 60.10 of SiO_2, 22.98-26.97 of Al_2O_3 and 4.67-8.01 of Fe_2O_3. For samples of bottom ash ranges were (wt.%): 46.14 to 61.95 of SiO_2, 19.20 to 23.88 of Al_2O_3 and 5.38 to 7.81 of Fe_2O_3.

The chemical composition found for ZBA is mainly silica, alumina, iron oxide and sodium oxide (Table 2). The main constituents for ZFA were 36.6 wt.% of SiO_2, 38.0 wt.% of Al_2O_3, 8.30 wt.% of Fe_2O_3 and 6,90 wt.% of Na_2O. A significant amount of Na element is incorporated in the final products due to hydrothermal treatment with NaOH solution.

The SiO_2/Al_2O_3 ratio for zeolites is associated to the cation exchange capacity. The values observed for ZFA was 0.96 and the value calculated for ZBA was 1.06 (Table 2). The SiO_2/Al_2O_3 ratios for the zeolites are lower than the values of raw fly and bottom ashes. The hydrothermal treatment contributed to the increase in the cation exchange capacity of these materials. The zeolitic material that exhibit lower the ratio SiO_2/Al_2O_3, have higher the cation exchange capacity.

Some physicochemical properties of coal bottom ash and its zeolitic material are given in Table 3. The same physicochemical properties for CFA and ZFA are presented in previous paper [26].

183

Orbital: Electron. J. Chem. 5 (3):179-191, 2013

Table 3. Physicochemical properties of coal bottom ash (CBA) and zeolite from coal bottom ash (ZBA).

Properties physicochemical	CBA	ZBA
Bulk density (g cm^{-3})	1.79	2.43
BET surface area (m^2 g^{-1})	5.33	84.9
Loss of ignition (%)	9.33	-
pH in water	7.6	8.4
pH$_{PZC}$[a]	-	7.3
Condutivity (µS cm^{-1})	110	367
CEC (meq g^{-1})[b]	0.109	1.19

(a) point of zero charge; (b) cation exchange capacity

The bulk density values ranged from 1.79 to 2.43 g cm^{-3} for ash and zeolites. Kreuz [33] found value of bulk density 1.81 g cm^{-3} for bottom ash from thermal power plant Jorge Lacerda, which is very close to the value found for the ash of this study.

The specific surface area value of the zeolite bottom ash was approximately 16 times greater than those of its precursor ash. The specific surface area value for ZFA was also higher (134.3 m^2 g^{-1}) than the value for CFA (9.6 m^2 g^{-1}). This area increase is due to the crystallization stage zeolitic on the smooth spherical particles of the ash after the hydrothermal treatment.

The CEC values of the ash are much low, and is similar to the value reported in the literature [34]. The CEC values of ZBA and ZFA were 10 and 50 times higher than CBA and CFA, respectively, due to hydrothermal treatment. Therefore, the synthesized zeolites can be used as good cation exchanger.

The pH of the coal ash is directly related to the availability of macro and micro nutrient and indicates whether coal ash is acidic or alkaline in nature. Based on the pH, coal ash has been classified into 3 categories, namely; slightly alkaline 6.5–7.5; moderately alkaline 7.5-8.5 and highly alkaline >8.5 [35]. The pH values of fly ash (8.0) and bottom ash (7.6) indicates that ashes were moderately alkaline in nature. This alkalinity is justified by the presence of compounds formed by the cations K$^+$, Na$^+$, Ca^{2+} and Mg^{2+} combined with carbonates, oxides or hydroxides [34]. The pH of zeolitic materials increased due to hydrothermal treatment with NaOH solution.

The conductivity values found for synthesized zeolites were higher than those of raw ashes. This increase is explained by presence of exchangeable cations in the structures of the zeolites formed by the hydrothermal treatment.

Depoi et al. [36] found a conductivity value of 119 µS cm^{-1} for bottom ash, which is accordance with the present study.

The point of zero charge (PZC) is defined as the pH at which the surface of the adsorbent has neutral charge. The pH$_{PCZ}$ adsorbents depends on several factors such as the nature of crystallinity, Si/Al ratio, impurity content, temperature, adsorption efficiency of electrolytes, degree of adsorption of H$^+$ and OH$^-$, and, therefore, it must vary adsorbent for adsorbing [37]. The value of pH$_{PZC}$ of ZBA (Table 3) was lower than the pH in water indicating that the surface presented negative charge in aqueous solution (pH> pH$_{PZC}$). The value of the pH$_{PZC}$ of ZFA obtained in this study was 6.5. This value is lower than the pH and the surface of ZFA also showed negative charge.

The data of loss on ignition of coal ash may indicate the combustion efficiency of a thermoelectric power plant. The high levels of this property make it difficult the synthesis of zeolites, as the non-reactive phase may be a lesser amount during conversion. The loss on ignition is usually indicative of the presence of unburned carbon and mineral phases stable at high temperatures [38]. The loss on ignition values found for CFA and CBA were 15.1% and 9.33%, respectively. According to the obtained values of loss on ignition of Brazilian fly ash was suggested that the Jorge Lacerda Thermal Power Plant has a low efficiency [26].

Kinetics studies

Figure 5 shows the effect of contact time on adsorption process of CV on ZFA and on ZBA. The efficiency of dye removal was increased as the agitation time increased until equilibrium. The adsorption equilibrium with ZFA and ZBA were reached at 10 min. The process shows the removal of 71% and 50% with ZFA e ZBA, respectively.
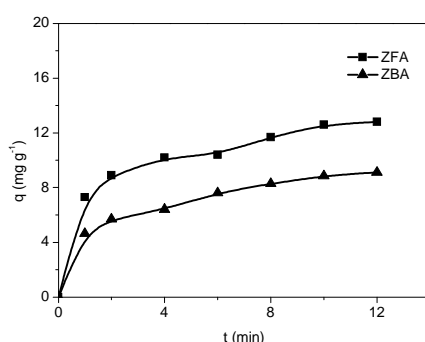

Figure 5. Effect of contact time on the adsorption of CV onto ZFA and ZBA.

Kinetic models

184

Orbital: Electron. J. Chem. 5 (3):179-191, 2013

In order to investigate the adsorption processes of CV onto adsorbents, pseudo-first order and pseudo-second order kinetic models were applied to the experimental data. The pseudo-first-order kinetic model, proposed by Lagergren, has been widely used to predict the dye adsorption kinetics. The dye adsorption kinetics following the pseudo-first-order model is given by [39]:

$$\frac{dq}{dt} = k_1(q_e - q) \qquad (3)$$

where q and q_e represent the amount of dye adsorbed (mg g^{-1}) at any time t and at equilibrium time, respectively, and k_1 represents the adsorption rate constant (min^{-1}). Integrating Eq. (3) with respect to boundary conditions $q = 0$ at $t = 0$ and $q = q$ at $t = t$, then Eq. (3) becomes:

$$\log_{10}(q_e - q) = \log_{10} q_e - k_1 t / 2{,}303 \qquad (4)$$

Thus the rate constant k_1 (min^{-1}) can be calculated from the plot of log $(q_e\text{-}q)$ *vs.* time *t*.

The kinetic data were further analyzed using a pseudo second- order relation proposed by [40] which is represented by:

$$\frac{dq}{dt} = k_2(q_e - q)^2 \qquad (5)$$

where k_2 is the pseudo-second-order rate constant (g mg^{-1} min^{-1}) and q_e and q represent the amount of dye adsorbed (mg g^{-1}) at equilibrium and at any time *t*. Separating the variables in Eq. (6) gives

$$\frac{dq}{(q_e - q)^2} = k_2 dt \qquad (6)$$

Integrating Eq. (6) for the boundary conditions $t = 0$ to $t = t$ and $q = 0$ to $q = q$ gives

$$\frac{t}{q} = \frac{1}{k_2 q_e^2} + \frac{1}{q_e} t \qquad (7)$$

A plot *of t/q vs. t* gives the value of the constants k_2 (g mg^{-1} min^{-1}), and also q_e (mg g^{-1}) can be calculated.

Because the above two equations cannot give definite mechanisms, the intraparticle diffusion model was tested. According to Weber and Morris [41], an intraparticle diffusion coefficient k_{dif} is defined by the equation:

$$q_t = k_{dif} t^{1/2} + C \qquad (8)$$

where k_{dif} is the intraparticle diffusion rate constant (mg g^{-1} min$^{-1/2}$), and C is the intraparticle diffusion constant (mg g^{-1}). The constants k_{dif} and C can be obtained, respectively, from the slope and intercept of the plot of qt versus $t^{1/2}$. The relative values of C give an idea about the boundary layer thickness, i.e., the larger the intercept value, the greater the boundary layer effect [41-43].

Figure 6 shows the fitting results using (a) first-order kinetic model; (b) second-order kinetic model, and (c) diffusion model. The parameters for all models are presented in Table 4.
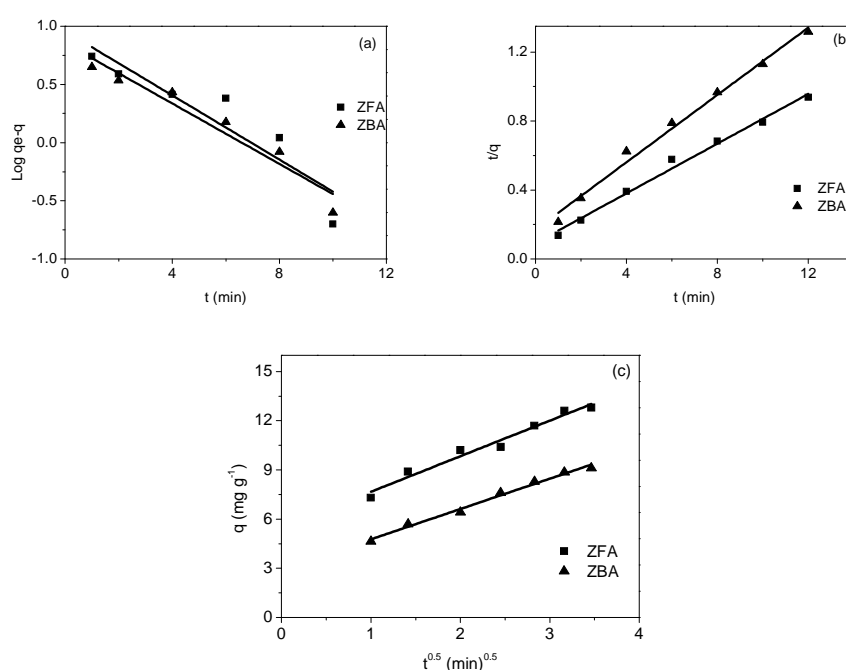

Figure 6. Comparison of kinetic models, and diffusion model of CV adsorption on ZFA and ZBA (a) first-order kinetics; (b) second-order kinetics; (c) diffusion model.

185

Orbital: Electron. J. Chem. 5 (3):179-191, 2013

Table 4. Kinetic parameters for CV removal onto ZFA and ZBA.

Adsorbents	Pseudo- first order				
	k_1 (min)$^{-1}$	q_e calc (mg g^{-1})	q_e exp (mg g^{-1})	R_1	
ZFA	3.17 x 10^{-1}	9.10	12.8	0.927	
ZBA	2.99 x 10^{-1}	7.16	9.11	0.970	
	Pseudo- second order				
	k_2 (gmg^{-1}min^{-1})	h (mg g^{-1}min^{-1})	q_e calc (mg g^{-1})	q_e exp (mg g^{-1})	R_2
ZFA	5.59 x 10^{-2}	10.8	13.9	12.8	0.996
ZBA	5.60 x 10^{-2}	5.88	10.2	9.11	0.995
	Intraparticle diffusion				
	C	k_{dif} (mg g^{-1}min$^{-0.5}$)	R_i		
ZFA	5.49	2.17	0.986		
ZBA	2.92	1.85	0.995		

The experimental q_e values (Table 4) did not agree with the calculated ones obtained from the linear plots, indicating that the pseudo-first order model does not reproduce the adsorption kinetics of CV onto ZFA and ZBA. The k_2 and qe determined from the model are presented in Table 4 along with the corresponding correlation coefficients. The values of the calculated and experimental q_e are close to ZFA and also to ZBA, and the calculated correlation coefficients (R) are also very close to unity. Hence, the pseudo-second order model better represented the adsorption kinetics.

The linearity of the fitting lines obtained from the application of the diffusion model (Fig. 6c) points

to the presence of intraparticle diffusion in the system. However, the fact that the lines do not pass through the origin of the plots indicates that, although intraparticle diffusion may be involved in the adsorption process, it was not the rate-controlling step [41].

A comparison of calculated and measurement results for kinetic of CV adsorption onto ZFA and ZBA are shown in Fig. 7a and 7b, respectively. As can be seen, the pseudo-first order model underestimates the adsorption and the pseudo second-order kinetic model provides the best correlation for both adsorption processes.
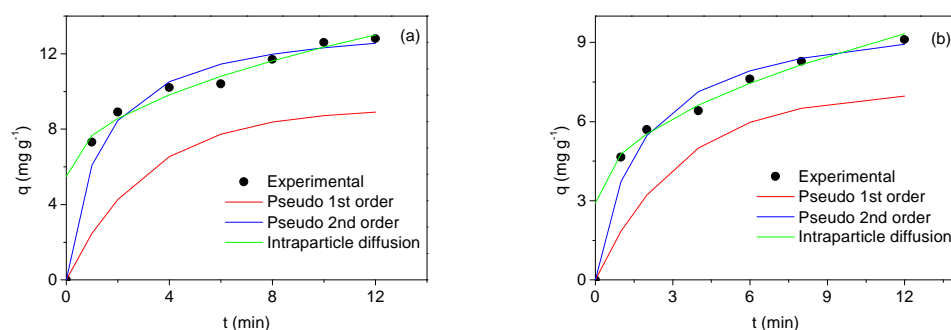

Figure 7. Comparison between the measured and modeled time profiles for adsorption of CV for (a) ZFA and (b) ZBA.

Adsorption equilibrium

In adsorption in a solid–liquid system, the distribution ratio of the solute between the liquid and the solid phases is a measure of the position of equilibrium. The preferred form of depicting this distribution is to express the quantity qe as a function of C_e at a fixed temperature and an expression of this type is termed an adsorption isotherm [44]. The

quantity q_e is the amount of solute adsorbed per unit weight of the solid adsorbent, and C_e is the concentration of solute remaining in the solution at equilibrium.

The analysis of the isotherm data is important to develop an equation which accurately represents the results and which could be used for design purposes [39]. In the present study, Langmuir,

186

Orbital: Electron. J. Chem. 5 (3):179-191, 2013

Freundlich and Dubinin-Radushkevich (*D-R*) models were used to describe the equilibrium data.

The Langmuir isotherm assumes that the sorption takes place at specific homogeneous sites within the adsorbent [45]. The linear form of Langmuir isotherm is represented by the Eq. 9:

$$\frac{C_e}{q_e} = \frac{1}{Q_o b} + \frac{C_e}{Q_o} \qquad (9)$$

where C_e is the equilibrium concentration (mg L^{-1}), q_e the amount adsorbed at equilibrium (mg g^{-1}), Q_0 the adsorption capacity (mg g^{-1}) and, *b* is the energy of adsorption (Langmuir constant, L mg^{-1}). The values of Q_0 and *b* were calculated from the slope and intercept of the linear plots C_e q_e^{-1} *versus* C_e which give a straight line of slope $1/Q_0$ that corresponds to complete monolayer coverage (mg g^{-1}) and the intercept is $1/Q_0 b$.

The Freundlich isotherm is derived by assuming a heterogeneous surface with a non-uniform distribution of heat of adsorption over the surface [46]. The logarithmic form is shown as Eq. 10:

$$\log q_e = \log K_f + \frac{1}{n}\log C_e \qquad (10)$$

where K_F [(mg g^{-1} (L mg^{-1})$^{1/n}$)] and n are the Freundlich constants related to adsorption capacity and adsorption intensity of adsorbents, respectively. They were calculated from the intercept and slope of the plot log qe versus log C_e.

Langmuir and Freundlich isotherms do not give any idea about adsorption mechanism. The Dubinin–Radushkevich isotherm (*D-R*) is generally applied to express the adsorption mechanism (physical or chemical) with a Gaussian energy distribution onto a heterogeneous surface [47]. This isotherm model is more general than Langmuir isotherm because it does not assume a homogeneous surface or a constant adsorption potential and is related to the porous structure of the adsorbent. The linear form of *D-R* isotherm equation is represented as:

$$\ln q_e = \ln K_{DR} - \beta\,\text{Є}^2 \qquad (11)$$

where K_{DR} is the theoretical saturation capacity (mol g^{-1}), β is a constant related to the mean free energy of adsorption per mole of the adsorbate (mol^2 J^{-2}), Є is Polanyi potential which is mathematically represented as:

$$\text{ε} = \ln(1 + 1/C_e)\; x\; RT \qquad (12)$$

where, C_e is the equilibrium concentration of adsorbate in solution (mol L^{-1}), *R* is the gas constant (J mol^{-1} K^{-1}) and *T* is the absolute temperature (K). The *D-R* model constants, K_{DR} and β, can be determined from the intercept and slope of linear plot of ln q$_e$ versus Є^2, respectively.

The constant β gives an idea about the mean free energy *E* (kJ mol^{-1}) of adsorption per molecule of the adsorbate when it is transferred to the surface of the solid from infinity in the solution and can be calculated from the relationship:

$$E = \frac{1}{\sqrt{-2\beta}} \qquad (13)$$

If the magnitude of *E* is between 8 and 16 kJ mol^{-1}, the adsorption process is supposed to proceed via ion-exchange or chemisorption, while for values of *E*<8 kJmol^{-1}, the adsorption process is of physical nature [48].

Figures 8 and 9 show the adsorption isotherms of CV on ZFA and ZBA, respectively, where the experimental values and curves achieved from the values estimated by the Langmuir, Freundlich and D-R models are presented. The adsorption efficiency was between 78 to 99% ZFA and 65 to 96% for ZBA at equilibrium time.

Giles et al. [49] state that isotherm shapes are largely determined by the adsorption mechanism, and thus can be used to explain the nature of adsorption. The adsorption isotherm for solution may be classified into four main classes relating to their shapes termed S, L, H and C and subgroups 1, 2, 3, 4 or max. The equilibrium isotherms for the system CV/ZFA showed sigmoidal curve in the class with the corresponding behavior L2. In processes where such isotherms are obtained, the adsorption of solute onto the adsorbent proceeds until a monolayer is established; the formation of further layers is not possible in this case [50].

Comparing the isotherm for the system CV/ZBA with those given by Giles et al [49], L4 type of isotherm (Langmuir type with two layers) appears to fit the adsorption data well. After the first degree of saturation of the surface, further adsorption takes place on new surface.

Figures 10 and 11 illustrate the Langmuir, Freundlich and *D-R* plots for the removal of CV by ZFA and ZBA, respectively. The Langmuir, Freundlich, and *D-R* isotherm constants are given in Table 5 along with the corresponding correlation coefficients.

187

Orbital: Electron. J. Chem. 5 (3):179-191, 2013
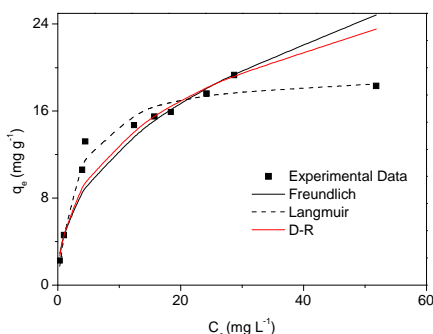
**Figure 8.** Adsorption isotherm of CV onto ZFA (T = 25 °C; t agitation = 10 min).
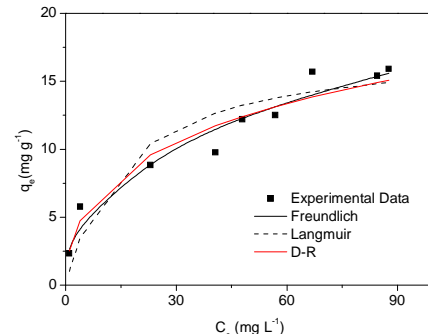
Figure 9. Adsorption isotherm of CV onto ZBA (T = 25 °C; t agitation = 10 min).
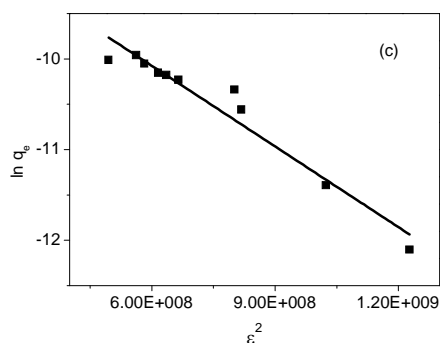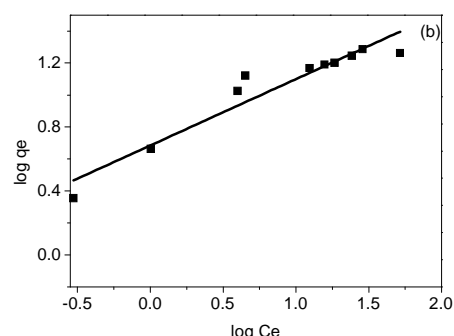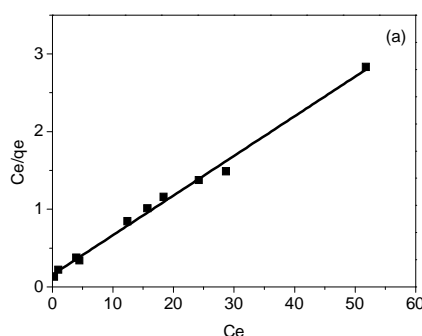

Figure 10. Langmuir (a), Freundlich (b) and D-R (c) plots for adsorption of CV onto ZFA.

Table 5. Parameters of the models of Langmuir isotherm, Freundlich and *D-R* for the CV dye on adsorbents and values and Chi-square (χ^2)

	Adsorbents	
Lagmuir	ZFA	ZBA
Q_o (mg g^{-1})	19.6	17.7
B (L mg^{-1})	0.329	0.0630
R	0.997	0.961
X^2	0.706	4.53
Freundlich		
K_F (mg g^{-1})(L mg^{-1})$^{1/n}$	4.83	2.66
N	2.41	2.53
R	0.959	0.981
X^2	4.42	0.869
D-R		
β (mol^2 J^{-2})	2.96 x 10^{-9}	3.03 x 10^{-9}
K_{DR} (mol g^{-1})	2.49 x 10^{-4}	1.39 x 10^{-4}
E (kJ mol^{-1})	13.0	12.8
R	0.973	0.983
X^2	3.01	0.966

188

*Orbital: Electron. J. Chem. 5 (3):179-191, 2013*
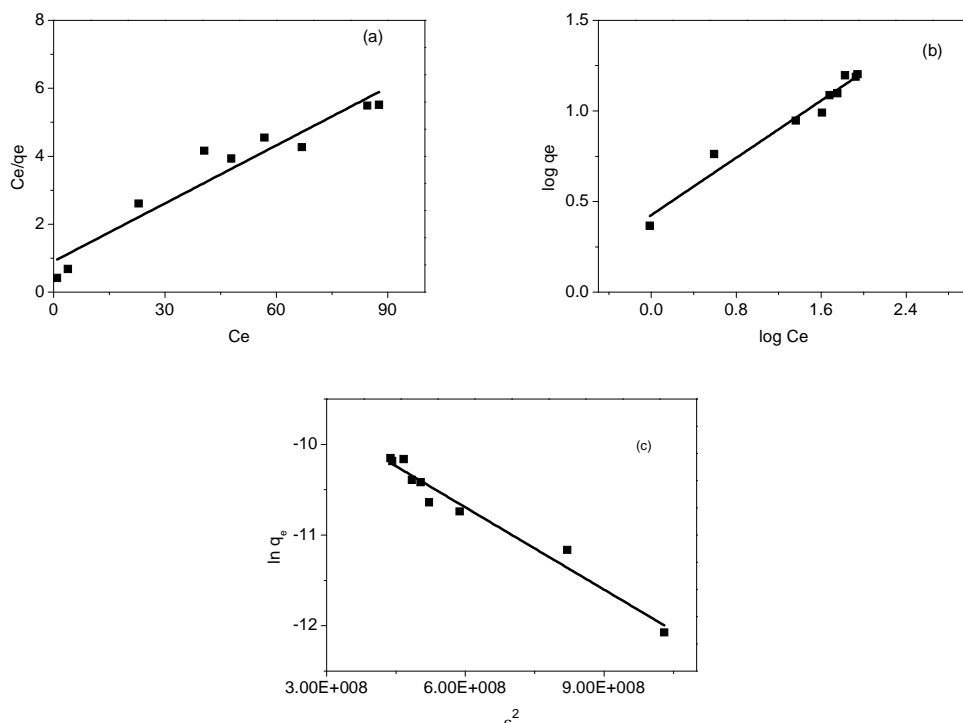
Figure 11. Langmuir (a), Freundlich (b) and *D-R* (c) plots for adsorption of CV onto ZBA.

By comparing the correlation coefficient values obtained from the Langmuir, Freundlich and D-R isotherm models, it can be concluded that the Langmuir isotherm model is more suitable for CV/ZFA while the experimental data obtained for CV/ZBA were fitted well by the Freundlich isotherm model. This may be due to both homogeneous and heterogeneous distribution of active sites on the surface of the ZBA. Both energy distributions induce single and multilayer adsorption. These might occur simultaneously or subsequently by order of time, both in a random manner [51].

The adsorption for the system CV/ZFA obeys Langmuir isotherm better, indicating predominantly homogeneous distribution of active sites on the ZFA surface, since the Langmuir equation assumes that the adsorbent surface is energetically homogeneous.

The Freundlich isotherm constant, n, gives an idea for the favorability of the adsorption process. The value of n should be less than 10 and higher than unity for favorable adsorption conditions. As can be seen from Table 5, the n values for ZFA and ZBA were in the range of 1-10, indicating that the adsorption is a favorable process. By evaluating the *D-R* isotherm model, the mean adsorption energy, *E*, values were found to be 13.0 kJ mol^{-1} for ZFA and 12.8 kJ mol^{-1} for ZBA, suggesting that the adsorption mechanisms of CV onto zeolitic materials are chemical in nature.

The non-linear regression Chi-square (X^2) test was employed as a criterion for the fitting quality due to the inherent bias resulting from linearization of isotherm models. Therefore, it is necessary to analyze the data set using the Chi-square test to confirm the best fit isotherm for the adsorption system combined with the values of the correlation coefficient. This statistical analysis is based on the sum of the squares of the differences between the experimental and model calculated data, of which each squared difference was divided by the corresponding data obtained by calculating from models [52]. The Chi-square can be represented by

$$\chi^2 = \sum \frac{(q_e \exp - q_e calc)^2}{q_e calc} \qquad (14)$$

where $q_e$exp is the equilibrium capacity of the adsorbent obtained from experiment (mg·g^{-1}), and $q_e$calc is the equilibrium capacity obtained by calculating from the model (mg·g^{-1}). A low value of X^2 indicates that experimental data fit better to the value from the model.

Table 5 also shows the values obtained in non-linear test or Chi-square (X^2). The values of regression coefficients, *R* and the linear error functions, X^2, are in agreement to one another. The

189

Orbital: Electron. J. Chem. 5 (3):179-191, 2013

lower value of X^2 confirmed statistically a better fit to the Langmuir isotherm for the CV/ZFA system and the Freundlich isotherm for the CV/ZBA system.

The maximum adsorption of capacity of CV, according Langmuir, was about 10% higher on the zeolite ZFA than on the zeolite ZBA, not being a very significant difference. The result of performance of the ZFA was expected because this material will have particles sizes smaller than the zeolite from coal botton ash due granulometric characteristics of the ash sample that served as raw material. Thus, decreasing the particle size increases the externa surface area, which means increasing the number of active sites available for adsorption of the adsorbate and thus increases the efficiency of adsorption [53].

Adsorbents like zeolites consist primarily of silicon and aluminium oxides, whose hydroxylated surface develop negative charges in aqueous solution. The adsorption of CV on the zeolite of coal ash will occurs by electrostatic attraction between the negatively charged sites of the adsorbent and the positively charged dye molecules ($=N^+(CH_3)_2$) and also by cation exchange.

Table 6 lists a comparison of maximum monolayer adsorption capacity of CV on various adsorbents. A close look at the values displayed reveals that the present adsorbents (ZFA and ZBA) have a maximum CV dye uptake value comparable with the reported values in some cases. The adsorption capacity varies, and it depends on the characteristics of the individual adsorbent and the initial concentration of the adsorbate. However, the present experiments are conducted to find the technical applicability of the low-cost adsorbents to treat CV.

Table 6. Comparison of the maximum adsorption of capacities of CV dye onto various adsorbents

Adsorbents	Q_o (mg g^{-1})	References
Fly ash	74.6	[54]
Bottom ash	12.1	[55]
Sepiolite	77.0	[56]
Sulphuric acid	85.8	[5]
Activated carbon	19.8	[57]
ZFA	19.6	This study
ZBA	17.6	This study

4. CONCLUSION

The present study showed that is possible to convert coal ash into zeolitic materials by alkaline hydrothermal treatment. The X-ray diffraction analysis demonstrated that hydroxy-sodalite and NaX zeolites were formed after the synthesis. These zeolites synthesized from fly ash (ZFA) and bottom ash (ZBA) are effective adsorbents for removal the cationic dye crystal violet from aqueous solution. The pseudo-second order model provides the best correlation of the experimental data for both adsorbents and intraparticle diffusion is involved in the adsorption process, but it is not the only rate-limiting step. The equilibrium data fit with the Langmuir isotherm for ZFA and the Freundlich isotherm for ZBA. The adsorption capacity for ZFA was found to be 19.6 mg g^{-1} and for ZBA 17.6 mg g^{-1}. The use of the southern Brazilian coal ash generated in power plants for the production of zeolites can constitute an alternative and noble use for a residue which has contributed to the degrading of wide areas.

6. REFERENCE AND NOTES

[1]   Kant, R. *Nat. Sci.* **2012**, *4*, 22. [CrossRef]

[2]   Carneiro, P. A.; Pupo Nogueira R. F.; Zanoni, M. V. B. *Dye. Pigment*. **2007**, *74*, 127. [CrossRef]

[3]   Adak, A.; Bandyopadhyay, M.; Pal, A. *Sep. Purif. Technol.* **2005**, *44*, 139. [CrossRef]

[4]   Ayed, L.; Chaieb, K.; Cheref, A. *World J. Microbiol. Biotechnol.* **2009**, *25*, 705. [CrossRef]

[5]   Senthilkumaar, S.; Kalaamani, P.; Subburaam, C. V. *J. Hazard. Mater*. **2006**, *136*, 800. [CrossRef]

[6]   Mittal, A.; Mittal, J.; Malviya, A.; Kaur, D.; Gupta, V. K. *J. Colloid Interface Sci.* **2010**, *343*, 463. [CrossRef]

[7]   Dabrowski, A. *Adv. Coll. Interface Sci.* **2001**, *93*,135.

190

Orbital: Electron. J. Chem. 5 (3):179-191, 2013

[CrossRef]

[8] Orthman, J.; Zhu, H. Y.; Lu, G. Q. *Sep. Purif. Technol.* **2003**, *31*, 53. [CrossRef]

[9] Fungaro, D. A.; Magdalena, C. P.; *Int. J. of Chem. Environ. Eng. Sci.* **2012**, *3*, 74.

[10] Ahmaruzzaman, M. Adv. Colloid and Interface Sci. **2011**, *166*, 36.

[11] Bhatnagar, A.; Sillanpää, M. *Chem. Eng. J.* **2010**, *157*, 277. [CrossRef]

[12] Gupta V. K.; Carrott, P. J. M.; Ribeiro-Carrot, M. M. L.; Suhas. *Crit. Rev. Environ. Sci. Technol.* **2009**, *39*, 783. [CrossRef]

[13] Gupta, V.K.; Suhas *J. Environ. Manage.* **2009**, *90*, 2313. [CrossRef]

[14] Fungaro, D. A.; Grosche, L. C.; Pinheiro, A. S.; Izidoro, J. C.; Borrely, S. I. *Orbital Elec. J. Chem.* **2010**, *2*, 235. [Link]

[15] Levandowski, J.; Kalkreuth, W. *Int. J. Coal Geol.* **2009**, *77*, 269. [CrossRef]

[16] Fungaro, D. A.; Bruno, M., Grosche, L. C. *Desalin. Water Treat.* **2009**, *2*, 231. [CrossRef]

[17] Cheriaf, M., Péra, J., Rocha, J. C. *Cem. Concr. Res.* **1999**, *29*, 1387. [CrossRef]

[18] Fungaro, D. A.; Silva, M. G. *Quim. Nova* **2002**, *25*, 1081. [CrossRef]

[19] Fungaro, D. A.; Flues, M. S-M; Celebroni, A. P. *Quim. Nova* **2004**, *27*, 582. [CrossRef]

[20] Fungaro, D. A.; Izidoro, J. C.; Almeida, R. S.; *Eclética Quim.* **2005**, *30*, 31. [CrossRef]

[21] Fungaro, D. A.; Izidoro, J. C. *Tchê Quím.* **2006a**, *3*, 21.

[22] Fungaro, D. A.; Izidoro, J. C. *Quim. Nova* **2006b,** *29*, 735. [CrossRef]

[23] Querol, X.; Moreno, N.; Umaña, J. C.; Alastuey, A.; Hernández, E.; López-Soler A.; Plana, F. *Int. J. Coal Geol.* **2002**, *50*, 413. [CrossRef]

[24] Rayalu, S. S.; Bansiwal, A. K.; Meshram, S. U.; Labhsetwar, N.; Devotta, S. *Catal. Sur. Asia* **2006**, *10*, 74. [CrossRef]

[25] Carvalho, T. E. M.; Fungaro, D. A.; Magdalena, C. P.; Cunico, P. *J. Radioanal. Nucl. Chem.* **2011**, *289*, 617. [CrossRef]

[26] Izidoro, J. C.; Fungaro, D. A.; Santos, F. S.; Wang, S. *Fuel Process Technol.* **2012a**, *97*, 38. [CrossRef]

[27] Izidoro, J. C.; Fungaro, D. A.; Wang, S. *Adv. Mater. Res*. **2012b**, *356-360*, 1900. [CrossRef]

[28] Fungaro, D. A.; Yamaura, M.; Carvalho, T. E. M. *J. At. Mol. Sci.* **2011**, *2*, 305.

[29] Fungaro, D. A.; Graciano, J. E. A. *Adsorpt. Sci. Technol.* **2007**, *10*, 729. [CrossRef]

[30] Henmi, T. *Soil Sci. Plant Nutr.* **1987**, *33*, 517. [CrossRef]

[31] Scott, J.; Guang, D.; Naeramitmarnsuk, K.; Thabuot, M. J. *Chem. Technol. Biotechnol.* **2002**, *77*, 63. [CrossRef]

[32] Shigemoto, N.; Hayashi, H.; Miyaura, K. *J. Mater. Sci.* **1993**, *28*, 4781. [CrossRef]

[33] Kreuz, A. L. Utilização de cinzas pesadas de termelétricas na substituição de cimento e areia na confecção de concretos. [Master's thesis.] Florianópolis, Brazil: Departamento de Engenharia Civil da Universidade Federal de Santa Catarina, 2002.

[34] Paprocki, A. Síntese de zeólitas a partir de cinzas de carvão visando sua utilização na descontaminação de drenagem ácida de mina. [Master's thesis.] Porto Alegre, Brazil, Pontifícia Universidade Católica do Rio Grande do Sul, 2009.

[35] Sijakova-Ivanova, T.; Panov, Z.; Blazev, K.; Zajkova-Paneva, V. *Int. J. Eng. Sci. Technol.* **2011**, *3*, 8219.

[36] Depoi, F. S.; Pozebon, D.; Kalkreuth, W. D. *Int. J. Coal Geol.* **2008**, *76*, 227. [CrossRef]

[37] Fungaro, D. A.; Borrely, S. I. *Ceram.* **2012**, *58*, 77 (in Portuguese with English abstract). [CrossRef]

[38] Umaña-Peña, J.C. Síntesis de zeolitas a partir de cenizas volantes de centrales termoeléctricas de carbón. [PhD Thesis.] Barcelona, Espanha, Universitat Politécnica de Catalunya, 2002.

[39] Ho, Y. S.; McKay, G. *Can. J. Chem. Eng.* **1998**, *76*, 822. [CrossRef]

[40] Ho, Y. S.; Wase, D. A. J.; Forstera C.F. *Environ. Technol.* **1996**, *17*, 71. [CrossRef]

[41] Weber, W. J.; Morris, J. C. *Sanit J. Engin. Div., ASCE*, **1963**, *89*, 31.

[42] Allen, S. J.; McKay, G.; Khader, K.Y.H. *Environ. Pollut.* **1989**, *56*, 39. [CrossRef]

[43] Helby, W. A. *Chem. Eng.* **1952**, *59*, 153.

[44] Weber, W. J. Jr In: Weber W.J. Jr (ed) Physicochemical processes for water quality control, New York: Wiley-Interscience, 1972.

[45] Zou, W.; Zhao, L.; Han, R. *J. Radioanal. Nucl. Chem.* **2011**, *288*, 239. [CrossRef]

[46] Mall, I. D.; Srivastava, V. C.; Agarwal, N.; K.; Mishra, I. M. *Chemosphere* **2005**, *61*, 492. [CrossRef]

[47] Dubinin, M. M.; Radushkevich, L. V. *Proc. Acad. Sci. USSR Phys. Chem. Sect*. **1947**, *55*, 331.

[47] Giles, C. H.; MacEwan, T. H.; Nakhwa, S. N.; Smith, D. *J. Chem. Soc. London* **1960**, 3973.

[48] Helfferich, F. Ion Exchange; McGraw-Hill: New York, 1962.

[49] Giles, C. H.; Smith, D.; Huitson, A. *I. Theoretical. J. Colloid Interface Sci.* **1974**, *47*, 755. [CrossRef]

[50] Giles, C. H.; MacEwan, T. H.; Nakhwa, S. N.; Smith, D. *J. Chem. Soc. London* **1960**, 3973.

[51] Mohd Din, A.T.; Hameed, B. H. *J. Appl. Sci. in Environ. Sanitation* **2010**, *5*, 161.

[52] Ho, Y. S., *Carbon* **2004**,42, 2115. [CrossRef]

[53] Ali, A. A.-H.; El-Bishtawi, R. *J. Chem. Technol. Biotechnol.* **1997**, *69*, 27. [CrossRef]

[54] Çoruh, S.; Geyikçi, F.; Nuri O. N. ATINER'S Conference Paper Series, Athens, Greece, 2012.

[55] Gandhimathi, R.; Ramesh S.T.; Sindhu, V., Nidheesh P.V. *Iran J. Energy & Environ.* **2012**, *3*, 52.

[56] Eren E.; Cubuk, O.; Ciftci H.; Eren, B.; Caglar, B. *Desalin.* **2010**, *252*, 88. [CrossRef]

[57] Malarvizhi, R.; Ho, Y. S. *Desalin.* **2010**, *264*, 97. [CrossRef]

191

Orbital: Electron. J. Chem. 5 (3):179-191, 2013

Full Paper

Estudo das Propriedades do Pseudofruto do Cajueiro na Adsorção de Cr (VI)

Thiago C. Medeiros, Fátima I. C. C. Martins, Ronaldo F. do Nascimento, Maria das G. Gomes*

Departamento de Química Analítica e Físico-Química, Universidade Federal do Ceará, Centro de Ciências, Bloco 940, Campus Universitário do Pici, Caixa Postal 6021, CEP 60455-970 Fortaleza, Ceará, Brasil.

Abstract: In this study, the Cr (VI) adsorption properties by cashew (*Anacardium occidentale* L.) were studied in a batch system. The effects of pH (5.0 and 7.0), drying process – S (oven-dried and lyophilized), particle size – P (0.10 – 0.25 and 0.25 – 0.84 mm), mass of adsorbent – m (1.0 and 1.5 g) initial chromium concentration – C (500 and 1000 mg L^{-1}) contact time – t (1 and 3 h) and stirring rate – v (0 and 150 rpm), on the adsorption process were studied using a fractional factorial design (2^{7-4}). Under ideal conditions the efficiency of adsorption of 87.24% for total chromium and 100.00% for Cr (VI) were achieved. The maximum adsorption capacity achieved was 11.43 mg/g. The adsorbent was characterized by infrared and X-ray fluorescence spectroscopy. Test reactions performed with Cr (VI) in conjunction with the aqueous extract of the adsorbent and pH monitoring during adsorption were carried out to better understand the mechanisms of adsorption. The proposed mechanism consists of two steps: reduction of Cr (VI) in solution or at the surface of the adsorbent and subsequent adsorption of Cr (III) by ion exchange or complexation.

Keywords: adsorption; chromium; cashew; factorial design

1. INTRODUÇÃO

O cromo é um metal tóxico utilizado em vários processos dentre eles: fabricação de aço e outras ligas metálicas, na preservação de madeira, curtimento de couro, eletrodeposição, na fabricação de tijolos refratários, pigmentos, corantes, fluidos de perfuração, inibidores de corrosão e produtos têxteis [1, 2].

A especiação deste metal é de extrema importância, pois as duas espécies mais estáveis de cromo em solução, Cr (III) e Cr (VI), diferem muito em seus níveis de toxicidade. O cromo (III) em níveis traços é considerado nutriente essencial para o organismo humano, estando envolvido no metabolismo da glicose, lipídeos e proteínas, onde sua deficiência na dieta alimentar está relacionada à elevada taxa de glicose no sangue, insulina, colesterol e triglicerídeos [3]. A forma hexavalente, entretanto, é cinco mil vezes mais tóxica que a trivalente [4]. Cromo (VI) é extremamente tóxico para animais e vegetais e a exposição por inalação, toque ou ingestão pode provocar ulceração e perfuração do septo nasal, irritação do trato respiratório, dores de cabeça, ulcerações na pele, danos na córnea, vómito, possíveis efeitos cardiovasculares, gastrointestinais, hematológicos, hepáticos e renais, além do risco elevado de câncer pulmonar [5, 6].

Os efluentes contendo cromo têm se tornado um sério problema ambiental. Ao serem despejados no meio ambiente contaminam água, solo e ar. As duas formas de contaminação possíveis para o homem são por exposição direta ou indireta. A exposição direta pode ocorrer através do contato dérmico com água e solo, inalação de particulados contendo cromo, ou ingestão acidental de solo ou água contaminados. A exposição indireta ocorre devido à sua capacidade de bioacumulação, contaminando vegetais, peixes e outros alimentos e chegando ao homem por ingestão destes [7]. Dessa forma a remoção de cromo dos efluentes é extremamente importante, de forma a evitar que o seu despejo contamine os mananciais e os organismos vivos causando danos irreparáveis.

A remoção de íons em efluentes industriais pode ser feita através de processos como precipitação,

---
*Corresponding author. E-mail: gracinha@ufc.br

coagulação, troca iônica, extração com solvente, osmose reversa, adsorção em carvão ativo, redução e separação por membrana [8-10]. As resinas de troca iônica são muito utilizadas nas indústrias para remoção de íons em água potável ou em águas de caldeira e na purificação de substâncias orgânicas e inorgânicas. Entretanto, o emprego destas resinas para tratar efluentes contendo metais tóxicos torna-se economicamente inviável [11].

Devido ao alto custo de algumas técnicas, tem crescido o interesse dos pesquisadores por métodos eficientes, de baixo custo e que não afetem o meio ambiente. Sendo assim, várias pesquisas vêm sendo feitas com a finalidade de utilizar adsorventes ou trocadores iônicos naturais [12-16].

Na adsorção de cromo pode ser utilizada uma série de adsorventes de origem natural como, por exemplo, casca do coco [17], bagaço de milho [18], bagaço de azeitona [19], flor de palmeira [9], palha de arroz [20], pó de café [21], farinha de canola [22], plantas aquáticas [23], cascas de caranguejo [24] etc.

Por conter em sua composição celulose, hemicelulose e lignina o pedúnculo do caju é caracterizado como um material lignocelulósico [25]. Nos materiais lignocelulósicos a celulose e a hemicelulose se encontram ligadas à lignina por ligações covalentes e ligações de hidrogênio [15]. Sabe-se que a lignina e a celulose são biopolímeros que possuem capacidade de adsorção de metais tóxicos [12,26-28]. Portanto, este trabalho objetivou estudar as propriedades adsorventes do pseudofruto do cajueiro (*Anacardium occidentale L.*) para adsorção de Cr (VI). O cajueiro pertence à família *Anacardiaceae* que é representada por 76 gêneros e mais de 600 espécies [29]. Trata-se de uma planta rústica, típica de regiões de clima tropical [30].

2. MATERIAIS E MÉTODOS

Obtenção e preparo do material adsorvente

O bagaço de caju (*Anacardium occidentale L.*) foi fornecido pela empresa Embrapa Agroindústria Tropical situada no Campus do Pici da Universidade Federal do Ceará (UFC). Foi realizada secagem em estufa a 65°C e liofilização do bagaço de caju obtido por prensagem. Na secagem em estufa foi utilizada estufa com circulação de ar forçado (Marconi, MA035/3, Brasil), sem controle de velocidade do ar e de umidade. O processo simples de secagem, foi escolhido para verificar a possibilidade de seu uso sem muitos recursos financeiros ou equipamentos mais sofisticados. A espessura inicial obtida não pôde ser medida em peneiras ABNT já que o material se apresentou na forma de fibra. A liofilização foi realizada em liofilizador piloto (Liobraz, LT 510, Brasil). Após secagem o adsorvente foi triturado em moinho de facas (Marconi, MA-048, Brasil) e separado em várias faixas de granulometria entre 0,074 e 0,84 mm em agitador (CERTECH, ST 023, Brasil) provido de peneiras ABNT. Em seguida as frações foram acondicionas em recipientes plásticos e mantidas em dessecador.

Soluções utilizadas

Foram preparadas soluções estoque, para diversos experimentos, nas concentrações de 500 e 1000 mg L^{-1} em Cr (VI) a partir do reagente K_2CrO_4 de grau analítico, fabricante Vetec. Soluções de $KHC_8H_4O_4$ 0,1 mol L^{-1}, KH_2PO_4 0,1 mol L^{-1} e NaOH 0,1 mol L^{-1} foram utilizadas no preparo de soluções tampão de pH 5 e 7 para utilização nos ensaios de adsorção [31] (Tabela 1)

Tabela 1. Composição das soluções tampão utilizadas.

Tampão	$KHC_8H_4O_4$ 0,1 mol L^{-1} (mL)	KH_2PO_4 0,1 mol L^{-1} (mL)	NaOH 0,1 mol L^{-1} (mL)	Volume Total (mL)	Força Iônica calculada (mol L^{-1})
pH 5	50,0	-	22,6	100,0	0,08
pH 7	-	50,0	29,1	100,0	0,09

Instrumentação

A determinação do teor de cromo total foi realizada utilizando-se chama de ar/acetileno redutora e comprimento de onda de 357,9 nm em espectrômetro de absorção atômica (EAA) Varian, AA240FS, Austrália. O teor de Cr (VI) foi determinado por método espectrofotométrico da difenilcarbazida [32] utilizando espectrofotômetro UV-Vis Varian, Cary 1E, Canadá. O teor de Cr (III) foi determinado pela diferença entre o teor de cromo total e Cr (VI).

193

Orbital: Electron. J. Chem. 5 (3):192-205, 2013

Estudo do efeito das variáveis na adsorção

Foram conduzidos experimentos de adsorção em batelada conforme planejamento fatorial fracionário para estudar o efeito das variáveis no processo de adsorção. A Tabela 2 mostra as variáveis utilizadas nos experimentos de adsorção.

Tabela 2. Variáveis codificadas utilizadas no planejamento fatorial fracionário 2^{7-4} para estudar a adsorção de cromo pelo bagaço do caju.

Código	Variável	(-)	(+)
pH	pH	5,0	7,0
S	Secagem	Estufa	Liofilizado
P	Tamanho de part. (mm)	0,10 – 0,25	0,25 – 0,84
m	Massa de adsorvente (g)	1,0	1,5
C	Conc. inicial cromo (mg L^{-1})	500	1000
t	Tempo (h)	1	3
v	Taxa de agitação (rpm)	0	150

Os únicos parâmetros fixos nestes experimentos foram o volume de solução padrão de K$_2$CrO$_4$ (15 mL) e o volume de solução-tampão utilizado (10 mL). As respostas utilizadas nesse planejamento foram o rendimento de adsorção de cromo total e de Cr (VI) e a capacidade de adsorção de cromo total pelo bagaço do caju.

O rendimento do processo de adsorção para cromo total foi calculado através da seguinte expressão:

$$\eta_{Crtotal} = \frac{C_0 - C_e}{C_0} \times 100 \qquad \text{(Equação 1)}$$

Onde C_0 e C_e (mg/L) são as concentrações de cromo total em solução no início e no equilíbrio, respectivamente, e $\eta_{Crtotal}$ (%) é o rendimento do processo de adsorção.

O rendimento do processo de adsorção de Cr (VI) foi calculado pela expressão:

$$\eta_{Cr(VI)} = \frac{C_0' - C_e'}{C_0'} \times 100 \qquad \text{(Equação 2)}$$

Onde C'_0 e C'_e (mg/L) são as concentrações de Cr (VI) em solução no início e no equilíbrio, respectivamente, e $\eta_{Cr(VI)}$ (%) é o rendimento do processo de adsorção de Cr (VI).

O cálculo da capacidade de adsorção foi feito através da seguinte expressão:

$$q_e = \frac{V(C_0 - C_e)}{m} \qquad \text{(Equação 3)}$$

Onde V (L) é o volume de solução, m (g) é a massa de adsorvente utilizada e q_e (mg/g) é a capacidade de adsorção de cromo total.

Com os resultados deste planejamento fatorial fracionário foi feito o estudo da influência das variáveis sobre o processo de adsorção. Cada experimento foi realizado em duplicata. Os resultados obtidos foram ajustados a um modelo linear para cada uma das respostas através do uso de Análise de Variância (ANOVA). Os diagramas de Pareto foram construídos com os resultados da aplicação do teste *t* de Student.

Espectroscopia no Infravermelho

Os espectros de absorção na região do infravermelho (IV) [33] foram obtidos a partir da dispersão das amostras de caju em pastilhas de brometo de potássio (KBr), utilizando um espectrômetro ABB BOMEM, modelo FTLA 2000, Canadá. Os espectros de IV dos extratos aquosos do adsorvente também foram investigados. Os extratos, após secagem, foram dispersos em pastilhas de KBr para determinação dos espectros.

Fluorescência de Raios-X

A Espectroscopia por Fluorescência de Raios X é uma técnica não destrutiva que permite a análise qualitativa e quantitativa, estabelecendo uma proporção de cada elemento presente numa amostra. A técnica consiste em expor a amostra a um feixe de radiação para excitação e medição da radiação fluorescente proveniente da amostra [34].

As análises de fluorescência de raios-X do adsorvente foram realizadas em espectrômetro de fluorescência de raios-X marca RIGAKU, modelo ZSX II mini, Japão. A análise foi realizada nas

194

Orbital: Electron. J. Chem. 5 (3):192-205, 2013

amostras de caju *in natura* e após adsorção de cromo.

3. RESULTADOS E DISCUSSÃO

Estudo do efeito das variáveis na adsorção

Realizou-se um planejamento fatorial fracionário para se estudar o processo de adsorção de Cr (VI) pelo bagaço do caju. Foram estudados os efeitos de sete variáveis na adsorção. Com base nos resultados do planejamento foi possível se entender como cada variável afeta o rendimento de adsorção. A tabela 3 apresenta os resultados de rendimento de adsorção de cromo total e Cr (VI) e na capacidade de adsorção de cromo total para cada ensaio do planejamento realizado.

Tabela 3. Resultados obtidos no planejamento fatorial fracionário 2^{7-4} para estudar a adsorção de cromo pelo bagaço de caju.

	Variáveis codificadas									
Ensaio	*pH*	*S*	*P*	*m**	*C**	*t**	*v**	$\eta_{Cr\ total}$ (%)	$\eta_{Cr\ VI}$ (%)	$q_{e\ Cr\ total}$ (mg/g)
1	-	-	-	+	+	+	-	49,07 ± 3,07	69,72 ± 5,52	4,90 ± 0,31
2	+	-	-	-	-	+	+	86,27 ± 0,18	100,00 ± 0,03	6,45 ± 0,01
3	-	+	-	-	+	-	+	76,80 ± 1,19	93,74 ± 0,29	11,43 ±0,05
4	+	+	-	+	-	-	-	66,31 ± 1,08	98,45 ± 0,94	3,31 ± 0,06
5	-	-	+	+	-	-	+	78,58 ± 2,04	100,00 ± 0,03	3,92 ± 0,11
6	+	-	+	-	+	-	-	9,13 ± 7,57	34,06 ± 8,67	6,26 ± 0,25
7	-	+	+	-	-	+	-	48,13 ± 1,66	84,86 ± 0,96	3,61 ± 0,13
8	+	+	+	+	+	+	+	87,24 ± 0,32	100,00 ± 0,00	8,72 ± 0,03

* Relações geradoras: I = 124 = 135 = 236 = 1237

O experimento de número 8 foi o que mostrou melhor rendimento de adsorção de cromo total (87,24%). Já para o rendimento de adsorção de Cr (VI) os experimentos de número 2, 5 e 8 apresentaram rendimento máximo (100,00%). Isso mostra que o experimento de número 8, no qual todas as variáveis estão no nível máximo, apresentou melhores resultados para o rendimento de adsorção de Cr (VI) e cromo total. Analisando os dados de capacidade de adsorção o experimento de número 3 foi o que mostrou melhores resultados (11,43 mg/g). Neste experimento as variáveis secagem, concentração inicial e taxa de agitação foram mantidas no nível máximo e as demais no nível mínimo. A capacidade de adsorção atingida neste trabalho para o bagaço de caju apresenta valor similar a outros adsorventes reportados na literatura (Tabela 4).

Tabela 4. Capacidade de adsorção de vários adsorvente reportados na literatura.

Biomaterial	q_e (mg/g)		Referência
	Cr (VI)	Cr (III)	
flor de palmeira	4,90	6,24	[9]
palha de arroz	3,15	-	[20]
folhas de mangue	8,87	2,63	[23]
junco	1,66	7,18	[23]
carvão ativo comercial	15,47	-	[35]
carvão ativo obtido de casca de coco	10,88	-	[35]
Aspergillus niger	Cr total: 15,2		[36]
bagaço de cana	5,75	-	[37]
sabugo de milho	3,0	-	[37]
torta de *Jatropha*	11,75	-	[37]
farelo de trigo	-	93	[38]
casca de eucalipto	45	-	[39]
bagaço de caju	Cr total: 11,43		este trabalho

195

Orbital: Electron. J. Chem. 5 (3):192-205, 2013

Os resultados foram analisados através do software Minitab® 16, e as estimativas dos efeitos principais foram determinadas. O efeito de um fator é definido pela mudança observada na resposta devido à alteração no nível do fator.

Os modelos matemáticos codificados empregados para o planejamento fatorial fracionário 2^{7-4} foram:

$$\eta_{Cr\ total} = 62,69 - 0,45pH + 6,93S - 6,92P + 7,61m - 7,13C + 4,99t + 19,53v \quad \text{(Equação 4)}$$

$$\eta_{Cr\ VI} = 85,11 - 1,98pH + 9,15S - 5,37P + 6,94m - 10,73C + 3,54t + 13,33v \quad \text{(Equação 5)}$$

$$q_{e\ Cr\ total} = 5,46 - 0,50pH + 1,30S - 1,06P - 0,25m + 1,14C + 0,46t + 2,17v \quad \text{(Equação 6)}$$

As equações 4 a 6 apresentam modelos matemáticos lineares que descrevem o comportamento do sistema. Com o uso dessas equações pode-se calcular a eficiência de remoção de cromo total (Equação 4) ou de Cr (VI) (Equação 5) e a capacidade de adsorção de cromo total (Equação 6) através da substituição das variáveis pelos seus valores codificados (–1 ou +1). Essas equações são importantes, pois resumem toda a informação do planejamento realizado de forma compacta e através delas podemos calcular todos os resultados da Tabela 3 com bastante exatidão.

Os efeitos de cada variável podem ser representados graficamente para facilitar sua visualização. Na Figura 1 estão representados os valores dos efeitos no rendimento de adsorção de cromo total. Analisando os dados da Figura 1 é possível se entender como cada variável afeta a resposta. O aumento do pH não provocou uma mudança significativa no percentual de cromo adsorvido (–0,91%). Dentre os dois tipos de secagem utilizados o caju liofilizado mostrou melhores resultados no percentual médio de remoção de cromo total (+13,86%). O tamanho de partícula apresentou efeito negativo (–13,84%) na eficiência de remoção de cromo total. Isto significa que a faixa de granulometria que mostrou melhores resultados foi a de 0,10 – 0,25 mm. Por ser formada por partículas de menor tamanho esta faixa apresenta maior área superficial o que significa mais sítios de adsorção disponíveis. O aumento da massa também promoveu um aumento na eficiência do processo (+15,22%). Isto se deve ao simples fato de o sistema ter maior quantidade de adsorvente e, portanto mais sítios de adsorção. O aumento da concentração inicial de cromo apresentou um efeito negativo na resposta (–14,26%). Em um nível de concentração maior há mais adsorbato no meio para uma mesma quantidade de adsorvente o que provoca uma redução no rendimento do processo. O tempo apresentou efeito positivo na resposta (+9,97%). O efeito mais significativo no processo de adsorção foi o da taxa de agitação do sistema (+39,06%). O rendimento médio de adsorção no sistema com agitação (82,22%) foi quase o dobro do rendimento no sistema sem agitação (43,16%). O aumento da agitação facilita o contato entre adsorbato e adsorvente. Dessa forma o sistema leva um tempo consideravelmente menor até atingir o estado de equilíbrio.
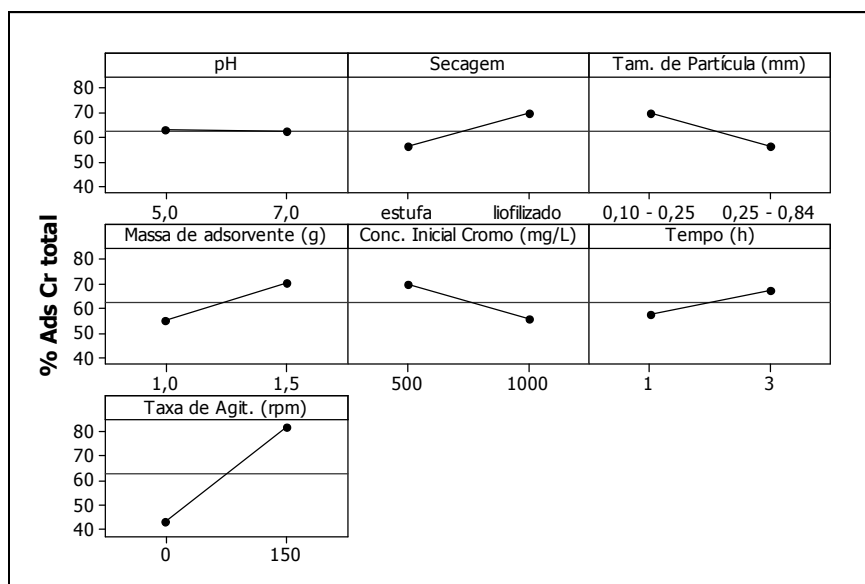

Figura 1. Efeitos das variáveis no rendimento de adsorção de cromo total pelo bagaço do caju.

196

Orbital: Electron. J. Chem. 5 (3):192-205, 2013

Na Figura 2 estão representados os valores dos efeitos no rendimento de adsorção de Cr (VI). Uma mudança entre os níveis mínimo e máximo das variáveis *pH*, *S*, *P*, *m*, *C*, *t* e *v*, resulta em variações de, respectivamente, –3,95; +18,31; –10,74; +13,88; –21,46; +7,08 e +26,67% na eficiência de remoção.
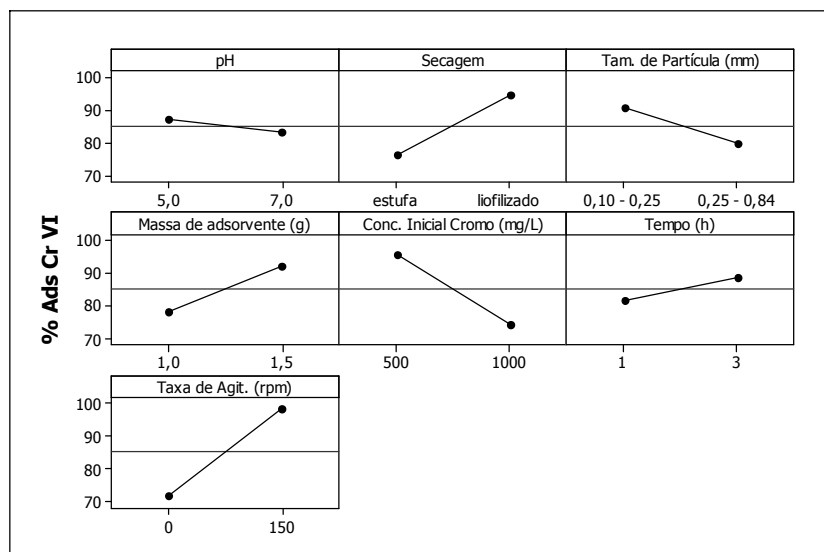

Figura 2. Efeitos das variáveis no rendimento de adsorção de Cr (VI) pelo bagaço do caju.

Na Figura 3 estão representados os valores dos efeitos na capacidade de adsorção de cromo total. Uma mudança entre os níveis mínimo e máximo das variáveis *pH*, *S*, *P*, *m*, *C*, *t* e *v*, resulta em variações de, respectivamente, –1,00; +2,61; –2,12; –0,50; +2,28; +0,91 e +4,34 mg/g. Observa-se que o aumento da massa apresenta um efeito negativo na capacidade de adsorção e o aumento da concentração um efeito positivo, ao contrário do que ocorre com o rendimento de adsorção. Isto se deve ao fato de a capacidade de adsorção levar em conta a quantidade de cromo adsorvida por unidade de massa de adsorvente. Para uma dada concentração inicial de cromo ao se aumentar a massa de adsorvente a capacidade de adsorção diminui, pois uma massa maior entra no denominador da equação 3. De modo similar uma concentração inicial maior provoca um aumento da diferença entre C_0 e C_e na equação 3 resultando em um aumento de q_e.
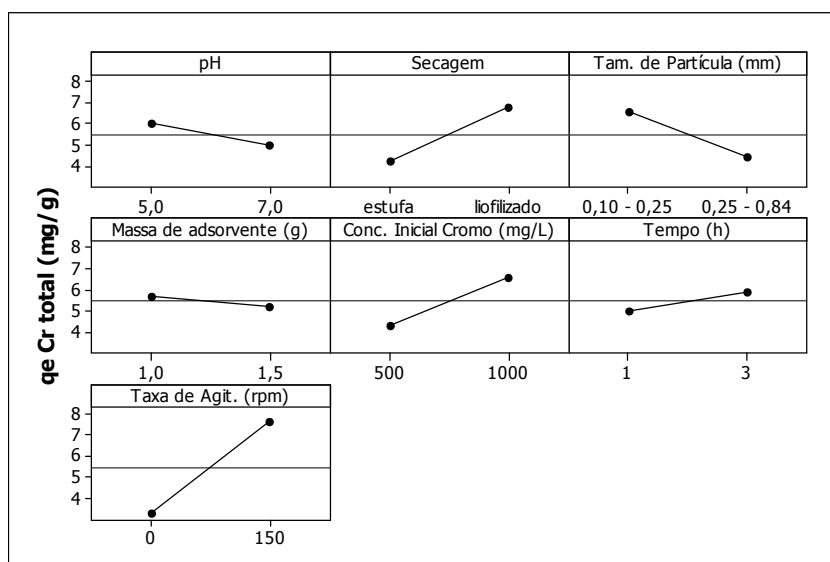

Figura 3: Efeitos das variáveis na capacidade de adsorção de cromo total pelo bagaço do caju.

197

Orbital: Electron. J. Chem. 5 (3):192-205, 2013

Para analisar a significância de cada efeito foram gerados diagramas de Pareto. A Figura 4 apresenta o diagrama de Pareto para a eficiência de remoção de cromo total. Pode-se observar que todas as variáveis estudadas são influentes no processo de adsorção com 95% de confiança, com exceção do pH. Isto significa que não há diferença estatística significativa na resposta ao se variar o valor de pH nessa faixa de valores. Observou-se que a variável mais influente na resposta foi a taxa de agitação.
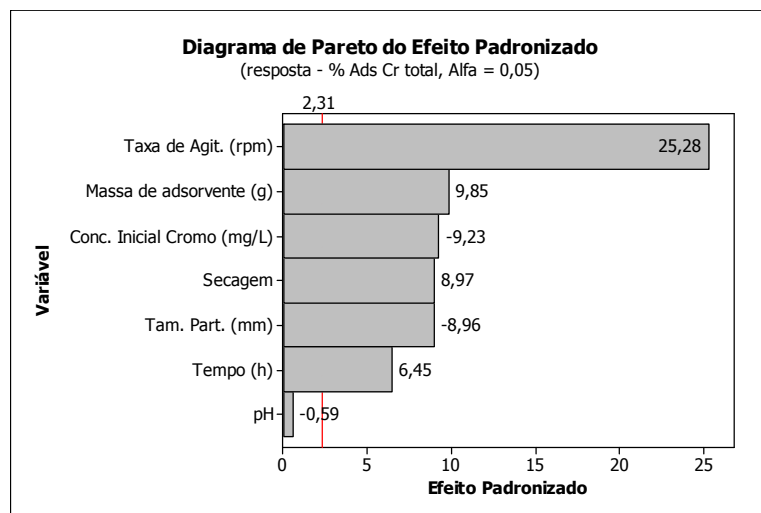

Figura 4. Diagrama de Pareto do efeito padronizado em termos de adsorção de cromo total.

A Figura 5 apresenta o diagrama de Pareto para a eficiência de remoção de Cr (VI). Da mesma forma que na Figura 4, todas as variáveis são influentes no processo com 95% de confiança, com exceção do pH, sendo a taxa de agitação a variável mais influente.
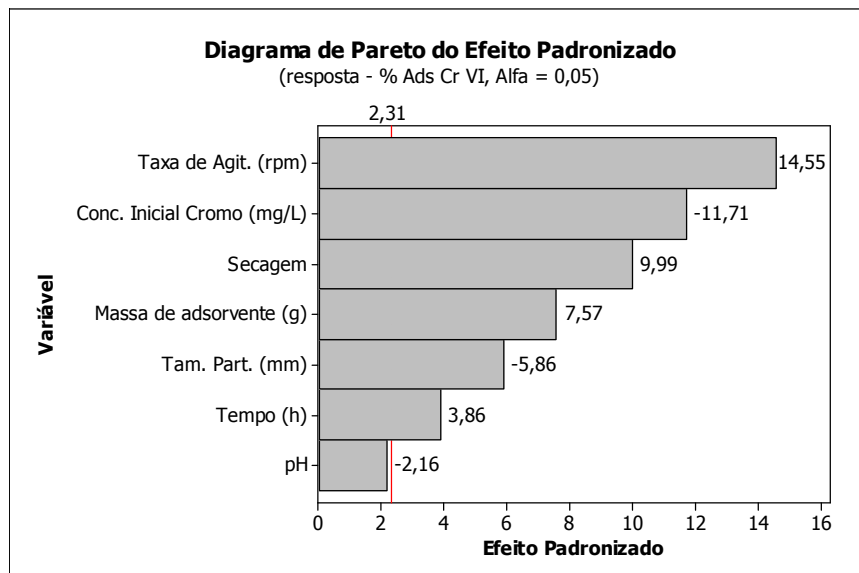

Figura 5. Diagrama de Pareto do efeito padronizado em termos de adsorção de Cr (VI).

A Figura 6 apresenta o diagrama de Pareto para a capacidade de adsorção de cromo total. Todas as variáveis são influentes com 95% de confiança sendo a taxa de agitação a variável mais influente. O pH se mostrou uma variável influente, ao contrário do que ocorre ao se considerar o

198

Orbital: Electron. J. Chem. 5 (3):192-205, 2013

rendimento de adsorção como resposta. É conhecido na literatura que valores de pH mais ácidos favorecem o processo de adsorção de cromo por materiais lignocelulósicos [40, 41].
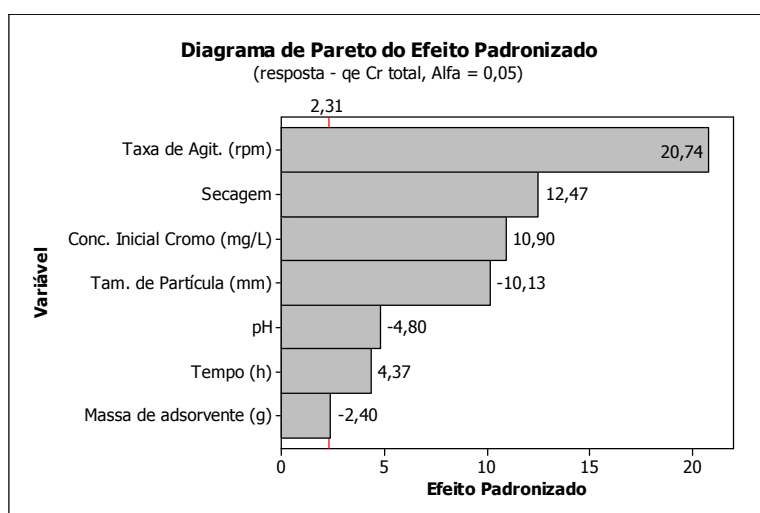

Figura 6. Diagrama de Pareto do efeito padronizado em termos de capacidade de adsorção de cromo total

Espectroscopia no Infravermelho

Os espectros de absorção na região do infravermelho (IV) das amostras de caju seco em estufa e liofilizado estão apresentados na figura 7. Os gráficos estão deslocados no eixo das ordenadas para facilitar visualização. Os espectros apresentam perfil típico de materiais lignocelulósicos. A banda de absorção larga em 3381 cm⁻¹ indica a presença de estiramentos dos grupos –OH e –NH, mostrando assim a presença de grupos hidroxil e amino no adsorvente. As bandas em 2926 e 2854 cm⁻¹ são devido a estiramento assimétrico e simétrico de grupos –CH$_2$, respectivamente. As bandas de absorção em 1744 e 1641 cm⁻¹ são devido ao estiramento C=O em aldeídos e cetonas conjugados (1744 cm⁻¹) e não-conjugados (1641 cm⁻¹) a anéis aromáticos. A banda de absorção em 1537 cm⁻¹ é devido ao estiramento da ligação C=C de anel aromático. O íon carboxilato apresentou duas bandas: estiramento C=O em 1447 e 1373 cm⁻¹. A banda em 1236 cm⁻¹ representa estiramento do grupo –SO$_3$. As bandas de absorção em 1034 e 1154 cm⁻¹ são referentes ao estiramento C–OH em álcoois primários e secundários, respectivamente.
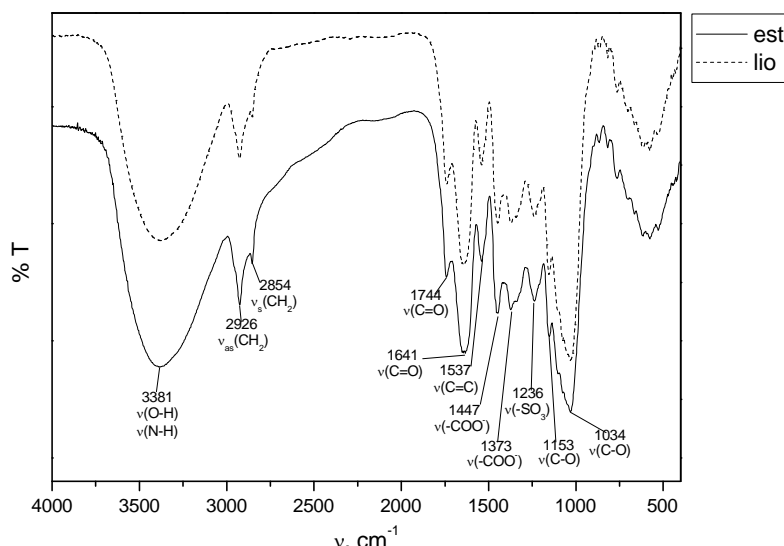
**Figura 7.** Espectros de IV do bagaço do caju seco em estufa (est) e liofilizado (lio).

199

Orbital: Electron. J. Chem. 5 (3):192-205, 2013

A Figura 8 mostra os espectros das amostras de adsorvente após contato com solução contendo Cr (VI). Observou-se uma diminuição na intensidade do pico C–O após adsorção do Cr (VI). Por outro lado houve um aumento na banda de absorção C=O. Sabe-se que o Cr (VI) é um forte agente oxidante, que pode oxidar álcoois primários e secundários a suas correspondentes, cetonas, ácidos carboxílicos e outros compostos tendo hidrogênios benzílicos a ácidos benzoicos [23]. Isto indica que o Cr (VI) pode ter provocado a oxidação branda de álcoois primários e secundários na estrutura lignocelulósica a seus correspondentes aldeídos e cetonas.
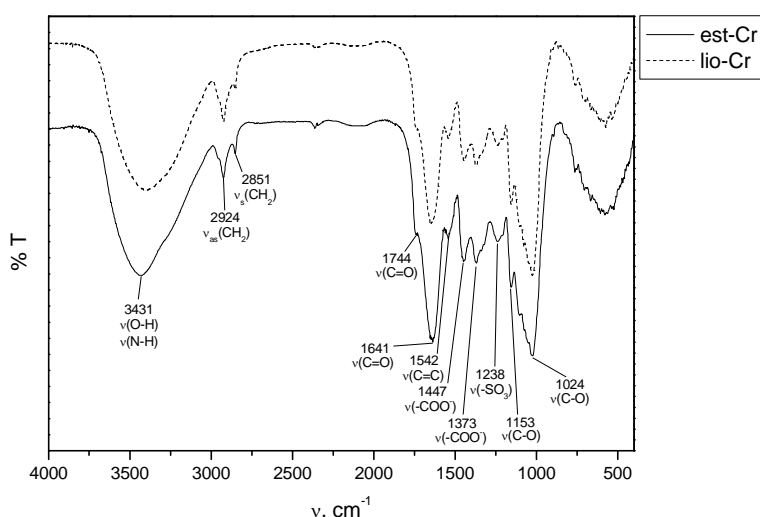

Figura 8. Espectros de IV do bagaço do caju seco em estufa (est-Cr) e liofilizado (lio-Cr) após adsorção.

Também foram analisados os espectros de absorção na região do infravermelho dos extratos aquosos do adsorvente seco em estufa e liofilizado. Após extração com água destilada, os extratos foram secos para obtenção dos espectros em fase sólida. Os espectros estão apresentados na Figura 9. Os espectros dos adsorventes (Figura 7) e os espectros dos extratos aquosos (Figura 9) apresentam diferença espectral na faixa de 1700–1100 cm^{-1} com ausência de algumas bandas de absorção nos espectros dos extratos e outras bandas com menor intensidade. Isso é devido a apenas alguns componentes do adsorvente, açúcares, fenóis, taninos etc., solúveis em água, estarem presentes nos extratos.
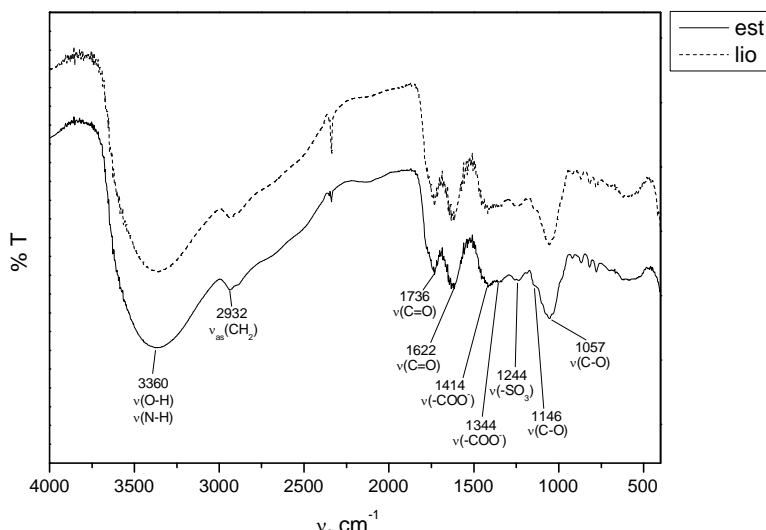

Figura 9. Espectros de IV do extrato aquoso seco obtido do bagaço do caju seco em estufa (est) e liofilizado (lio).

200

Orbital: Electron. J. Chem. 5 (3):192-205, 2013

A Figura 10 apresenta os espectros dos extratos aquosos do adsorvente após contato com solução contendo Cr (VI). Observou-se um aumento expressivo na intensidade da banda de absorção C=O (1630 cm^{-1}) e também da banda referente ao íon carboxilato (1387 cm^{-1}).
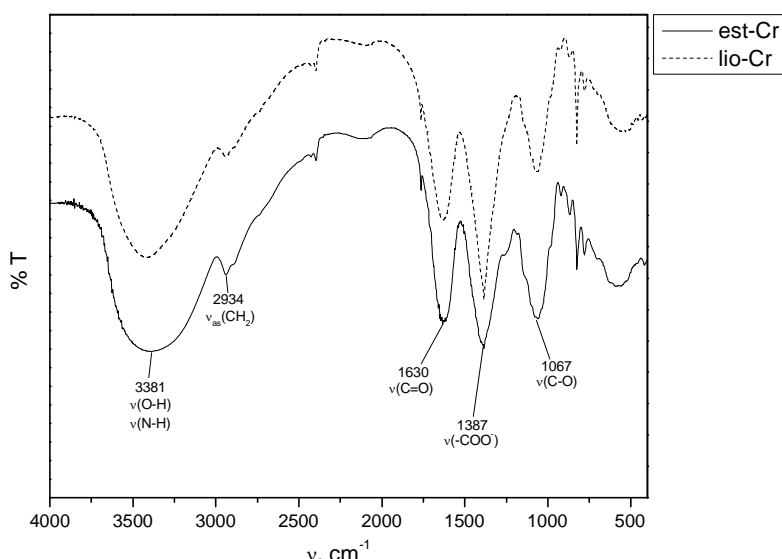

Figura 10. Espectros de IV do extrato aquoso seco obtido do bagaço do caju seco em estufa (est-Cr) e liofilizado (lio-Cr) após contato com solução contendo Cr (VI).

Isto indica que a oxidação dos compostos extrativos pelo Cr (VI) é mais intensa em solução, pois leva à formação de ácidos carboxílicos. Sugere-se, portanto, que a redução do cromo ocorra em maior extensão em solução por reação com os compostos extrativos do adsorvente e em menor extensão por contato com a estrutura lignocelulósica do adsorvente. Isto faz sentido, pois reações em solução são mais favorecidas devido ao contato íntimo entre os reagentes. Nas reações em superfície a área de contato está limitada pela interface entre sólido e líquido. Não se observou diferenças apreciáveis nos espectros com diferentes tipos de secagem (estufa e liofilização). Como os dois tipos de tratamento não apresentam diferenças estruturais o processo de secagem em estufa é recomendado devido ao custo mais baixo.

Fluorescência de Raios-X

Os resultados da análise de fluorescência de raios-X do bagaço do caju seco em estufa são mostrados na Tabela 5. A coluna 'adsorvente *in natura*' mostra os elementos naturalmente presentes no adsorvente. Após adsorção ocorre um aumento significativo do teor de cromo na superfície, passando de zero para 82,1% do total da superfície. Vale

ressaltar que os valores expressos na tabela 5 fazem jus a percentuais relativos dos elementos presentes na superfície do adsorvente, portanto não são valores absolutos. Os valores na coluna 'após adsorção' foram recalculados com base na entrada do cromo devido ao processo de adsorção não necessariamente implicando na redução da quantidade desses elementos no adsorvente. Observa-se, porém, uma redução significativa no teor de potássio na superfície. No adsorvente in natura o teor de potássio é de 59,4% enquanto o de cálcio é apenas 14,7%. Após a adsorção o teor de todos os elementos diminui devido à entrada do cromo. O teor de potássio passa a ser apenas 5,3% enquanto o de cálcio 9,3%. Isto indica que houve liberação de potássio para a solução, pois do contrário o teor de potássio ainda seria superior ao de cálcio. Esses resultados indicam a perda de potássio para solução, provavelmente por processo de troca iônica. O potássio por possuir alta mobilidade iônica, pode estar sendo substituído por íons Cr (III) nos sítios de adsorção.

Papel do pH na redução do Cr (VI)

Foi realizado experimento de adsorção em batelada com pH inicial igual a 7,0 sem adição de solução-tampão. O pH então ficou livre para variar

201

Orbital: Electron. J. Chem. 5 (3):192-205, 2013

no decorrer do processo de adsorção. O pedúnculo do caju possui caráter ácido apresentando um pH igual a 4,2 [42]. Observou-se, então, no decorrer da adsorção uma redução do pH inicial chegando a 4,4 ao final do processo (Figura 11).
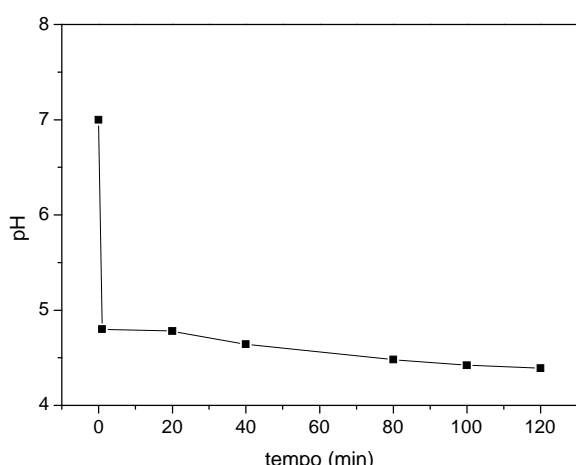

Figura 11. pH *versus* tempo de adsorção.

Tabela 5: Percentual relativo de elementos presente na superfície do adsorvente antes e após adsorção a partir de fluorescência de raios-X.

Elemento	Adsorvente *in natura* (%)	Após adsorção (%)
K	59,41	5,29
Ca	14,72	9,29
Fe	2,99	1,93
Cd	7,80	0,00
P	6,16	0,00
S	5,62	1,39
Si	2,22	0,00
Cl	1,08	0,00
Cr	0,00	82,11

No início do processo de adsorção o pH do meio era igual a 7,0. Neste pH a espécie de Cr (VI) predominante no meio é CrO_4^{2-} (Figura 12).

A redução do Cr (VI) pode ser então regida preferencialmente pela reação de redução do CrO_4^{2-} [43, 44]:

$$CrO_4^{2-} + 4H_2O + 3e^- \rightleftharpoons Cr(OH)_3 + 5OH^-$$

$E^o = -0,13$ V   (Equação 7)
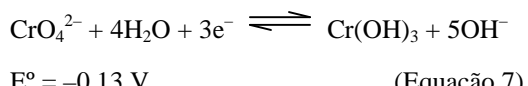
Porém, logo após o tempo 0 o pH cai abaixo de 5,0 provavelmente devido à liberação de compostos orgânicos de caráter ácido para o meio aquoso. O pH continua diminuindo com o tempo e estabiliza em 4,4 após 120 minutos. Na faixa de pH em que a maior

parte do processo se desenvolve (entre 4,5 e 5,0) as espécies de Cr (VI) predominantes no meio são $HCrO_4^-$ e $Cr_2O_7^{2-}$ (Figura 12). O processo de redução então pode ser descrito pelas reações [43-45]:

$$Cr_2O_7^{2-} + 14H^+ + 6e^- \rightleftharpoons 2Cr^{3+} + 7H_2O$$

$E^o = 1,33$ V   (Equação 8)

$$HCrO_4^- + 7H^+ + 3e^- \rightleftharpoons Cr^{3+} + 4H_2O$$
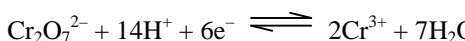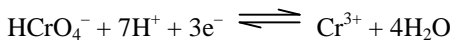
$E^o = 1,20$ V   (Equação 9)
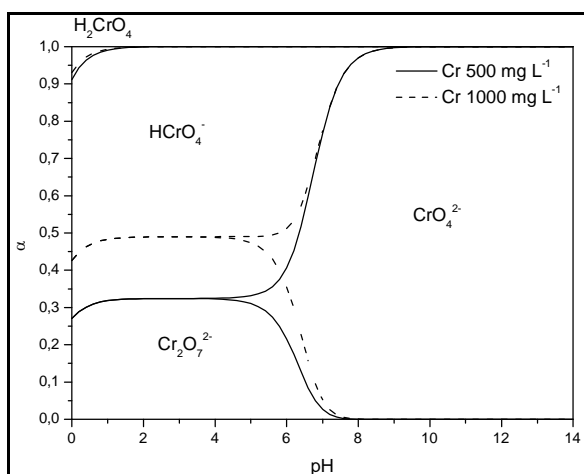
Figura 12. Diagrama de distribuição de espécies do Cr (VI) em solução (I = 0,05 mol L^{-1}).

O Cr (III) resultante da reação de redução pode participar de várias reações de equilíbrio em solução, estando presente majoritariamente na forma de *aqua* e hidroxo-complexos, na ausência de agentes complexantes [44, 46]:

$$Cr(H_2O)_6^{3+} + H_2O \rightleftharpoons Cr(OH)(H_2O)_5^{2+} + H_3O^+$$

(Equação 10)

$$Cr(OH)(H_2O)_5^{2+} + H_2O \rightleftharpoons Cr(OH)_2(H_2O)_4^+ + H_3O^+$$

(Equação 11)

$$Cr(OH)_2(H_2O)_4^+ + H_2O \rightleftharpoons Cr(OH)_3(H_2O) + H_3O^+$$

(Equação 12)
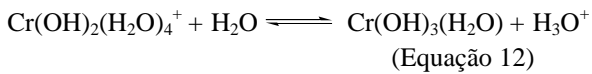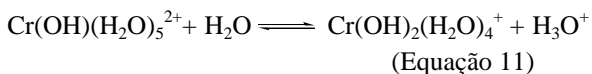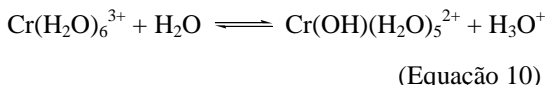
Porém, no sistema de adsorção aplicado neste trabalho existem outros agentes complexantes como, por exemplo, cloretos e sulfatos que são encontrados no adsorvente (Tabela 5) e podem ser liberados para a solução. Também existem compostos fenólicos e taninos liberados do adsorvente que podem complexar com o Cr (III) [47].

Em meios concentrados, o que é o caso deste trabalho, podem ser gerados também complexos

202

Orbital: Electron. J. Chem. 5 (3):192-205, 2013

polinucleares do Cr (III) como $Cr_2(OH)_2^{4+}$, $Cr_3(OH)_4^{5+}$ e $Cr_4(OH)_6^{6+}$ [46]. Nos níveis de concentração utilizados (entre 500 e 1000 mg L^{-1}) podemos considerar a espécie de Cr(III) predominante no pH 4,4 como sendo $Cr_3(OH)_4^{5+}$ (Figura 13).
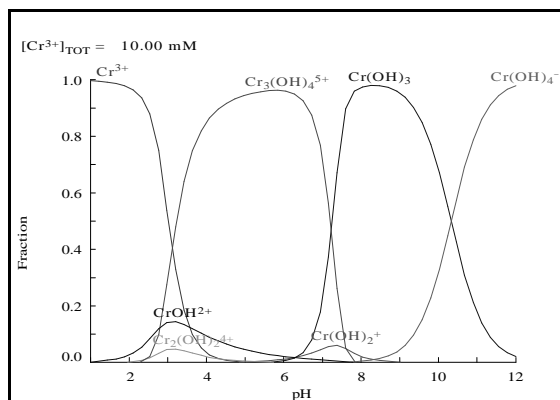

Figura 13. Diagrama de distribuição de espécies do Cr (III) em solução.

Esta espécie pode ser formada no sistema através da seguinte reação de hidrólise:

$$3Cr^{3+} + 4H_2O \rightleftharpoons Cr_3(OH)_4^{5+} + 4H^+ \text{ (Equação 13)}$$
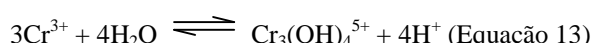
Além da reação de hidrólise também são liberados prótons da biomassa por adsorção via troca iônica do Cr (III) reduzido [48]. Conclui-se, portanto, que uma série de reações que envolvem prótons estão presentes durante a adsorção de Cr (VI). As reações de redução do Cr (VI) consomem prótons, porém o caráter ácido do adsorvente juntamente com as reações de hidrólise do Cr (III) e a liberação de prótons pelo mecanismo de adsorção por troca iônica prevalecem fazendo com que o pH final seja menor do que o pH inicial.

Papel da matéria orgânica na redução do Cr (VI)

Para melhor compreensão do mecanismo de adsorção uma solução contendo apenas Cr (VI) foi colocada em contato com o extrato aquoso do adsorvente (Tabela 6). Após 24 h de contato observa-se redução substancial do cromato. Em média 38,41% do cromo total foi reduzido a Cr (III) o que mostra que os compostos extrativos por si só possuem capacidade de redução do íon cromato. Elangovan *et al.* estudaram a adsorção de Cr (VI) por várias plantas aquáticas e associaram a redução do Cr (VI) ao conteúdo de fenóis totais e taninos na matéria

orgânica liberada pelos adsorventes [23]. Os autores afirmam que há uma correlação direta entre a quantidade de matéria orgânica liberada e o percentual de Cr (VI) reduzido.

Tabela 6. Percentual de Cr(III) e Cr(VI) após 24 h de contato de solução contendo inicialmente apenas Cr(VI) com extrato aquoso do adsorvente.

Ensaio	Cr III (%)	Cr VI (%)
1	31,30	68,70
2	46,60	53,40
3	40,59	59,41
4	35,16	64,84
Média ± DP	**38,41 ± 6,66**	**61,59 ± 6,66**

Esses resultados mostram que o extrato aquoso por si só possui capacidade de reduzir o Cr (VI) à sua forma menos tóxica, Cr (III). Entretanto, o processo de redução é mais intenso com a presença do adsorvente, pois neste caso, a redução do Cr (VI) também ocorre na superfície do adsorvente. Após a redução, parte do Cr (III) pode formar complexos com taninos e outros compostos fenólicos e ficar estável em solução não chegando a ser adsorvido na superfície. Outra parte do Cr (III) chega até à superfície e é adsorvida através de troca iônica ou através de ligações covalentes com a superfície. Romero-González *et al.* reportaram a biossorção de Cr (III) em *Agave lechuguilla* [49]. A biossorção foi devida a interação do íon Cr (III) com grupos carboxílicos na superfície do tecido celular do adsorvente. Suksabye *et al.* usaram casca de coco no tratamento de águas residuais de galvanoplastia e sugeriram que Cr (III) pode estar adsorvido através de ligações covalentes com os grupos C=O e O–CH$_3$ nos quais pares de elétrons livres nos átomos de oxigênio podem ser doados para formação da ligação com Cr (III) [17]. Os grupos amino e carboxil em aminoácidos e os átomos de nitrogênio e oxigênio das ligações peptídicas em proteínas podem estar disponíveis no adsorvente para formação de ligações coordenadas com íons metálicos [24].

Parte do cromo que não foi reduzida pode ser adsorvida também na forma de Cr (VI), porém este processo é menos efetivo devido à repulsão de cargas negativas do ânion com a superfície carregada negativamente do adsorvente [50]. Liu *et al.* reportaram que a redução do Cr (VI) é a etapa limitante na biossorção do mesmo [6].

De acordo com Park *et al.* Cr (VI) pode ser

203

Orbital: Electron. J. Chem. 5 (3):192-205, 2013

removido do meio aquoso por biomateriais através de dois mecanismos: redução direta (I) e redução indireta (II) [51]. Os dois mecanismos ocorrem na superfície do biomaterial. De acordo com os dados deste trabalho sugerimos que a redução ocorre também em solução por reação com os compostos extrativos do adsorvente. Estes resultados estão de acordo com dados encontrados na literatura [9, 23]. O mecanismo proposto consiste em duas etapas: redução do Cr (VI) em solução ou em contato com a superfície; e posterior adsorção do Cr (III) por troca iônica ou complexação. Os grupos de superfície envolvidos no processo de adsorção podem ser carboxil, carbonil, hidroxil, fenol e amino, dentre outros.

4. CONCLUSÃO

O estudo realizado através de planejamento fatorial fracionário foi adequado na determinação do efeito das variáveis no rendimento de adsorção de cromo total e Cr (VI). As melhores condições de rendimento de adsorção de cromo total, 87,24%, e Cr (VI), 100,00%, foram alcançadas ao se manter todas as variáveis no nível máximo. A capacidade de adsorção máxima, 11,43 mg/g, foi obtida ao se manter as variáveis secagem, concentração inicial e taxa de agitação no nível máximo e as demais no nível mínimo. Os modelos matemáticos gerados para o conjunto de dados obtidos por planejamento fatorial podem ser usados para prever a resposta em uma dada condição experimental.

Os espectros de infravermelho comprovaram a oxidação parcial do adsorvente devido à reação de redução do Cr (VI). Os dados de fluorescência de raios-X confirmaram a adsorção do cromo no adsorvente. Com o monitoramento do pH durante a adsorção foi possível se obter uma melhor compreensão da dinâmica do cromo durante o processo de adsorção.

Os ensaios realizados com o extrato aquoso do adsorvente em contato com Cr (VI) mostraram que o processo de redução pode ocorrer também em solução. Esses dados estão de acordo com a literatura e confirmam que o mecanismo de adsorção predominante é composto de duas etapas: redução do Cr (VI) em solução ou em contato com a superfície; e posterior adsorção do Cr (III) por troca iônica ou complexação.

5. AGRADECIMENTOS

6. REFERÊNCIAS E NOTAS

[1] Rifkin, E.; Gwinn, P.; Bouwer, E. *Environ. Sci. Technol.* **2004**, *38*, 267A. [CrossRef][PubMed]

[2] Suksabye, P.; Nakajima, A.; Thiravetyan, P.; Baba, Y.; Nakbanpote, W. *J. Hazard. Mater.* **2009**, *161*, 1103. [CrossRef][PubMed]

[3] Gomes, M. R.; Rogero, M. M.; Tirapegui, J. *Rev. Bras. Med. Esporte* **2005**, *11*, 262. [CrossRef]

[4] Available from: http://www.atsdr.cdc.gov/ToxProfiles/tp7.pdf. Access February, 2013.

[5] Janegitz, B. C.; Lourenção, B. C.; Lupetti, K. O.; Fatibello-Filho, O. *Quim. Nova* **2007**, *30*, 879. [CrossRef]

[6] Liu, C. C.; Wang, M. K.; Chiou, C. S.; Li, Y. S.; Lin, Y. A.; Huang, S. S. *Ind. Eng. Chem. Res.* **2006**, *45*, 8891. [CrossRef]

[7] Wang, Z.; Chen, J.; Chai, L.; Yang, Z.; Huang, S.; Zheng, Y. *J. Hazard. Mater.* **2011**, *190*, 980. [CrossRef][PubMed]

[8] Noeline, B. F.; Manohar, D. M.; Anirudhan, T. S. *Sep. Purif. Technol.* **2005**, *45*, 131. [CrossRef]

[9] Elangovan, R.; Philip, L.; Chandraraj, K. *Chem. Eng. J.* **2008b**, *141*, 99. [CrossRef]

[10] Shibi, I. G.; Anirudhan, T. S. *J. Chem. Technol. Biotechnol.* **2006**, *81*, 433. [CrossRef]

[11] Aguiar, M. R. M. P.; Novaes, A. C.; Guarino, A. W. S. *Quim. Nova* **2002**, *25*, 1145. [CrossRef]

[12] Bailey, S. E.; Olin, T. J.; Bricka, R. M.; Adrian, D. D. *Water Res.* **1999**, *33*, 2469. [CrossRef]

[13] Blais, J. F.; Shen, S.; Meunier, N.; Tyagi, R. D. *Environ. Technol.* **2003**, *24*, 205. [CrossRef][PubMed]

[14] Demirbas, A. *J. Hazard. Mater.* **2008**, *157*, 220. [CrossRef][PubMed].

[15] Miretzky, P.; Cirelli, A. F. *J. Hazard. Mater.* **2010**, *180*, 1. [CrossRef][PubMed]

[16] Sud, D.; Mahajan, G.; Kaur, M. P. *Bioresour. Technol.* **2008**, *99*, 6017. [CrossRef][PubMed]

[17] Suksabye, P.; Thiravetyan, P.; Nakbanpote, W.; Chayabutra, S. *J. Hazard. Mater.* **2007**, *141*, 637. [CrossRef][PubMed]

[18] Bosinco, S.; Roussy, J.; Guibal, E.; Cloirec, P. L. *Environ. Technol.* **1996**, *17*, 55. [CrossRef]

[19] Gharaibeh, S. H.; Abu-El-Shar, W. Y.; Al-Kofahi, M. M. *Water Res.* **1998**, *32*, 498. [CrossRef]

[20] Gao, H.; Liu, Y.; Zeng, G.; Xu, W.; Li, T.; Xia, W. *J. Hazard. Mater.* **2008**, *150*, 446. [CrossRef][PubMed]

[21] Orhan, Y.; Büyükgüngör, H. *Water Sci. Technol.* **1993**, *28*, 247.

[22] Al-Ashed, S.; Duvnjak, Z. *Water Qual. Res. J. Can.* **1996**, *31*, 319.

204

Orbital: Electron. J. Chem. 5 (3):192-205, 2013

[23]   Elangovan, R.; Philip, L.; Chandraraj, K. *J. Hazard. Mater.* **2008a**, *152*, 100. [CrossRef][PubMed]

[24]   Niu, H.; Volesky, B. *Hydrometallurgy* **2003**, *71*, 209. [CrossRef]

[25]   Hon, D. N. S. Chemical modification of lignocellulosic materials. 1st ed. New York: Marcel Dekker, 1996.

[26]   Gaballah, I.; Goy, D.; Allain, E.; Kilbertus, G.; Thauront, *J. Metall. Mater. Trans. B.* **1997**, *28*, 13. [CrossRef]

[27]   Guo, X.; Zhang, S.; Shan, X. *J. Hazard. Mater.* **2008**, *151*, 134. [CrossRef][PubMed]

[28]   LV, J.; Luo, L.; Zhang, J.; Christie, P., Zhang, S. *Environ. Pollut.* **2012**, *162*, 255. [PubMed]

[29]   Janick, J.; Paull, R. E. The Encyclopedia of fruit and nuts. 1st ed. Cambridge: Cambridge University Press, 2008.

[30]   Available   from: http://www.embrapa.gov.br/imprensa/artigos/2005/artigo.2005-12-29.6574944222. Acess May, 2012.

[31]   Kolthoff,   I.   M.;   Sandell, E.   B.; Meehan, E. J.; Bruckenstein, S. Quantitative chemical analysis. 4th ed. New York: Mcmillan, 1969.

[32]   American Public Health Association. Standard methods for examination of water and wasterwater. 21. ed. Washington: American Public Health Association, 2005.

[32]   Nakamoto, K. Infrared and Raman spectra of inorganic and coordination compounds, Part B. 6th ed. New Jersey: John Wiley & Sons, 2009.

[33]   Lachance, G. R.; Claisse, F. Quantitative X-Ray fluorescence analysis: theory and application, 1st ed. New York: John Willey & Sons, 1995.

[34]   Babel, S.; Kurniawan, T. A. *Chemosphere* **2004**, *54*, 951. [CrossRef][PubMed]

[35]   Mungasavalli, D. P.; Thiruvenkatachari, V.; Jin, Y. *Colloids Surf. A* **2007**, *301*, 214. [CrossRef]

[36]   Garg, U. K.; Kaur, M. P.; Garg, V. K.; Sud., D. *J. Hazard. Mater.* **2007**, *140*, 60. [CrossRef][PubMed]

[37]   Farajzadeh, M. A.; Monji, A. B. *Sep. Purif. Technol.* **2004**, *38*, 197. [CrossRef]

[38]   Sarin, V.; Pant, K. K. *Bioresour. Technol.* **2006**, 97, 15. [CrossRef][PubMed]

[39]   Nakano, Y.; Takeshita, K.; Tsutsumi, T. *Water Res.* **2001**, *35*, 496. [CrossRef]

[40]   Park, D.; Yun, Y.; Park, J. M. *Environ. Sci. Technol.* **2004**, *38*, 4860. [CrossRef][PubMed]

[41]   Paiva, F. F. A.; Garruti, D. S.; Silva Neto, R. M. Aproveitamento Industrial do caju. 1ª ed. Fortaleza: Embrapa-CNPAT/SEBRAE/CE, 2000.

[42]   Guenter, W. B. Química quantitativa: medições e equilíbrio. 1ª ed. São Paulo: Edgard Blücher, 1972.

[43]   Kotas, J.; Stasicka, Z. *Environ. Pollut.* **2000**, *107*, 263. [CrossRef]

[44]   Skoog, D. A.; West, D. M.; Holler, F. J.; Crouch, S. R. Fundamentos de Química Analítica. 8ª ed. São Paulo: Thomson Learning, 2006.

[45]   Rai, D.; Sass, B. M.; Moore, D. A. *Inorg. Chem.* **1987**, *26*, 345. [CrossRef]

[46]   Lavid, N.; Schwartz, A.; Yarden, O.; Tel-Or, E. *Planta*. **2001**, *212*, 323. [CrossRef][PubMed]

[47]   Deng, S.; Ting, Y. P. *Environ. Sci. Technol.* **2005**, *39*, 8490. [CrossRef][PubMed]

[48]   Romero-González, J.; Peralta-Videa, J. R.; Rodríguez, E.; Delgado, M.; Gardea-Torresdey, J. L. *Bioresour. Technol.* **2006**, *97*, 178. [CrossRef][PubMed]

[49]   Aggarwal, D.; Goyal, M.; Bansal, R. C. *Carbon*. **1999**, *37*, 1989. [CrossRef]

[50]   Park, D.; Lim, S. R.; Yun, Y. S.; Park, J. M. *Chemosphere* **2007**, *70*, 298. [CrossRef][PubMed]

205

Orbital: Electron. J. Chem. 5 (3):192-205, 2013

Full Paper

Cassava Root Husks as a Sorbent Material for the Uptake and Pre-concentration of Cadmium(II) from Aqueous Media

Alexandre de Oliveira Jorgetto[a]*, Adrielli Cristina Peres da Silva[a], Bruna Cavecci[a], Rodrigo Correa Barbosa[a], Marco Antonio Utrera[b], and Gustavo Rocha de Castro[a]

[a]Departamento de Química e Bioquímica, Instituto de Biociências de Botucatu, UNESP, Distrito de Rubião Júnior, S/N. CEP: 18618-970, Botucatu, SP, Brazil.
[b]Instituto de Química, UFMS – Av. Senador Filinto Müller, 1555. CEP: 79074-460, Campo Grande, MS, Brazil.

Abstract: Cassava husks were undergone to simple processes to obtain a fine powder whose particle diameter varied from 63 μm to 75 μm. The characterization of the material indicated the presence of the groups alcohol, amine and thiocarbonyl. The material was tested through batch experiments and the effect of the contact time and pH over the adsorption of Cd(II) ions were evaluated. The material presented a rapid kinetic equilibrium, which was reached in less than 1 min, and the highest Cd(II) uptake occurred at pH 5. The optimum conditions obtained were applied to determine the material's maximum adsorption capacity with the aid of the linearized Langmuir equation (0.109 mmol g^{-1}). A pre-concentration experiment was also carried out, and provided a pre-concentration factor of 43-fold.

Keywords: cassava; cadmium; adsorption; pre-concentration; solid-phase extraction

1. INTRODUCTION

Environmental pollution has become one of the greatest concerns in our modern society. Throughout history, mankind has been developing a wide variety of materials and substances to attend its own needs and to facilitate people's daily lives; nevertheless, this led to the development of toxic substances, which became environmental contaminants [1]. Some common examples of contaminants of the environment comprehend pesticides, dyes, fertilizers and heavy metals [2]. Concerning the heavy metals, such a type of contaminant encompasses a variety of metal elements such as cadmium, lead, nickel, copper and zinc among others [1, 2], which does not present any biological function, or is just required at trace levels by organisms; so, once their concentrations exceed such a level, they may become toxic to several living beings [2].

The most common sources of heavy metal contamination include fossil fuels, mining activities, industries and incineration plants. Once released in the environment, such substances may be dispersed through the atmosphere, hydrosphere or the soil to reach the most remote places in the world, causing the contamination of a vast area [2].

Yet, several diseases are associated to heavy metal contamination, being among them polycythemia, Alzheimer's, kidney damage, over-production of red blood cells, abnormal thyroid artery, fatal cardiac arrest, right coronary artery problems, blood pressure, lung cancer, stomach cancer, gliomas and etc [3-14].

In view of that, it is evident the great importance of regulating the emissions of metal contents to the environment, in order to prevent the damages caused by human activities. To do so, nowadays, many techniques have been developed to reduce/eliminate the amount of heavy metal contaminants from effluents based on principles like precipitation, co-precipitation, membrane filtration, solvent extraction, cementation, coagulation, reverse osmosis, ion exchange, electrodialysis and adsorption of the metal ions [15-26]. Obviously, every technique possesses its merits and drawbacks to accomplish the removal of metal contaminants, though solid-phase extraction using sorbent materials has attracted great attention by its simplicity, high efficiency, and low

---

*Corresponding author. E-mail: xjorgetto@gmail.com

cost (in general) [27-29]. This technique exploits the presence of chelating/complexing groups (*e.g.* carboxylic, amine, amide, thiol, phosphoryl *etc*.) on the surface of sorbents that are able to form coordinate covalent bonds with metal species, removing them from liquid media [30]. Nevertheless, solid-phase extraction is very dependent on parameters such as (but not only) contact time and pH. Since the sorption of pollutants has become a very important technique for the remediation of wastewaters, the study of such parameters has acquired great importance to evaluate the efficiency of sorbent materials. Whereas the elucidation of the kinetic process gives information over the mechanisms of sorption [31], the pH study allows us to uncover the optimum condition under which the sorption process is favored. One of the main effects of the medium's pH over the sorption process is related to presence of hydronium ions which may cause the protonation of the adsorption sites (obviously this process is more evident at low pHs). On the other hand, at higher pHs, another phenomenon takes place. In this case, the higher concentrations of hydroxyl ions may cause the precipitation of metal species due to hydrolysis reactions, not allowing them to coordinate to the material's adsorption sites [28].

Common materials that have being extensively applied for such a purpose include silicas, zeolites, clays, metal oxides, activated carbon and biosorbents [28]. Biosorbents, by their turn, present some advantages over other materials that include general large bioavailability, natural presence of chelating/complexing groups in their structure (without the need of previous functionalization, which could generate by-products and residues [27]) and simple preparation steps. Among the most studied biosorbents are fruit peels, vegetable husks, some agricultural wastes and etc [29].

In view of the promising properties provided by biomaterials for heavy metal solid-phase extraction, cassava (*Manihot esculenta*) root husks present a great potential for their application as a biosorbent in Brazil. Cassava is a plant of Brazilian origin, whose root is very appreciated in the native culinary. Its roots consist of a dark brown elongated root, which contains a white edible flesh in its interior. Some food industries in Brazil commonly extract the cassava root's inner flesh to trade it at supermarkets, but cassava root husks hardly ever have another destination rather than turning into vegetal manure. With that in mind, utilizing cassava husks as a heavy metal biosorbent would be a more interesting

application for this material. So, this work has as main aim, to produce a biosorbent made of cassava root husks, as well as to evaluate its adsorptive properties regarding the uptake and pre-concentration of cadmium(II) from aqueous media.

2. MATERIAL AND METHODS

Reagents and solutions

Cd(II) solutions were prepared using a high purity cadmium chloride (Merck) that was dissolved in ultrapure water (Elga system, Purelab). The standard solutions used in atomic absorption spectrometry were prepared by dilution of 1000 mg L^{-1} stock solutions (Tritisol Merck). For the adjustment of the pH, diluted HNO_3 (Carlos Erba) and NaOH (Synth) were used.

Equipments

The metal species were determined using an atomic absorption spectrometer (Shimadzu AA6800) equipped with a flame module, as appropriate. The monochromator of the equipment was adjusted to 228.8 nm, which are the most sensitive resonance line for cadmium. The infrared spectra were obtained using a Nicolet Nexus 670 spectrometer; samples were scanned 200 times at a resolution of 4 cm^{-1}, through reflectance mode. The pre-concentration experiments were carried out with the aid of dosing pumps Tecnopon DMC 100. Elemental analysis was performed on an EA 1110 CHNS-O analyzer from CE Instruments using 2.2 mg of material.

Preparation of the cassava husks biosorbent

Cassava roots were acquired from a conventional supermarket and washed with tap water to remove any earth particles that could be attached to them. Then, the clean roots had their husks manually extracted with the aid of a knife, and they were broken into pieces before being taken to a heated ventilated chamber at 100 °C. After 24 h in the chamber, the husks were grinded in a blade grinder to generate a gross powder of the material. Cassava root husks were later sieved in sieves of different particle sizes, and the powder fraction comprehended between 63 μm and 75 μm was chosen to perform the adsorption experiments. Prior to the adsorption experiments, it was accomplished a washing step, in order to remove any soluble organic substance that

207

Orbital: Electron. J. Chem. 5 (3):206-212, 2013

could be attached to the material. To do so, the husks were transferred to a becker containing 50 mL of 0.01 mol L^{-1} HCl solution, in which it was stirred for 2 h. After this step, the material was filtered in büchner funnel, and the material was rinsed several times with 100 mL of deionized water and, from time to time, 10 mL of the rinsing water was collected to perform pH analysis. When pH reached a value between 5 and 6, the material was removed from the funnel and taken to the heated ventilated chamber again at 55 °C, for drying. Since the material formed an agglomerate of the cassava husks powder, it was softly grinded manually so that powder particles could be released and used in the adsorption experiments.

Determination of the material's point of zero charge (PZC)

The procedure utilized to obtain the material's PZC was adapted from the one described by Regalbuto *et al.* [32]. The procedure applied to the cassava husks consisted of preparing solutions of different pHs (1, 2, 3, 4, 5, 6, 8, 9, 10 and 11), then, 25.0 mg of the cassava husks were transferred to flasks containing 20.0 mL of each solution and they were kept under agitation for 24 h. After the established time was completed, the solution of each flask had its pH measured, and a graph of final pH vs. initial pH was plotted. The PZC of the material consisted of the region in the graph in which it acted as a buffer.

Batch experiments

All the batch experiments were carried out using 1.8 mL of the metal solution and 20.0 mg of the biosorbent. Initially, it was performed a kinetic experiment, in which a 68.4 mg L^{-1} solution was shaken with the material for times varying from 1 min to 240 min. After the end of the established contact times, the material was filtered in a quantitative filter, and the supernatant was collected to have its concentration measured through Flame Atomic Absorption Spectrometry (FAAS). After the concentration analysis, it was possible to calculate the adsorption capacity of the material (N_f) for each contact time, what occurred by inserting the obtained data to Equation 1:

$$N_f = \frac{n_i - n_s}{m} \qquad (1)$$

in which n_i is the initial amount of Cd(II) (mmol) in the volume utilized for the experiment, n_s is the remaining amount of Cd(II) of the solution after the contact time (mmol), and m is the mass of the biosorbent (gram). This equation was also used to determine the adsorption capacity of all the subsequent batch experiments.

Later, it was studied the effect of the pH over the adsorption of Cd(II). For this parameter, 75 mg L^{-1} Cd(II) solutions, whose pH varied from 1 to 5, were prepared. The contact time established for this study was 10 min. The samples were subjected to the same procedure described for the kinetic study.

Finally, it was necessary to determine the maximum adsorption capacity of the material. To do so, the material was shaken with solutions of different concentrations (12.5 mg L^{-1} to 505.4 mg L^{-1}) for 10 min (the pHs of the solutions were adjusted to 5). As in the previous experiments, the concentrations before and after the contact time were analyzed and utilized to determine their N_f values for each condition.

Pre-concentration experiments

The pre-concentration experiments were carried out using a constant flow of 1.5 mL min^{-1}, and a mass of biosorbent of 5.00 mg. At first, the mass of the material was packed inside a 4 mm across cylindrical tube, which was connected to peristaltic pumps through Tygon tubes. At first, 50 mL of a 10 μg L^{-1} Cd(II) solution (pH ~ 5) was percolated through the material inside the column, and later, the retained metal species were eluted with 1 mL of a 2 mol L^{-1} HNO_3 solution. This procedure enabled to determine the pre-concentration factor of the cassava husks powder.

3. RESULTS AND DISCUSSION

Characterization of the biosorbent

The biosorbent was characterized through Fourier Transform Infrared Spectroscopy (FTIR) and elemental analysis.

According to the FTIR analysis, it indicated the presence of OH stretch band in the region of 3444 cm^{-1}, and CH stretch bands in 2929 cm^{-1} and 2846 cm^{-1}. These bands are expected since these groups are very common in materials constituted mainly by cellulose, which constitutes most of the vegetal structures on Earth. Moreover, C-N stretch band in

208

Orbital: Electron. J. Chem. 5 (3):206-212, 2013

1249 cm^{-1}, C=S stretch band in 1160 cm^{-1}, and NH wag bang in 928 cm^{-1} indicate the presence of amine and thiocarbonyl groups in the material. These are functional groups of interest for the occurrence of metal adsorption, since the presence of nitrogen and sulfur implies in the possibility of metal coordination to the non-bonding electron-pairs of such an elements. The presence of nitrogen-based groups was also verified through elemental analysis, which provided 1.01541758 wt % of nitrogen. The coordination phenomenon is attributed to the share of electron-pairs between Lewis bases and acids [33]. Since amine, hydroxyl and thiocarbonyl groups contain nitrogen, sulfur or oxygen atoms in their constitution (which possess non-bonding electron-pairs), such atoms may act as Lewis bases and form coordinated covalent bonds with metal ions (which, by their turn,

will behave as Lewis acids). So the presence of the as-mentioned groups plays a very important role in the adsorption process. Also, since pH exerts a great influence over the adsorption process, the PZC of the material was measured and found to be 5.33.

Batch Experiments

From the adsorption experiment in function of time, it was possible to know the minimum contact time in which the Cd(II) ions in solution reached the kinetic adsorption equilibrium onto the surface of the material. As it can be seen from Figure 1, the cassava husks powder presents a very rapid adsorption process, reaching kinetic equilibrium in less than 1 min.
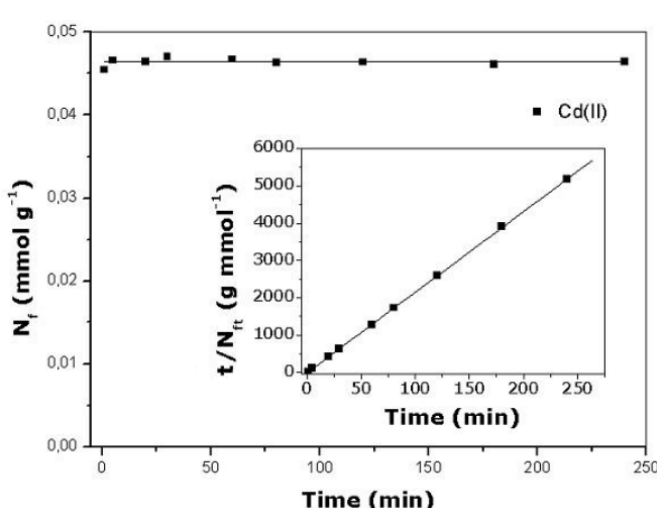

Figure 1. Isotherm of the kinetic experiment and its linearization according to the pseudo-second order kinetic model.

This short time to reach equilibrium indicates that the structure of the material provides high accessibility to its adsorption sites, so that Cd(II) ions could coordinate to them. This also implies that the material is adequate to perform pre-concentration experiments.

The data provided by the kinetic experiment were inserted to the pseudo-second-order kinetic model (Equation 2), which presented great accordance with this model, demonstrated by the high linear correlation coefficient ($r^2 = 1.0000$) (depicted in Figure 1 by the inserted graph), and by the great proximity of the experimental and theoretical N_f values at equilibrium (0.046 mmol g^{-1} and 0.0463 mmol g^{-1}, respectively). In Equation 2, t is the time (in min); N_{ft} is the adsorption capacity at time t (in mmol g^{-1}); N_f is the adsorption capacity at equilibrium (in

mmol g^{-1}); and K_2 is the pseudo-second order kinetic constant (g mmol^{-1} min^{-1}).

$$\frac{t}{N_{ft}} = \frac{1}{K_2 N_f^2} + \frac{1}{N_f} t \qquad (2)$$

Regarding the study about the influence of the pH over the material's adsorption capacity, it can be seen from Figure 2, that at pH 1, due to the high concentration of hydronium ions, the adsorption of Cd(II) is drastically reduced. This occurred because of the competition for the adsorption sites by the hydronium ions, which are in much higher concentration than the metal species, causing the protonation of the material's surface, as supported by the PZC of the material (5.33). Since the surface of the cassava husks is protonated under this pH value, it prevents the Cd(II) cations to bind to the material's

209

Orbital: Electron. J. Chem. 5 (3):206-212, 2013

coordinating groups not only because of the competition for the adsorption sites by the protons, but also because of the positively charged surface that repels Cd(II) cations.

Figure 2 also indicates that the material's adsorption capacity increases with the increase of the pH, till it attains the maximum Cd(II) uptake at pH 5, when the charge of the particles' surface is practically null, and the electron pairs of atoms such as nitrogen, sulfur, and oxygen are free to bind Cd(II) ions.
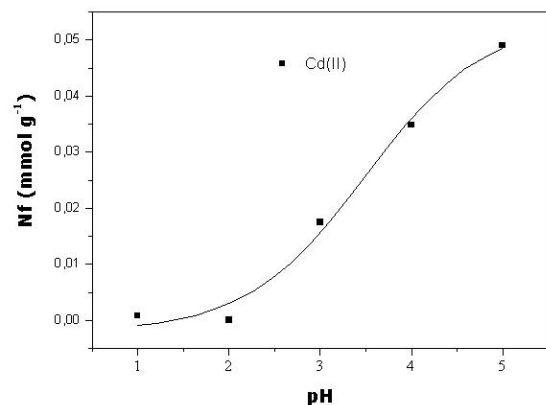

Figure 2. Effect of the pH over the adsorption of Cd(II).

At hand of the optimum contact time and pH obtained from the experiments, such conditions were applied to another experiment to uncover the material's maximum adsorption capacity. Hence, the moment in which cassava husks reached the saturation of its adsorption sites was evaluated as a function of Cd(II) concentration. Such a study is depicted in Figure 3 (a).

As it can be seen from Figure 3 (a), the isotherm as a function of the concentration approaches a maximum value of approximately 0.11 mmol g^{-1}, as the Cd(II) concentration increases. In Figure 3 (b), the obtained data were inserted to the linearized Langmuir equation (Equation 3), so that the maximum adsorption capacity could be estimated.

$$\frac{C_s}{N_f} = \frac{C_s}{N_s} + \frac{1}{N_s b} \qquad (3)$$

The linearized Langmuir equation was a good model to fit the data, since it provided a high linear correlation coefficient (r^2) of 0.9905. Such a model tells that Cd(II) adsorption occurs through the formation of a monolayer over the material's surface. The angular coefficient ($1/N_s$) of the best-fit straight line enabled to calculate the material's theoretical maximum adsorption capacity (N_s), obtaining a value

of 0.109 mmol g^{-1}, which is approximate to the experimental value, observed in Figure 3 (a). This indicates that practically all the adsorption sites were able to sequester Cd(II) ions. Moreover, the calculated empirical constant (*b*) of Equation 3 was 763 L mmol^{-1}. As a comparison, Table 1 shows some materials with their respective maximum adsorption capacities for Cd(II):


(a)

(b)
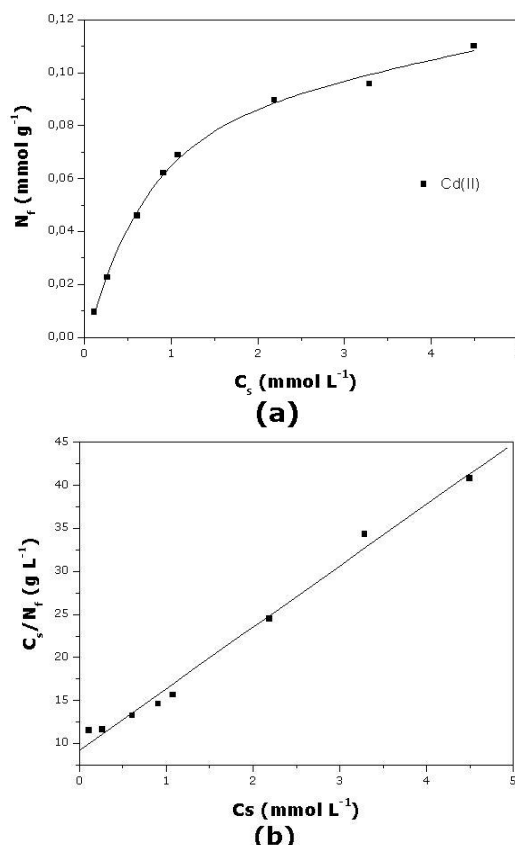
Figure 3. Isotherm for the adsorption of Cd(II) as a function of the concentration (a), and its linearization, according to the Langmuir equation (b).

Table 1 enables to compare the maximum adsorption capacity of cassava husks with other low-cost adsorbents. Among them, there are other crude biosorbents (coconut copra meal, raw rice husks, and broad bean peels), a chemically-treated biosorbent (NaOH-treated rice husks), functionalized adsorbents (dithiooxamide-modified cellulose and 2,2-bipyridine-modified silica gel), and a naturally occurring inorganic adsorbent (calcite). From such a table, it can be noted that there are materials much more efficient than cassava husks for the uptake of cadmium (*e.g.* broad been peels and 2,2-bipyridine-modified silica gel), however, less efficient materials also exist, like raw rice husks and coconut copra meal. Besides, functionalized cellulose also presented a

210

Orbital: Electron. J. Chem. 5 (3):206-212, 2013

lower cadmium maximum adsorption capacity than raw cassava husks. It is interesting to notice that a biosorbent material may have its efficiency improved by chemical treatment. In the table, this fact is illustrated by the increase in the adsorption capacity of rice husks, after a NaOH-treatment.

Table 1. Comparison of the maximum adsorption capacity of cassava husks powder and other adsorbents.

Material	*Maximum Adsorption Capacity (mmol g^{-1}) for Cd(II)*	*Reference*
Calcite	0.165	[34]
Dithiooxamide-modified cellulose	0.069	[35]
Coconut copra meal	0.044	[36]
2,2-bipyridine-modified silica gel	0.53	[37]
Raw rice husks	0.076	[38]
NaOH-treated rice husks	0.180	[38]
Broad bean peels	1.312	[39]
Cassava husks	0.109	This study

Pre-concentration experiments

Since pre-concentration experiments were carried out by percolating 50 mL of the metal solution and later eluting the retained metal with 1 mL of 2 mol L^{-1} HNO_3 solution, the pre-concentration factor is restricted to a maximum value of 50-fold. The experimental pre-concentration factor for Cd(II) obtained was 43-fold, what implies that the material recovered 86% of the metal content from the solutions. By uncovering the pre-concentration factor, this method allows to determine the amount of metal present in other samples through simple FAAS without resorting to more expensive and complex techniques (*e.g.* GFAAS, ICP-MS or ICP-OES).

4. CONCLUSION

Cassava husks infrared spectrum presented bands associated to the presence of alcohol, amine and thiocarbonyl groups. The material reached kinetic equilibrium in less than 1 minute, and its optimum pH to perform Cd(II) uptake was found to be 5, what is very approximate to the material's point of zero charge (5.33). The theoretical Cd(II) maximum adsorption capacity obtained was 0.140 mmol L^{-1}. The material's properties demonstrated to be adequate to perform pre-concentration experiments and it provided a pre-concentration factor of 43-fold.

5. ACKNOWLEDMENTS

6. REFERENCE AND NOTES

[1]   Manahan, S. E.; Environmental Science and Technology, Boca Raton: Lewis 2000.

[2]   REEVE, R. N.; Introduction to Environmental Analysis, Chichester: John Wiley & Sons LTD, 2002.

[3]   Knight, C.; Kaiser, G. C.; Robothum, L. H.; Witter, J. V. *Environ. Geochem. Health.* **1997**, *19*, 63. [CrossRef]

[4]   Loubieres, Y.; Lassence, A. D.; Bernier, M.; Baron, A. V.; Schmitt, J. M.; Page, B.; Jardin, F. *J. Toxicol. Clin. Toxicol.* **1999**, *37*, 333. [CrossRef]

[5]   Strachan, S. *Curr. Anaesth. Crit. Care* **2010**, *21*, 44. [CrossRef]

[6]   Robert, G.; Mari, G.; Human Health Effects of Metals, US Environmental Protection Agency Risk Assessment Forum, Washington, DC, 2003.

[7]   Dieter, H. H.; Bayer, T. A.; Multhaup, G. *Acta Hydroch. Hydrob.* **2005**, *33*, 72.

[8]   Nordberg, G.; Jin, T.; Bernard, A.; Fierens, S.; Buchet, J. P.; Ye, T.; Kong, Q.; Wang, H. *Ambio* **2002**, *31*, 478. [CrossRef]

[9]   Steenland, K.; Boffetta, P. *Am. J. Ind. Med.* **2000**, *38*, 295. [CrossRef]

[10] Mortada, W. I.; Sobh, M. A.; El-Defrawy, M. M.; Farahat, S. E. *Am. J. Nephrol.* **2001**, *21*, 274. [CrossRef]

[11] Jarup, L. *Brit. Med. Bull.* **2003**, *68*, 167. [CrossRef]

[12] Barbee, J. Y. Jr.; Prince, T. S. *South. Med. J.* **1999**, *92*, 510. [CrossRef]

[13] Jarup, L.; Hellstrom, L.; Alfven, T.; Carlsson, M. D.; Grubb, A.; Persson, B.; Pettersson, C.; Spang, G., Schutz, A., Elinder, C. G. *Occup. Environ. Med.* **2000**, *57*, 668. [CrossRef]

[14] Muhammad, S.; Shah, M. T.; Khan, S. *Microchem. J.* **2011**, *98*, 334. [CrossRef]

[15] Gabaldon, C.; Marzal, P.; Ferrer, J.; Seco, A. *Water Res.* **1996**, *30*, 3050. [CrossRef]

211

Orbital: Electron. J. Chem. 5 (3):206-212, 2013

[16] Kadirvelu, K.; Faur-Brasquet, C.; Le Cloirec, P. *Langmuir* **2000**, *16*, 8404. [CrossRef]

[17] Mohan, D.; Pittman Jr., C. U. *J. Hazard. Mater. B* **2006**, *137*, 762. [CrossRef]

[18] Mohan, D.; Singh, K. P.; Singh, V. K. *J. Hazard. Mater.* **2006**, *135*, 280. [CrossRef]

[19] Mohan, D.; Singh, K. P. *Water Res*. **2002**, *36*, 2304. [CrossRef]

[20] Atkinson, B. W.; Bux, F.; Kasan, H. C. *Water SA* **1998**, *24*, 129.

[21] Babel, S. *J. Hazard. Mater.* **2003**, *97*, 219. [CrossRef]

[22] Mellah, A.; Chegrouche, S.; Barkat, M. *J. Colloids Interf. Sci.* **2006**, *296*, 434. [CrossRef]

[23] Prasad, M.; Saxena, S. *Ind. Eng. Chem. Res.* **2004**, *43*, 1512. [CrossRef]

[24] Liu, C. C.; Wang, M. K.; Li, Y. S. *Ind. Eng. Chem. Res.* **2005**, *44*, 1438. [CrossRef]

[25] Özcan, A.; Özcan, A. S.; Tunali, S.; Akar, T.; Kiran, I. *J. Hazard. Mater. B* **2005**, *124*, 200. [CrossRef]

[26] Kobya, M. *Adsorpt. Sci. Technol.* **2004**, *22*, 51. [CrossRef]

[27] Castro, R. S. D.; Caetano, L.; Ferreira, G.; Padilha, P. M.; Saeki, M. J.; Zara, L. F.; Martines, M. A. U.; Castro, G. R. *Ind. Eng. Chem. Res.* **2011**, *50*, 3446. [CrossRef]

[28] Walcarius, A.; Mercier, L. *J. Mater. Chem.* **2010**, *20*, 4478. [CrossRef]

[29] Rao, K. S.; Mohapatra, M.; Anand, S.; Venkateswarlu, P. *Int. J. Eng. Sci. Technol.* **2010**, *2*, 81.

[30] Jal, P. K.; Patel, S. B.; Mishra, K. *Talanta* **2004**, *62*, 1005. [CrossRef]

[31] Ho, Y. S.; McKay, G.; *Proc. Biochem.* **1999**, *34*, 451. [Crossref]

[32] Regalbuto, J. R.; Robles, J.; *The engineering of Pt/Carbon Catalyst Preparation,* University of Illinois: Chicago, 2004.

[33] Pearson, R. G. *J. Am. Chem. Soc.*, **84**, *16*, 1962.

[34] Yavuz, Ö.; Guzel, R.; Aydin, F.; Tegin, I.; Ziyadanogullari, R. *Pol. J. Environ. Stud.* **2007**, *16*, 467.

[35] Jorgetto, A. O.; Silva, R. I. V.; Longo, M. M., Saeki, M. J., Padilha, P. M.; Martines, M. A. U.; Rocha, B. P.; Castro, G. R. *Appl. Surf. Sci*. **2013**, *264*, 368. [CrossRef]

[36] Ho, Y. S.; Ofomaja, A. E. *Biochem. Eng. J.* **2006**, *30*, 117. [CrossRef]

[37] Souza, E. J.; Cristante, V. M.; Padilha, P. M.; Jorge, S. M. A.; Martines, M. A. U.; Silva, R. I. V.; Carmo, D. R.; Castro, G. R. *Pol. J. Chem. Tech.* **2011**, *13*, 28.

[38] Kumar, U.; Bandyopadhyay, M. *Bioresour. Technol.* **2006**, *97*, 104. [CrossRef]

[39] Benaissa, H. *J. Hazard. Mater.* **2006**, *132*, 189. [CrossRef]

212

Orbital: Electron. J. Chem. 5 (3):206-212, 2013

Full Paper

The Use of Converter Slag (Magnetite) and Bentonite Clay for Amoxicillin Adsorption from Polluted Water

Fernanda Maichin, Lidiane Cunha Freitas and Nilce Ortiz*

Center of Environmental Chemistry – CQMA. Institute for Energy and Nuclear Research, IPEN. Av. Lineu Prestes, 2242, CEP 05508-000, São Paulo-Brasil http://www.ipen.br

Abstract: The presence of pharmaceuticals compounds in the aquatic environment has attracted much interest from the academic community, since these compounds are potential endocrine disrupters and persist in the environment causing irreversible damage to the ecosystem. In Brazil little research has been conducted to measure, treat and remove β-lactam antibiotics such as amoxicillin present in surface water. Thus, the development and implementation of new treatment method which allow the removal or reduction of these compounds in surface waters are need. This study, focus on the development of low cost adsorbent material composed by steel manufacture converter slag (magnetite) and bentonite clay to adsorb and remove amoxicillin (amox) from water under laboratory conditions. To demonstrate the favorable aspects, the study was performed by experimental calculations of thermodynamics, kinetic and empirical model. The obtained results were similar with others found in literature which indicate the steel industry residue -magnetite and bentonite clay can be use to remove amoxicillin, with approximately 50% of removal percentage.

Keywords: amoxicillin; magnetite; bentonite clay; endocrine disrupters

1. INTRODUCTION

The drinking water supply have been suffered numerous challenges in recent years, this is a complex issue that requires reflection and actions to ensure water quality for this and future generations. The introduction of toxic substances in water is one of the most complex causes of its deterioration. One of the higher concerns is the presence of micro pollutants, toxic compounds in concentrations on the order of $\mu g.L^{-1}$ and $ng.L^{-1}$, and that has increasing significantly in recent years. Among these micro pollutants are many pharmaceutical compounds, endocrine disruptors, and persistent organic pollutants.

In aquatic environment, the pharmaceuticals compounds and its derivatives can be found in surface water, underground, marine sediments, soils, effluents, biological sludge from STP – Sewage treatment plant and drinking water [1]. They have been introduced continuously into the environment at detectable concentrations resulting in water quality lost, ecosystem health and potentially impact on drinking water supply. The presence of pharmaceutical compound as β-lactam antibiotic amoxicillin and its derivatives in the effluent of sewage treatment plants demonstrates the need to improve the treatment efficiency before discharge in water resources [2].

Antibiotics as amoxicillin are important to human and veterinary health. They were specially designed to control disease due its high bacteria resistance and large spectrum against a wide variety of microorganisms. The US top 200 prescriptions were prescribed more than two billion times within the United States in 2003, with amoxicillin being prescribed the most (3.4% of all sales) among those included in this study, followed by atorvastatin (3.1%) [3].

The discharge of amoxicillin and its derivatives in water resources result in an environmental disorder, odor, and may cause microbial resistance among pathogen organisms [4]. For those reasons, amoxicillin waste need to be removed before water disposes in to the environment [1].

There are many methods to remove amoxicillin from sewage water, such as membrane process, ion exchange, biological degradation and

---

*Corresponding author. E-mail: nortiz@ipen.br

adsorption using various kinds of adsorbents. The adsorption process was already proved to be effective to remove various pollutants from aqueous solutions in wide range of concentrations [5]. The process involves the rate of adsorption (K_{ab}) which indicates the velocity of the amoxicillin molecules and its derivatives toward active sites in solid adsorbent surface [6].

The amoxicillin solubility increase with the temperature, but in the adsorption processes the temperature increase also reduce the interaction forces between amoxicillin and the solid adsorbent surface, consequently the amoxicillin surface adsorption became more difficult. The processes temperatures higher than 23 °C can also result in amoxicillin decomposition [5].

The use of converter slag from steel industry, main composed by magnetite will allow adsorbing and removing the pharmaceutical compound from water in a low cost adsorption process. The magnetite has high pore structure and adsorption capacity, primarily related to pore size distribution, surface area and pore volume. After adsorption process the satured magnetite can be remove form the solution using a simple magnetic separation [7].

The bentonite clay was added to the magnetite to improve the absorbent properties [8]. The clay was chosen due its affinity to the organic compounds, such characteristic have been used historically in industrial clarification process of comestible vegetable oils. It's natural clay, abundant in most continents, chemically inert with low acquisition cost.

Main composed by montmorilonite, the bentonite crystal structure consists of two layers of tetrahedral silica sheets sandwiching one octahedral alumina sheet, it has a net negative charge on its layer lattice due isomorph substitutions. Their chemical nature and pore structure generally determine the clay sorption ability.
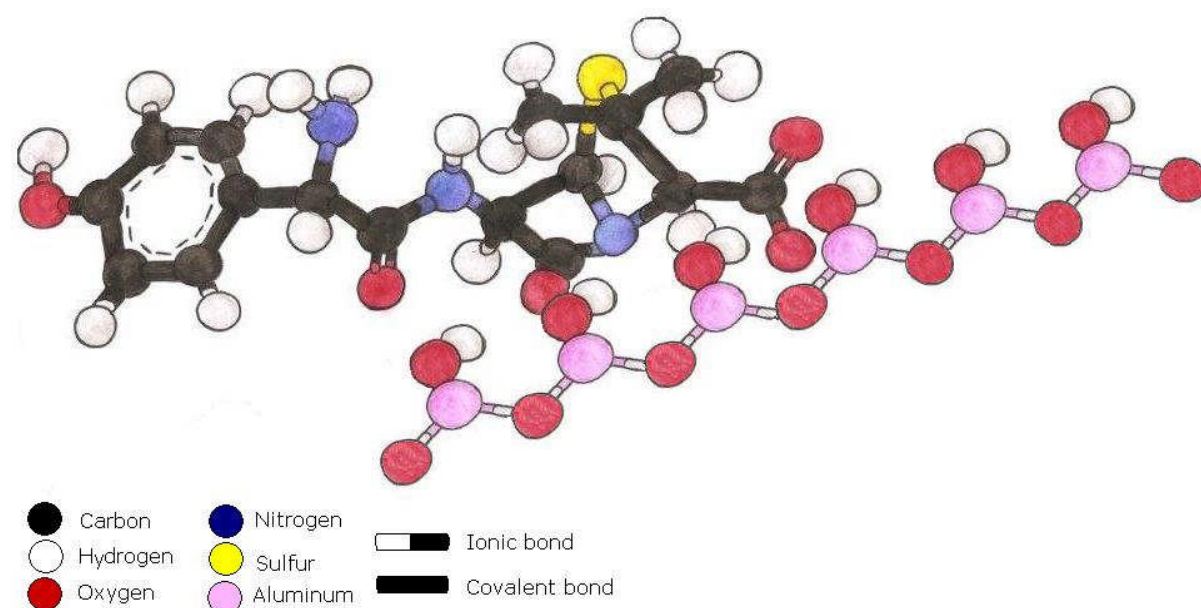

Figure 1. The schematic physical adsorption of the amoxicillin molecule and the alumina sheet (octahedral) of the bentonite clay.

The project was developed aiming the adsorption process improvement using a mixture of converter slag-magnetite with bentonite clay to adsorb and reduce the presence of amoxicillin and its derivatives from contaminated water, pharmaceutical effluents and polluted surface water resources. The experimental results were applied on thermodynamic calculations, the determination of the empirical kinetic model and adsorption process rate (K_{ab}).

2. MATERIAL AND METHODS

The converter slag (magnetite) was collected in air filters of the converter unit in steel manufacture plant, it is main composed by iron oxide (98%). After the sampling procedure, it was dried, sieved and the

214

Orbital: Electron. J. Chem. 5 (3):213-217, 2013

granulometric fractions of #12>Ө>#16 mesh (ASTM) were used to prepare the adsorbent mixture with bentonite clay (1/8 weight). The thermodynamic and kinetic studies were developed using the results obtained in adsorption processes performed under laboratory conditions using heating bath to keep temperatures on 16-21 ^{o}C. The amoxicillin stock solution was prepared dissolving 0.20g in 0.5 L of distilled water for 30 min. the initial concentration (C_o) were obtained using different volumes of the stock solution diluting in 250 mL to perform adsorption processes studies. The 2 g of the adsorbent composite (magnetite and bentonite clay) was added to the amoxicillin solution and the mixture was keep homogeneous using mechanical agitation for 8 h to reach the equilibrium condition. Nine aliquots were collected form the adsorption process on 0, 10, 30, 60, 120, 240, 360, 420 e 480 minutes of stirring. The aliquots were centrifuged on 15000 rpm for 15 minutes and the amoxicillin content were determined as adsorbance using the spectrophotometer UV-Vis Varian Cary–E1 in λ= 273 nm and λ= 194 nm. The amoxicillin concentrations were determined using a calibration curve prepared previously with standards solutions, those values were used on thermodynamics and kinetics calculations.

3. RESULTS AND DISCUSSION

The thermodynamic constants of the adsorption indicate whether the process was spontaneous, exothermic or endothermic and if the adsorbent has a high affinity for the adsorbate. Moreover, these parameters may provide information concerning the heterogeneity of the solid surface and if the process involves physical or chemical adsorption.

The thermodynamic parameters of the adsorption process as Gibbs free energy (ΔG^0), enthalpy (ΔH^0) and entropy (ΔS^0) can be calculated using the following equations:

$$Kc = C_A / C_s \qquad \qquad \qquad I$$

$$\log Kc = \Delta S^0 / 2.303\,R - \Delta H^0 / 2.303\,RT \qquad II$$

$$\Delta G^0 = -2.303\,RT \log Kc \ (kJ\ mol^{-1}) \qquad III$$

Where: Kc is the equilibrium constant from the adsorption isotherm; C_A is the concentration of amoxicillin adsorbed on the adsorbent in the equilibrium condition, Cs is the concentration of amoxicillin in solution at equilibrium, R is the gas

constant (8.314 J. $mol^{-1}.K^{-1}$) and T the temperatures in Kelvin.

The value of Gibbs free energy (ΔG^0) of physical adsorption is in the range of 1 to 5 kJ mol^{-1}, for chemical adsorption the ΔG^0 values is usually higher of 20 kJ mol^{-1} and the ΔG^0 values for activated adsorption are in the range of 5 to 20 KJ mol^{-1}.

The adsorption kinetics of amoxicillin on magnetite and bentonite mixture has been mathematically analyzed using a kinetic empirical model. The kinetic model is used to calculate the amoxicillin concentration in each time stirring, usually the modeling results are compared with those measured experimentally. The constants K'' and A depends of the C_o, the adsorbent density and its particle size. The K'' and A were determined from the plots $\log(C_o-C_e)$ vs log [log(t+1)]. The straight lines obtained indicate the applicability of the kinetic model to the present study. The study were performed on different initial concentrations to confirm the K'' and their variations.

$$\log (t+1) = K''(C_o-C)^A$$

$$\log (\log(t+1)) = \log K'' + A \log (C_o-C)$$

$$\log (C_o-C) = -\log K''/A + 1/A \log [\log(t+1)] \qquad IV$$

Where: t-stirring time (min), C- amoxicillin concentration (mg L^{-1}), C_o-initial concentration of amoxicillin mg L^{-1}), K"- kinetic constant of the empirical model, A - empirical constant of the kinetic model.

The adsorption constant rate (K_{ab}) was calculated using the equation V following the first order rate expression, given by Langergren expression [9, 10]

$$\log (C_o-C_e) = \log C_e - (K_{ab}/2.303)t \qquad V$$

Where: t-stirring time (min), C_e equilibrium concentration, and C_o initial concentration, K_{ab} constant rate of adsorption (min^{-1}).

Linear plots of $\log(C_o-C_e)$ *vs* t indicate the applicability of the equation V. The obtained K_{ab} values, calculated from the slopes of the line equation indicate the tendency of the K_{ab} change with the increasing of the temperature (Figure 2). In literature was found K_{ab}= 0.0198 $min.^{-1}$ for adsorption process of amoxicillin with bentonite clay [5].

The experimental results and the equations I to III were used to calculate the thermodynamic constants, the values can be observed in Table 1.

215

Orbital: Electron. J. Chem. 5 (3):213-217, 2013

Table 1. The thermodynamic constants for the adsorption process.

Thermodynamic constants	(kJ/mol)
ΔS^0	1.5
ΔH^0	438.8
R^2	0.86
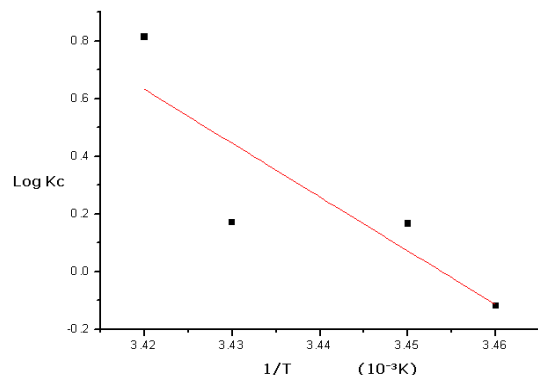
Figure 2. Thermodynamic plots for line equation calculation.

The ΔH^0 and ΔS^0 were obtained from the slope and intercept of the Van't Hoff plot [10]. The positive value of enthalpy (ΔH^0) confirms the endothermic adsorption of the amoxicillin and the positive value of ΔS^0 suggests the increase randomness at the solid-solution interface during the amoxicillin adsorption. The effect of the solvent molecules displaced by the amoxicillin molecules in solid surface, increase the system energy with more translation entropy than the amoxicillin molecules alone, also allowing the improvement of the randomness of the system. The negative values for Gibbs energy indicate that the adsorption is spontaneous, Table 2.

Table 2. Gibbs energy on different temperatures (K).

Temperatures (K)	$-\Delta G^0$ (kJ Mol^{-1})
292	4.5
291	-0.95
290	9.2
289	-0.66

The empirical kinetic model was calculated using the experimental results and equation IV. The adsorption constant rate (K_{ab}) was calculated using the equation V.

The value of K_{ab} found in the experiment was 0.0167 min^{-1}, very similar with 0.0198 min^{-1} found in literature for amoxicillin adsorption with bentonite clay. It means that the value of the parameters was consistent with published results [5].

Table 3. Constants calculated using the empirical model.

K"	1.26(min^{-1})	R^2	0.861
A	2.36	R^2	0.861
K_{ab}	0.017	R^2	0.793
$K_{ab\,*}$	0.0198(min^{-1})		

*K_{ab} reference values.

The kinetic empirical model were considered with reasonable response, the comparison between the amoxicillin concentrations obtained experimentally with those obtained empirically indicate the difference of only 0.4 mgL^{-1}, Table 4.

Table 4. Experimental concentrations of amoxicillin in different time stirring and the calculated values obtained using the empirical model.

C_o (mgL^{-1})	C_{exp} (mgL^{-1})	C_{calc} (mgL^{-1})
3.06	2.14	2.37
7.08	5.37	5.73
12.4	11.8	11.2
18.46	16.62	16.98

4. CONCLUSION

The magnetite and bentonite clay can be used to adsorb and remove amoxicillin compound from contaminated water. The adsorbent mixture was efficient, chemically inert, and abundant, with low cost and has a removal rate of 50% of amoxicillin in water. The adsorption processes were physical and activated depending of the temperature. The thermodynamic indicates a spontaneous, endothermic adsorption reaction with concentration results of the empirical model very close with the experimental. The adsorption modeling equations were confirmed to reduce the amoxicillin concentration from contaminated water and possibly from common effluents from pharmaceutical industries. In future experiments the magnetic properties of the adsorbents will be also considered to improve the amoxicillin removal percentage.

5. ACKNOWLEDMENTS

216

Orbital: Electron. J. Chem. 5 (3):213-217, 2013

6. REFERENCES AND NOTES

[1]   Ternes, T. A. *Wat. Res.* **1998**, *32*, 32. [CrossRef]

[2]   Longhim, R. S. Degradation of the pharmaceuticals amoxicillin and ampicillin and evaluation of toxicity and biodegradability of derived-products. [Doctoral dissertation.] Brasília, Brazil: Chemistry Institute of Brasília University, 2008. [Link]

[3]   Coillie, R. V.; Junqua, G.; Robinson, I.; Thomas, O. *Anal Bioanal Chem.* **2007**, *387*, 1143. [CrossRef][PubMed]

[4]   Ghiselli, G.; Jardim, W. F. *Quím. Nova* **2007**, *30*, 695. [CrossRef]

[5]   Budyanto, S.; Soedjono, S.; Irawaty, W.; Indraswat, N. *J. Environ. Prot. Sci.* **2008**, *2*, 72.

[6]   Adriano, W. S.; Gonçalves, L. R. B; Santana, C. C.; Veredas, V. *Biochem. Engin. J.* **2005**, *27*, 132. [CrossRef]

[7]   Ortiz, N. Study of the use of magnetite as adsorber of Cu^{2+}, Pb^{2+}, Ni^{2+} and Cd^{2+} in aqueous solution. [Doctoral dissertation.] São Paulo, SP, Brazil: Instituto de Pesquisas Energéticas e Nucleares, Universidade de São Paulo, 2000. [Link]

[8]   Putra, E. K.; Pranowo, R.; Sunarso, J.; Indraswati, N.; Ismadji, S. *Wat. Res.* **2009**, *43*, 2419. [CrossRef][PubMed]

[9]   Singh, A. K.; Singh, D. P.; Pandey; K. K.; Singh, V. N. *J. Chem. Technol. Biotechnol.* **1988**, *42*, 39. [CrossRef]

[10]   Namasivayam, C.; Ranganathan, K. *Environ.Pollut* **1993**, *82*, 255. [CrossRef]

217

Orbital: Electron. J. Chem. 5 (3):213-217, 2013